Old Dominion University
ODU Digital Commons

OES Theses and Dissertations | Ocean & Earth Sciences

Winter 2004

Inner Shelf Circulation in Coastal Virginia: A Data Assimilation Approach

Hector Hito Sepulveda
Old Dominion University

Follow this and additional works at: https://digitalcommons.odu.edu/oeas_etds

Part of the Oceanography Commons

Recommended Citation

Sepulveda, Hector H.. "Inner Shelf Circulation in Coastal Virginia: A Data Assimilation Approach" (2004). Doctor of Philosophy (PhD), Dissertation, Ocean & Earth Sciences, Old Dominion University, DOI: 10.25777/jykj-n513
https://digitalcommons.odu.edu/oeas_etds/161

This Dissertation is brought to you for free and open access by the Ocean & Earth Sciences at ODU Digital Commons. It has been accepted for inclusion in OES Theses and Dissertations by an authorized administrator of ODU Digital Commons. For more information, please contact digitalcommons@odu.edu.

INNER SHELF CIRCULATION IN COASTAL VIRGINIA: A DATA ASSIMILATION APPROACH

by

Héctor Hito Sepúlveda
B.S. in Physics - March 1996, University of Chile

A Dissertation Submitted to the Faculty of
Old Dominion University in Partial Fulfillment of the
Requirement for the Degree of

DOCTOR OF PHILOSOPHY

OCEANOGRAPHY

OLD DOMINION UNIVERSITY
December 2004

Approved by:

Arnoldo Valle–Levinson (Director)

Larry P. Atkinson

Chester E. Grosch

Thomas C. Royer

Keith R. Thompson

Reproduced with permission of the copyright owner. Further reproduction prohibited without permission.

ABSTRACT

INNER SHELF CIRCULATION IN COASTAL VIRGINIA: A DATA ASSIMILATION APPROACH

Héctor Hito Sepúlveda
Old Dominion University, 2004
Director: Dr. Arnoldo Valle–Levinson

The primary objective of this dissertation is to describe the tidal and subtidal flow patterns over the inner shelf of the Delmarva Peninsula, located in the Mid–Atlantic Bight of the United States (36.6–38.0 N), north of the Chesapeake Bay. The objective is pursued with a combination of direct measurements and numerical assimilative techniques. The dynamic balance of the study area is little known, and the distribution of tidal properties has not been described for this area since very rough descriptions in the 1950's. Hydrographic and current velocity profiles from four regional cruises in the inner shelf were used to study the area. The tidal and subtidal fields were studied using data assimilation techniques on a numerical model. The model described the spatial and temporal dynamics of the area and included vertically averaged shallow water equations. Current velocity measurements were assimilated into the model using the adjoint method. Concurrent predicted sea level data from inside the Chesapeake Bay were also assimilated in order to incorporate the sea level signal in the model. Measured current velocities were not able to represent adequately the tidal signal in the location of sea level stations, except for one cruise. In turn, sea level data were not able to recover shipboard current measurements. A weighted combination of both data sources and a regularization term that penalized vorticity, gave the best results in terms of minimizing the root mean square error of un-assimilated information. The mean circulation obtained over the inner shelf was less than 10 cm s^{-1} and oriented along shelf. The mean flow and elevation reflected semigeostrophic dynamics with along shore pressure gradient balanced by friction and rotation, and cross shore pressure gradient balanced by rotation. The mean flow and elevation had spatial scales of 15-40km in the along shelf direction. The across shelf direction presented smaller scales (3–5 km). In terms of tidal flows, the semidiurnal constituent was dominant, with magnitudes of 30 cm s^{-1}. The diurnal constituent was less than 10 cm s^{-1}. The propagation of the semidiurnal tide could be explained as combination of a Kelvin and a Poincaré wave that transform into a coastal trapped Kelvin wave as it moves into the Chesapeake Bay.

Reproduced with permission of the copyright owner. Further reproduction prohibited without permission.

©Copyright, 2004, by Héctor Hito Sepúlveda, All Rights Reserved

Reproduced with permission of the copyright owner. Further reproduction prohibited without permission.

To my parents, for their love.

To my family, for their unconditional affection.

To my grandma Hortensia, for bringing us together.

Reproduced with permission of the copyright owner. Further reproduction prohibited without permission.

ACKNOWLEDGMENTS

I would like to thank my advisor, Dr. Arnoldo Valle–Levinson, for his patience, guidance, and all the opportunities he provided to explore the fascinating realm of oceanography.

My committee members, Dr. Larry Atkinson, Dr. Chet Grosch, Dr. Tom Royer, and Dr. Keith Thompson, all have shown a deep understanding of their fields; a level of insight and intuition we should aspire to achieve. The dedication and hospitality shown by Dr. Keith Thompson while I was visiting Dalhousie University is greatly appreciated.

My fellow students at Old Dominion University always provided companionship, counsel, support (food included), and fun. Among them I have found brothers, I have found sisters. Let us continue sharing, there are many adventures ahead. The faculty and staff at CCPO were very helpful to learn beyond the books, a very important step in this process. All the friends I met in Norfolk, who helped me to learn beyond the school, a very important step in life.

Reproduced with permission of the copyright owner. Further reproduction prohibited without permission.

LIST OF SYMBOLS

g	Gravity acceleration
u	East-West component of velocity
v	North-South component of velocity
η	Sea Level (m)
ρ	Sea water density
σ_θ	Water Density Anomaly (kg m^{-3})
z	Water Depth (m)
h	Height of Water Column (m)
t	Time (s)
ω	Tidal Constituent Frequency (rad s^{-1})
r	Linear Bottom Drag Coefficient
N	Buoyancy Frequency (s^{-1})
U	East-West component of wind velocity
V	North-South component of wind velocity
J	Total cost function
J_a	ADCP component of cost function
J_p	Sea Level component of cost function
J_v	Vorticity component of cost function
J_t	Tidal component of cost function
A_{M_2}	Amplitude of Semidiurnal Tidal Constituent
P_{M_2}	Phase of Semidiurnal Tidal Constituent
A_{K_1}	Amplitude of Diurnal Tidal Constituent
P_{K_1}	Phase of Diurnal Tidal Constituent
$\epsilon_{A_{M_2}}$	Error of Amplitude of Semidiurnal Tidal Constituent
$\epsilon_{P_{M_2}}$	Error of Phase of Semidiurnal Tidal Constituent
$\epsilon_{A_{K_1}}$	Error of Amplitude of Diurnal Tidal Constituent
$\epsilon_{P_{K_1}}$	Error of Phase of Diurnal Tidal Constituent
r^2	Coefficient of Determination
RMSE	Root Mean Square Error
aRMS	RMSE of non–assimilated ADCP data
sRMS	RMSE of non–assimilated Sea Level data

Reproduced with permission of the copyright owner. Further reproduction prohibited without permission.

TABLE OF CONTENTS

Page

List of Tables ix
List of Figures x

CHAPTERS

1 INTRODUCTION 1
1.1 Background 1
1.2 Geographical area of interest 2
1.2.1 Climate 2
1.2.2 Water Masses and Large Scale Circulation 4
1.2.3 Coastal Circulation 5
1.3 Research questions 6
1.4 Significance of Research 6
2 DATA COLLECTION 8
2.1 Data Quality Control 9
2.2 Ancillary Data 9
2.3 Data Processing 15
2.4 Repeated Transects 24
3 DATA ASSIMILATION APPROACH 26
3.1 Numerical Model - Shallow Water Equation 26
3.2 Variational Adjoint Technique 27
3.2.1 Cost Function 30
3.2.2 Mean Current and Residual Dispersion 31
4 RESULTS 32
4.1 Sensitivity Analysis 32
4.1.1 Bottom drag coefficient 32
4.1.2 Cost function weight 34
4.2 MAY2000 Runs 36
4.3 SEP2000 Runs 36
4.4 NOV2000 Runs 38
4.5 FEB2001 Runs 39
4.6 Optimal Runs 39
4.6.1 Results Repeated Transects 45
4.7 Physical Analysis of Optimal Model Runs 47
4.7.1 Semidiurnal and Diurnal Ellipses 50
4.7.2 Mean Circulation 50
4.7.3 Cotidal Maps 53
4.7.4 Spatial Scales 56
4.7.5 Dynamic Balance 60
5 DISCUSSION 72

Reproduced with permission of the copyright owner. Further reproduction prohibited without permission.

6 SUMMARY AND CONCLUSIONS 75
6.1 Future Work 76

REFERENCES 77

APPENDICES

A SCALING ANALYSIS 83
A.1 Across shelf circulation 84
A.2 Along shelf circulation 84
B ASSIMILATION MODEL DETAILS 86
C NUMERICAL MODEL RUNS 88

VITA 95

Reproduced with permission of the copyright owner. Further reproduction prohibited without permission.

LIST OF TABLES

		Page
1	Characteristics of the Virginia Shelf	6
2	Data collected at each cruise	9
3	Spearman's rank correlation of wind data. C is the rank correlation coefficient, and P is the two-sided significance of its deviation from zero.	11
4	Selected Sea Level Stations (NOAA)	13
5	Data Spatial Autocorrelation Scales	24
6	Sea Level Validation. Data not assimilated in the model.	70
7	Spatial Autocorrelation Scales of Model Output	71
8	Regularization Terms. MAY2000	89
9	Regularization Terms. SEP2000	90
10	Regularization Terms. SEP2000 (Cont.)	91
11	Regularization Terms. NOV2000	91
12	Regularization Terms. FEB2001	92
13	Cost Function - MAY2000 ($r = 0.15$ m s^{-1})	92
14	Cost Function - MAY2000 ($r = 0.15$ m s^{-1}) (Cont.)	93
15	Cost Function - SEP2000	93
16	Cost Function - NOV2000	93
17	Cost Function - FEB2001	94

Reproduced with permission of the copyright owner. Further reproduction prohibited without permission.

LIST OF FIGURES

		Page
1	Study Area. The numbers mark the location of the sea level stations used in this study (Table 4). **CLT** marks the location of the Chesapeake Light Tower.	3
2	Cruise Tracks.	10
3	Wind Time Series. Data from Chesapeake Light Tower (CLT) and onboard measurements. Shaded areas indicate the time when each survey was done. Vertical lines mark significant changes in direction in the cruise track.	12
4	Wavelet Power Spectral Analysis of Wind. Data from Chesapeake Light Tower. Wind components are rotated, so U corresponds to the along shore direction, and V to the across shore direction. Solid bars indicate when ADCP data were collected. The darker shades indicate a lower power and the lighter shades a higher power. The thick contour is the 95% confidence level for the corresponding red–noise spectrum. The length of the time series analyzed was longer than the interval shown and is located inside the cone of influence, so there are no edge effects on the results.	14
5	Predicted sea level. Data from seven NOAA stations in Chesapeake Bay for MAY2000, SEP2000, NOV2000, and FEB2001 cruises. Shaded areas indicate the time when each survey was done. See Fig. 1 for the location of each station. The mean has been removed from each time series.	16
6	Buoyancy frequency N. Results for MAY2000, NOV2000, and FEB2001 cruises. Maximum (+) and average (diamonds) values for each cast are represented. These values are calculated adjacent bins. Triangles represent N calculated using the top and bottom bins of the hydrographic profile.	17
7	Surface Density Anomaly (σ_θ) fields - MAY2000, SEP2000, NOV2000, and FEB2001 Cruises. Dots represent the cruise track. σ_θ is in kg m^{-3}. Isolines are every one unit.	19
8	MAY2000 Sections. The sections are sequentially numbered.	20
9	Density Sections Contours - MAY2000. * represent the position of the casts. σ_θ is in kg m^{-3}. Isolines are every one unit. The location of each section is specified in Fig. 8.	21
10	FEB2001 Sections. The sections are sequentially numbered.	22
11	Density Sections Contours - FEB2001. * represent the position of the casts. σ_θ is in kg m^{-3}. Isolines are every one unit. The location of each section is specified in Fig. 10.	23

Reproduced with permission of the copyright owner. Further reproduction prohibited without permission.

12 Orientation and coverage of the numerical model grid. Dots represent water, dashes represent land. The solid line and the dashed lines on the oceanic edges of the model represent the location and length of the first and second structure functions of each open boundary. 28

13 Sensitivity of Cost Function to the linear drag coefficient r. Data from FEB2001 Cruise, Table 17, runs 63–65,67–82. 33

14 Sensitivity of Cost Function to the ADCP/Sea Level weight ratio. ADCP weight has been set to 1 and the Sea Level weight has been renormalized accordingly. Data from MAY2000 Cruise, Table 13. 35

15 Hindcast skill of Vorticity Term. Standard deviation as a function of the weight of the regularization term. The ADCP RMSE (upper panel) is an average of the u and v components, $.5\times(\sigma_u + \sigma_v)$. The sea level RMSE is the average RMSE of sea level stations 1, 2, 4, and 7. 37

16 Predicted and Assimilated ADCP - MAY2000, SEP2000, and FEB2001. Solid line represents the assimilated data and dotted line the predicted data. Shaded area marks the withheld ADCP data. Each panel shows statistics of the data included in the model (RMSE and r^2) and of the withheld data (NA-RMSE and NA-r^2). Every 3rd data point is plotted. 41

17 Model Sea Level Validation. The sea level predicted by the model (diamonds) is compared with the sea level predicted by NOAA at stations that were not assimilated during the model run. See Table 6 for the results of a least squares analysis. 42

18 Final Cost Function Value. The panel shows the decrease of the total cost function after each iteration for the optimal runs. The results are normalized by the maximum value. 43

19 Optimal Boundary Conditions - MAY2000, SEP2000, FEB2001. The across shelf and along shelf boundaries of the numerical model were partially open. Each boundary was represented by two structure functions that were obtained by the data assimilation procedure. Solid line represent the temporal evolution of the first structure function and the dotted line represent the second structure function. 44

Reproduced with permission of the copyright owner. Further reproduction prohibited without permission.

20 Wavelet Analysis of Boundary Conditions - MAY2000 and SEP2000. The upper panel shows the Wavelet Power Spectrum of the elevation during MAY2000 and the lower panels during SEP2000. Panels a), b), e), and f) represent the right open boundary and panels c), d), g), and h) represent the bottom boundary condition. The open boundary conditions were obtained with the data assimilation process. The darker shades indicate a lower power and the lighter shades a higher power. The V-shaped contour separates the areas where edge effects become important. The thick contour is the 95% confidence level for the corresponding red–noise spectrum. 45
21 Wavelet Analysis of Boundary Conditions - FEB2001. Same as in Fig. 20. 46
22 Repeated Transect - MAY2000. Mean velocity, semidiurnal and diurnal tidal velocities. Transect was measured for 24 hours. Velocities are vertically averaged. Vectors and ellipses are plotted every 2 km. 48
23 Repeated Transects - NOV2000. Mean velocity and semidiurnal tidal velocities. Each transect was measured for 13 hours. Velocities are vertically averaged. Vectors and ellipses are plotted every 2 km. 49
24 Semidiurnal Ellipses - MAY2000, SEP2000, and FEB2001 optimal runs. . 51
25 Diurnal Ellipses - MAY2000, SEP2000, and FEB2001 optimal runs. 52
26 Mean Velocities - MAY2000 (top panel), SEP2000 (middle panel) and FEB2001 (lower panel). 54
27 Residuals - Dispersion of velocities not explained by the mean and tidal flow. Superimposed are the confidence ellipses of each group of residuals, calculated using EOF analysis. Panels show the MAY2000 (top), SEP2000 (middle), and FEB2001 (lower) results. The confidence interval shown is 50%. 55
28 Cotidal Elevation - MAY2000. The panels are (top to bottom) the semidiurnal and diurnal components, RMSE and map of variance explained. Phase is in hours, elevation in cm. Time reference for phase is GMT. 57
29 Cotidal Elevation - SEP2000. Same as in Fig. 28. 58
30 Cotidal Elevation - FEB2001. Same as in Fig. 28. 59
31 Grid for spatial scales analysis. 61
32 Spatial Autocorrelation Scales of Model Results. MAY2000 (solid line), SEP2000 (dotted line), and FEB2001 (dashed line). 62
33 Along Shore Dynamic Terms - MAY2000. The panels are, a) the Coriolis term, b) pressure gradient, and c) frictional term. Solid lines represent positive values; dotted lines negative values. 64
34 Across Shore Dynamic Terms - MAY2000. Same as in Fig. 33. 65
35 Along Shore Dynamic Terms - SEP2000. Same as in Fig. 33. 66
36 Across Shore Dynamic Terms - SEP2000. Same as in Fig. 33. 67

Reproduced with permission of the copyright owner. Further reproduction prohibited without permission.

37 Along Shore Dynamic Terms - FEB2001. Same as in Fig. 33. 68
38 Across Shore Dynamic Terms - FEB2001. Same as in Fig. 33. 69

Reproduced with permission of the copyright owner. Further reproduction prohibited without permission.

CHAPTER 1

INTRODUCTION

This dissertation is oriented to understand the circulation of the inner shelf in front of the Delmarva Peninsula, in the Virginia coast; to characterize and separate the tidal and subtidal components of the currents measured in this area during four cruises. This is with the double purpose of characterizing the inner shelf circulation and learning a working methodology that helps to optimize the extraction of current dynamics information obtained from shipboard surveys. The study area was selected due to the feasibility of conducting short term cruises (1-4 days). Also, this region has been rarely described in the literature, and this study seeks to contribute to understand the dynamic balance and the characteristics of the tidal flow in this area.

The approach used separated tidal and subtidal currents from velocity measurement done with an acoustic Doppler current profiler (ADCP). This type of measurement has been used previously in studying the circulation in coastal areas, e.g. Munchow et al. (1992a). Since the measured current is aliased with respect to the tidal phase, several methods have been proposed to separate the tidal and subtidal signal (Foreman and Freeland, 1991; Griffin and Thompson, 1996; Bogden and O'Donnell, 1998) Of the described methods, the combination of numerical models and data assimilation techniques (Griffin and Thompson, 1996), is the approach of this dissertation since it combines a simple numerical model, a 2D shallow water equation model, and an implementation of the variational adjoint technique to assimilate sea level and acoustic Doppler current profiler data, information that is available in most current shipboard surveys.

1.1 BACKGROUND

The early work of Redfield (1958) described tidal currents in the study area based on calculations of volumetric transport. A recent study by Lentz et al. (2001) showed a void in the distribution of tidal properties between the Delaware and Chesapeake Bays. Other studies done in the area consist of modeling efforts of the interaction between an estuary and the coastal ocean (Valle-Levinson et al., 1996) that emphasize the effect of the ambient flow. The dynamic balance of the Mid Atlantic Bight (MAB) continental shelf was described in a review by Epifanio and Garvine (2001). Compared to the tides and the Gulf Stream influence, the along shore component of wind and the buoyancy–driven flow were considered the most important for larval transport. These two forces are expected to dominate the subtidal variability in the inner shelf of Virginia. The entrance

This dissertation follows the style of *Continental Shelf Research*

Reproduced with permission of the copyright owner. Further reproduction prohibited without permission.

to the Chesapeake Bay has been the object of studies which focused on the importance of the channels in the volume exchange (Valle-Levinson et al., 1998), and wind influence on the subtidal exchange (Wong and Valle-Levinson, 2002). Garvine (1995) established a dynamic classification of buoyant discharge where he characterized, among others, the Delaware Bay buoyant discharge, but not the outflow from the Chesapeake Bay.

Munchow et al. (1992b) has studied the spatial and temporal variability of currents near the entrance of the Delaware Bay. They found one order of magnitude changes in tidal currents in a 30 km area. They observed that tidal current rectification contributed significantly to mean currents on the shelf. The work of Shay et al. (2001) describe the dominance of the M_2 on the barotropic tide (60% of the signal) by analyzing ocean current surface radar (OSCR) and ADCP moorings. The subsequent work of Hallock et al. (2003) assimilated ADCP, OSCR, and sea level data into a linear, barotropic model of Griffin and Thompson (1996) that the adjoint method. Their results show the feasibility of using this approach to predict the M_2 currents and elevation within a few cm s^{-1} and cm, respectively. On a larger scale, Noble et al. (1983) observed strong correlation among along shelf currents in the MAB throughout a 600 km span. In their study, wind-forced motions and free-propagating waves accounted for 75 to 90% of the along shelf energy. The study of the interaction of tides and mean currents has also been addressed in estuarine environments (Ianniello, 1977). Free and forced propagating waves were described by Ou et al. (1981), from current meter measurements. Yankovsky et al. (2000) studied the influence on across-and along shelf circulation in the New Jersey inner shelf due to buoyancy and wind forcing. They found that the velocity field adjusted geostrophically to the density disturbances created by these factors, even when the water depth was 20-30 m and friction was important.

1.2 GEOGRAPHICAL AREA OF INTEREST

The coastline in the study area has a general northeast–southwest orientation, interrupted by the entrance to the Delaware and Chesapeake Bays (Fig. 1). The continental shelf is wide ($\approx$ 100–150 km) and narrows toward the south with a gentle slope (Sherman et al., 1988). The general characteristics of the meteorology and hydrography of this area follow in this section.

1.2.1 Climate

Two major atmospheric pressure systems, the Bermuda High and the Icelandic Low, control the regional wind patterns. Episodically, land air masses and influx from the cold Labrador Sea water change the wind patterns. Frequent storms associated with strong

Reproduced with permission of the copyright owner. Further reproduction prohibited without permission.

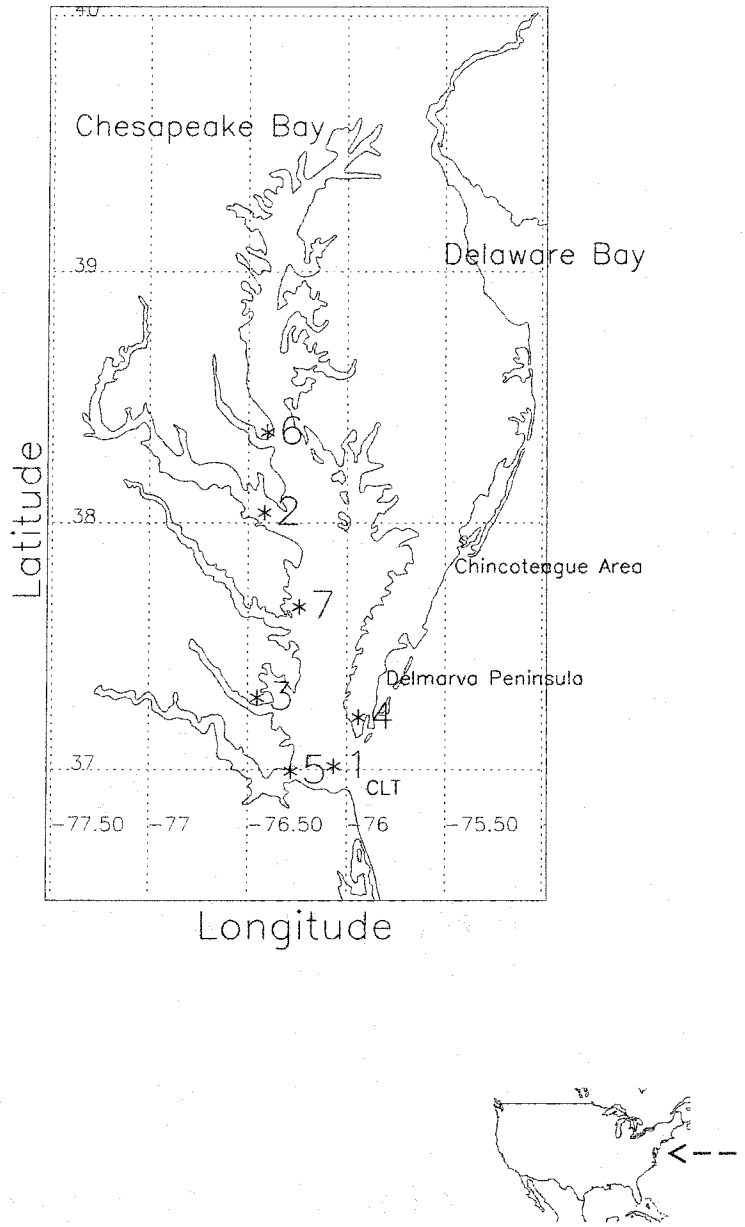

Fig. 1. Study Area. The numbers mark the location of the sea level stations used in this study (Table 4). **CLT** marks the location of the Chesapeake Light Tower.

Reproduced with permission of the copyright owner. Further reproduction prohibited without permission.

northeasterly winds produce high seas due to the long fetch to the northeast. Prevailing winds in summer are southerly. Mean monthly precipitation is 112 mm. Hurricanes are rare; they move faster than northeasters and generate stronger winds, but affect a smaller area. Hurricane season is between June and October. Most hurricanes move north or northeastward, and infrequently make landfall. These strong wind events can have a mixing power greater than that provided by tides (Atkinson and Blanton, 1986).

The meteorological flushing of the Delaware, Narragansett, and Chesapeake estuaries was studied by Goodrich (1988), who points out the role of wind–induced exchanges in 2–20 days time scales and their influence on salinity at the Chesapeake Bay entrance. Recent studies have analyzed the directional effect of local and remote winds and the water exchange between the bay and the adjacent ocean (Valle-Levinson et al., 2001; Wong and Valle-Levinson, 2002). The effect of wind in the circulation of the inner shelf near the Delaware Bay entrance has been studied by Wong (1999), who observed an along shelf orientation in the wind stress (35°T) and a temporal variability of 2–4 days. In the Chesapeake Bay, northeasterly winds dominate from early autumn to early spring while southwesterly winds are dominant in summer (Paraso and Valle-Levinson, 1996). Energetic winds can occur during any season from any direction except southeasterly. In particular, those from the northeast or northwest occur in late fall and winter (Valle-Levinson et al., 1998).

1.2.2 Water Masses and Large Scale Circulation

Three main water masses are present in the Middle Atlantic Bight (MAB): shelf water, whose properties have large seasonal variations, Gulf Stream water and slope water that is a mix of the previous two. Shelf water originates from the coastal region off Canada and moves southward, being continuously modified by river runoff and air–sea interaction. In winter, its temperature can be lower than the slope water due to atmospheric cooling, and its salinity is the lowest out of the three water masses due to river runoff.

The slope water mass is a mixture of the shelf and the Gulf Stream water and has more oceanic than shelf water characteristics. Below 200 m, it is fresher than the waters of the North Atlantic Ocean, while at 900 m it has the same salinity as the North Atlantic Deep Water (NADW). The slope water gyre between the continental shelf and the Gulf Stream exists 85% of the year and is driven by the cyclonic wind stress curl (Csanady and Hamilton, 1988).

The Gulf Stream current is a permanent feature with current velocities up to 2 m s^{-1} in summer. After leaving the continental shelf at Cape Hatteras, the Gulf Stream acquires meandering motions that may create warm core rings that drift into slope water zones.

Reproduced with permission of the copyright owner. Further reproduction prohibited without permission.

1.2.3 Coastal Circulation

Currents over the MAB shelf have a strong southwestward component, especially in the winter season. The currents parallel the coast and range from 5 to 20 cm s^{-1}. Portions of these currents move south along the coastline towards Cape Hatteras and turn seaward, thus forming the cyclonic gyre mentioned previously. The outer area of the slope water gyre merges into the Gulf Stream, where a few warm anticyclonic gyres may develop due to Gulf Stream instabilities.

During summer, when the water column is highly stratified and the wind is southerly, a northward flow may appear in the area. Upwelling events occur most frequently from mid–July to September. During spring, half of the annual runoff occurs (Sherman et al., 1988). Runoff coupled with increased heating yields a strong thermocline between 15–40 m depth in early summer, isolating a near–bottom cool pool of water across the middle and outer portions of the shelf. In fall, storm winds and cooling are largely responsible for the breakdown of thermal stratification in the water column.

Of particular importance to this area is the Delaware buoyancy–driven coastal current (Münchow, 1992), which flows over the inner shelf of Delaware, Maryland and Virginia. The magnitude of this flow has been estimated at 10 to 20 cm s^{-1} (Wong and Münchow, 1995), with a width of 4–6 km (Sanders and Garvine, 1996). A distinctive feature of the coastal current is that it generally contacts the bottom and flows next to the adjacent heavier shelf water rather than above it. Other findings indicate that this may be modulated by changes in tidal mixing (Wong, 1998b).

Semidiurnal (M_2) tides characterize most of the MAB, accounting for over 70% of the current variance. Amplitude of the semidiurnal tide increases shoreward and the S_2 and O_1 constituent have amplitudes of 25–30% of the dominant M_2. The semidiurnal currents at the Chesapeake Bay mouth were studied by Shay et al. (2001) using high-frequency radar measurements, observing tidal amplitudes up to 50 cm s^{-1} for the M_2 constituent, and 8 cm s^{-1} for S_2. Subtidal circulation in time scales of a week or less have been analyzed to show a strong wind influence (Beardsley et al., 1976). South of Cape May, at the entrance to Delaware Bay, wind is the dominant force in producing sub–tidal sea level fluctuations at frequencies higher than 0.3 cycles day^{-1}. At lower frequencies, non-local free waves are dominant (Wong, 1998a). Table 1 resumes the main characteristics of the area.

The general characteristics of the study area are summarized as follows:

- Wind forcing is seasonal. The area is also affected by storms (Salas-Monreal, 2002).
- M_2 is the most important tidal constituent.
- Freshwater is mainly introduced to the Virginia coast by the Chesapeake and Delaware Estuaries.

Reproduced with permission of the copyright owner. Further reproduction prohibited without permission.

Table 1
Characteristics of the Virginia Shelf

Continental Shelf	Broad ($\approx$ 100 km)
Temperature Range°C	2–23
Salinity range	30-35 (shelf); 27 (near shore)
Storm Events	Yes
Stratification	Yes
Frontal Systems Variability	3–7 days
f = Coriolis Parameter (s^{-1})	8.6×10^{-5}
Inertial Period	20 hours
Barotropic Rossby Radius (h=10 m)	115 km

- Geostrophic balance plays a role for the along shelf component of the flow. It can be overridden by the meridional wind stress. The along shore balance is between frictional, Coriolis and pressure gradient terms. A scaling analysis of the dynamic balance in the Virginia shelf is detailed in Appendix A.

1.3 RESEARCH QUESTIONS

The primary objective of this dissertation is to describe the tidal and subtidal flow patterns in the research area, Virginia's inner shelf coast and to investigate the dynamic balances driving those patterns.

This dissertation addresses the following questions:

1. What are the main subtidal circulation features and the dynamics driving them?
2. What is the spatial variability of these features?
3. What are the characteristics of the diurnal and semidiurnal tidal ellipses?
4. What dynamics explain the characteristics of the cotidal charts in this area?

The working hypothesis for the above questions is:
The dynamics in the area is semi-geostrophic, with the across shelf component being in geostrophic balance and the along shelf balance is between the frictional, Coriolis and pressure gradient term. This is drawn from studies in other continental shelf areas.

1.4 SIGNIFICANCE OF RESEARCH

Little is known about the dynamic balance of the inner shelf in front of the Delmarva peninsula. This area is connected with regions of high biological importance such as

Reproduced with permission of the copyright owner. Further reproduction prohibited without permission.

the entrance to the Chesapeake Bay and Delaware Bay. Thus, understanding the shelf circulation would contribute to a better understanding of the processes modifying transport of chemicals and biota.

The use of simultaneous ADCP and hydrographic measurements has become routine in recent years. As mentioned before, the information derived from surveys is tidally biased and the data from transect repetitions are spatially limited. In addition to statistical approaches to detide data, a numerical model that considers the spatial and temporal dynamics of an area, while using the available data to produce a minimum–variance estimation of the parameters of the model, is desirable. It is hoped that the approach described in this dissertation can be used in similar situations to enhance the amount of information extracted from such surveys.

In the following chapters the data collected and the first observations that emerge from the hydrographic information are described. The assimilation method used to analyze this information is detailed in Chapter III. Chapter IV describes the results from the data assimilation and the dynamics inferred from using this method. The final chapters contain a discussion, followed by a summary and conclusions.

Reproduced with permission of the copyright owner. Further reproduction prohibited without permission.

CHAPTER 2

DATA COLLECTION

Underway velocity profiles and surface hydrography (temperature and conductivity) data were combined with hydrographic stations during four cruises onboard either NOAA R/V Ferrel or R/V Cape Hatteras between May 2000 and February 2001. Each cruise is named by the first three letters of the month and the year in which it was done. The MAY2000 and FEB2001 cruises were designed to survey inner shelf portions of the Virginia coastal ocean in different seasons. The SEP2000 and NOV2000 cruises were part of a larger study from which the information relevant to this study area was extracted. In MAY2000, SEP2000 and FEB2001 cruises, the navigation tracks consisted of a series of oblique transects about 10 n.m. each, northward and southward along the Delmarva peninsula. The NOV2000 cruise information concentrated on the inner shelf off the Chesapeake Bay mouth. In addition, some transects were repeated for periods of 24 and 13 h in the MAY2000, and NOV2000 cruises (Fig. 2).

In each cruise, an acoustic current Doppler profiler (ADCP, BB-600 kHz RD Instruments) was mounted on a catamaran (1.2 m long) and towed at an average speed of 2.5 m s^{-1} at the side of the ship, in order to avoid the ship's wake. The instrument was set up with 1 m bin resolution, 1 ping every second, and 1 min averaging. The current velocity data was then binned into 10 minute intervals, a spatial resolution of 1.5 km. In order to obtain surface temperature and salinity data, a thermosalinograph (TSG, SB-16/21 Sea Bird Electronics) was set to sample every 10 s the ship's sea-water system during MAY2000. During the cruises on the R/V Cape Hatteras (SEP2000 and NOV2000), the onboard thermosalinograph data were saved every minute. In the last cruise, FEB2001, a Conductivity-Temperature (CT, SBE–37M SeaBird Electronics) sensor was attached to the bottom frame of the catamaran, sampling every 10 s.

During MAY2000, NOV2000, and FEB2001 cruises, hydrographic casts were taken every 2–2.5 n.m. using a conductivity-temperature-depth instrument (CTD, SB-19 Sea Bird Electronics). In the SEP2000 cruise, an underwater undulating body (Acrobat, Sea-Sciences Inc) with a CTD (Falmouth Scientific) was towed from the ship's stern in order to measure the temperature and salinity of the water column. However, the quality of the data obtained was questionable owing to noise contamination. Because of this, the data will not be used in this study. The only hydrographic information available for the NOV2000 cruise is the surface data obtained from the CT and three CTD profiles.

During portions of the MAY2000 cruise, the hydrographic observations were done from a small boat to avoid interference with the towed ADCP operations. Navigation information was obtained from the ship's DGPS, when available, or from our DGPS (either a

Reproduced with permission of the copyright owner. Further reproduction prohibited without permission.

Trimble or a Garmin unit). The main characteristics of each cruise are detailed in Table 2.

Table 2
Data collected at each cruise

Name	Ship	Duration	Repetitions	Hydrography
MAY2000	R/V Ferrel	08–12 May 2000	Yes	CTD/TSG
SEP2000	R/V Cape Hatteras	17–20 Sep 2000	No	CTD/TSG
NOV2000	R/V Cape Hatteras	13–16 Nov 2000	Yes	CTD/TSG
FEB2001	R/V Ferrel	20–23 Feb 2001	No	CTD/CT

2.1 DATA QUALITY CONTROL

Hydrographic Measurements

Hydrographic casts were processed using the manufacturer's software (SeaBird) for sensor alignment and edition of loops. CT and TSG files were averaged every 10 minutes. Density values were derived using UNESCO's equation of state of seawater (UNESCO, 1981).

ADCP

The ADCP data were screened for bad values. Data points were rejected according to the following criteria: measurements where the error velocity (the difference between redundant vertical velocity measurements) was greater than 10 cm s^{-1} were eliminated, values recorded in the lower 15% of the water column were rejected due to side-lobe effects in the measurements, data with a signal return criteria of less than 85% good were also eliminated, measurements done where the ship velocity was less than 1 m s^{-1} were also discarded due to data being taken at CTD stations. Magnitude and heading corrections were done to the ADCP measurements using DGPS data, according to the calibration method described by Joyce (1989), where a magnitude, β, and heading correction coefficient, α, are obtained for each pre-defined segment. Calibrated velocities from this method were not significantly different from the results obtained using the method described by Trump and Marmorino (1997).

2.2 ANCILLARY DATA

Wind

Wind measurements for this area were compiled from records at the Chesapeake Light Tower (CLT, NOAA C-MAN meteorological station CHLV2) (Fig. 3, left panels).

Reproduced with permission of the copyright owner. Further reproduction prohibited without permission.

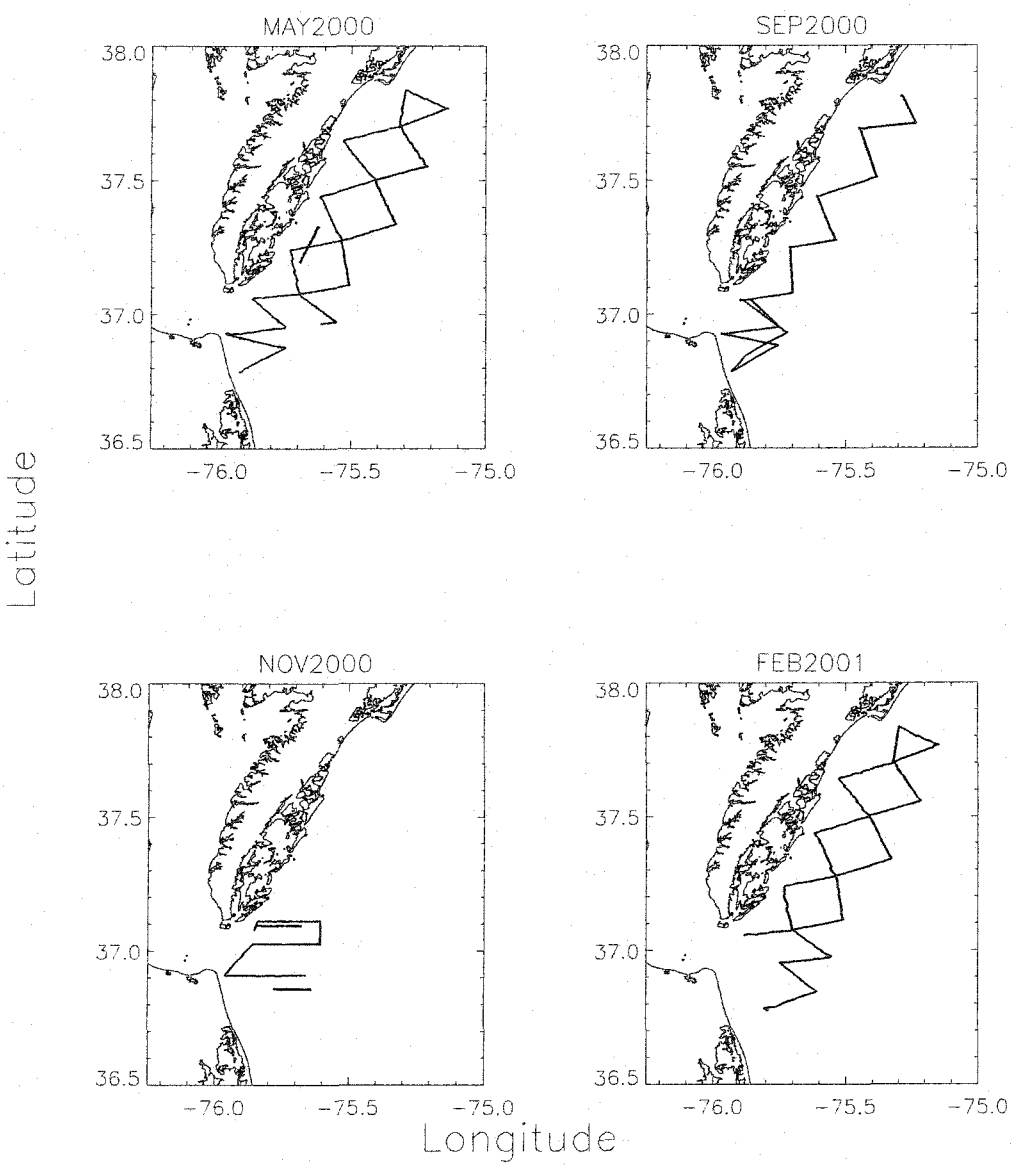

Fig. 2. Cruise Tracks.

Reproduced with permission of the copyright owner. Further reproduction prohibited without permission.

Shipboard wind measurements were collected every minute on the R/V Cape Hatteras (SEP2000 and NOV2000), and every 10 seconds on the NOAA R/V Ferrel (MAY2000 and FEB2001). Onboard data were corrected for ship's motion and averaged every hour in order to compare it to the CLT data (Fig. 3, right panels). The Spearman's Rank Correlation (Kendall and Gibbons, 1990; Press et al., 1992) was calculated between the U (east-west) and V (north-south) wind components (Table 3). In all cases, the rank correlation coefficient (C) between CLT and onboard wind measurements was greater than .70, and all correlations were significant. The significance (P) range is [0,1] and a small value indicates significant correlation.

Table 3
Spearman's rank correlation of wind data. C is the rank correlation coefficient, and P is the two-sided significance of its deviation from zero.

Cruise	U Component		V Component	
	C	P	C	P
MAY2000	0.71	0.00	0.82	0.00
SEP2000	0.95	0.00	0.88	0.00
NOV2000	0.93	0.00	0.97	0.00
FEB2001	0.69	0.00	0.94	0.00

The comparison of the CLT data and onboard wind records in all four cruises indicates that the CLT station can be used as a good approximation for the wind patterns in the entire area. Onboard winds during all cruises showed similar orientation and a slightly lesser magnitude than those of CLT. This is due in part to the difference in height between the Chesapeake Light Tower and the wind sensors in both the R/V Ferrel and the R/V Cape Hatteras. Further analysis of these time series could provide a translation factor for the magnitude and direction of the CLT measurements into the onboard wind records, however the high correlation obtained is encouraging.

MAY2000 measurements at CLT showed upwelling favorable winds (northward, following the oceanographic convention) of about 10 m s^{-1} during all the spatial surveys. During the last 24 hours, when the repeated track was measured, downwelling winds of about 10 m s^{-1} were measured. SEP2000 winds were northward with an average magnitude of 5 m s^{-1}, while in NOV2000 the magnitude was less than 5 m s^{-1}, mostly pointing S-SE. FEB2001 presented winds of about 10 m s^{-1} during the entire cruise. The direction changed 180° from N–NE at the first half of the cruise to SE–S during the second half. The upwelling favorable winds have the effect of depressing the coastal sea level and favoring and development of an upshelf geostrophic current, by driving an offshore surface Ekman transport. This should have been the effect of the wind influence during MAY2000, SEP2000, and the first half of the FEB2001 cruise.

Reproduced with permission of the copyright owner. Further reproduction prohibited without permission.

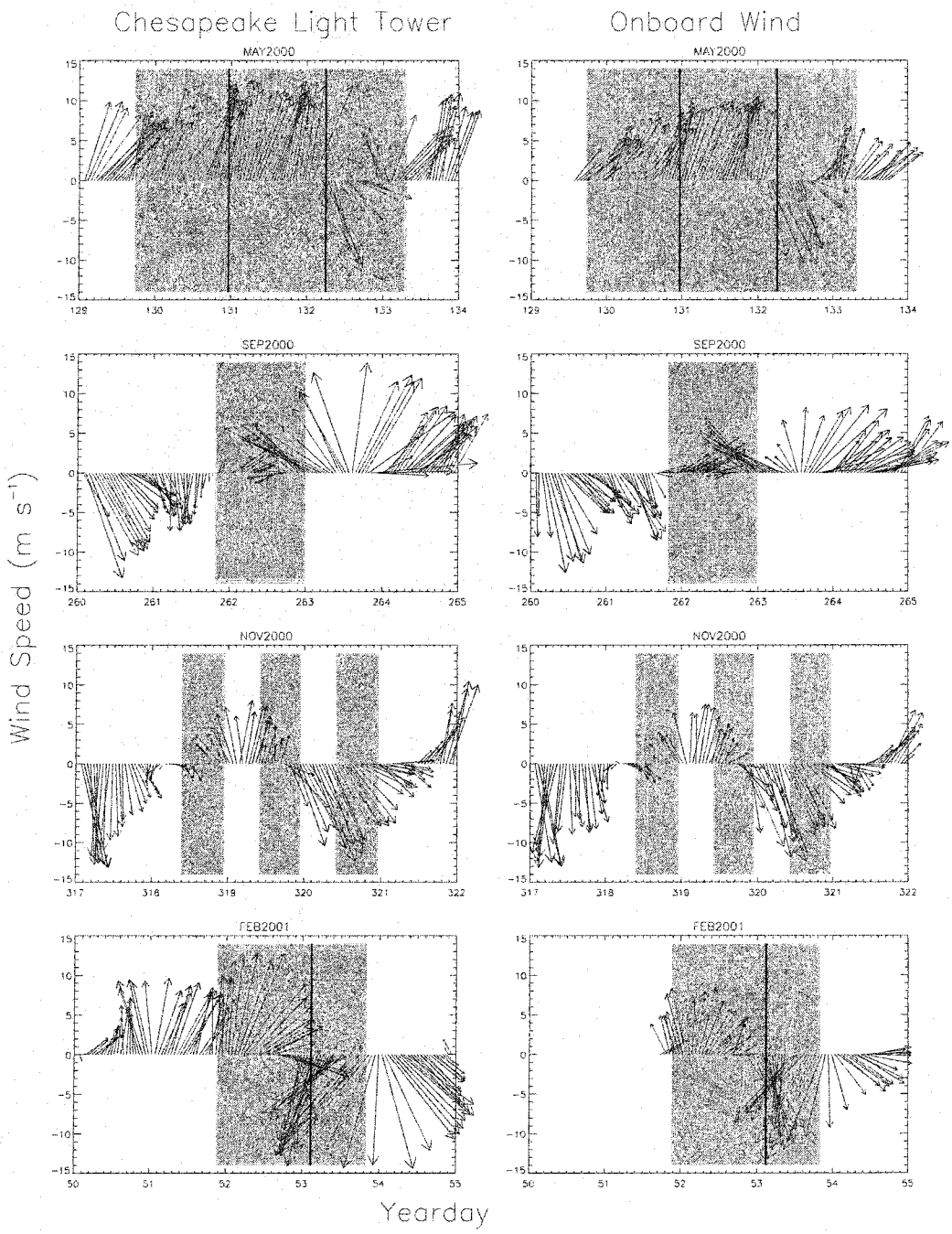

Fig. 3. Wind Time Series. Data from Chesapeake Light Tower (CLT) and onboard measurements. Shaded areas indicate the time when each survey was done. Vertical lines mark significant changes in direction in the cruise track.

Reproduced with permission of the copyright owner. Further reproduction prohibited without permission.

A wavelet analysis of the U (east–west) and V (north–south) components of the wind measured at the Chesapeake Light Tower was done to understand the influence of wind forcing in the mean circulation. Hourly wind data were rotated 50 degrees to orient the U component along shelf and the V component in the across shelf, relative to the orientation of the Delmarva peninsula. The analysis used a Morlet mother wavelet (Torrence and Compo, 1998), and showed the energy of different periodicities in the wind signal, as well as their level of significance Qiu and Er (1995). Before the analysis the mean value of time series was removed, the anomaly was normalized by σ^2, and the time series was padded with zeros for the analysis. The results show the significant periodicities in the along shore and across shore wind direction. Across–shelf wind data for MAY2000 shows statistically significant signals in the diurnal and semidiurnal band during the last day of the cruise (Fig. 4, panel b)). FEB2001 across-shelf wind observations show a peak near the 2–day period, during the last day of the cruise (Fig. 4, panel h)).

Sea Level

Hourly predicted sea level was obtained for seven NOAA stations located inside the Chesapeake Bay (Fig. 5). These sea level predictions have been produced with the harmonic constituents derived from extensive records at each station. The data obtained are in meters above the Mean Lower Low Water (MLLW) calculated over the National Tidal Datum Epoch to ensure a common datum for all sea level station. The sea level data show a semidiurnal signal with weak diurnal inequalities, therefore the diurnal and semidiurnal constituents will be analyzed from the model results. Table 4 shows the list of stations used in this analysis. The predicted sea level was preferred instead of the measured records in order to dynamically propagate only the astronomical tidal signal. Recorded sea level has the influence of wind events and inverse barometric effects, which are not considered in the dynamic model used. The open boundary conditions will then include the effect of these forcing factors that, due to simplicity, are not explicitly included in the dynamic equations.

Table 4
Selected Sea Level Stations (NOAA)

Symbol	Name	Latitude	Longitude
1	Chesapeake Bay-Bridge Tunnel, VA	36° 58.0' N	76° 06.8' W
2	Lewisetta, VA	37° 59.7' N	76° 27.9' W
3	Gloucester Point, VA	37° 14.8' N	76° 30.0' W
4	Kiptopeke, VA	37° 10.0' N	75° 59.3' W
5	Sewells Point, VA	36° 56.8' N	76° 19.8' W
6	Solomons Island, MD	38° 19.0' N	76° 27.1' W
7	Windmill Point, VA	37° 36.9' N	76° 17.4' W

Reproduced with permission of the copyright owner. Further reproduction prohibited without permission.

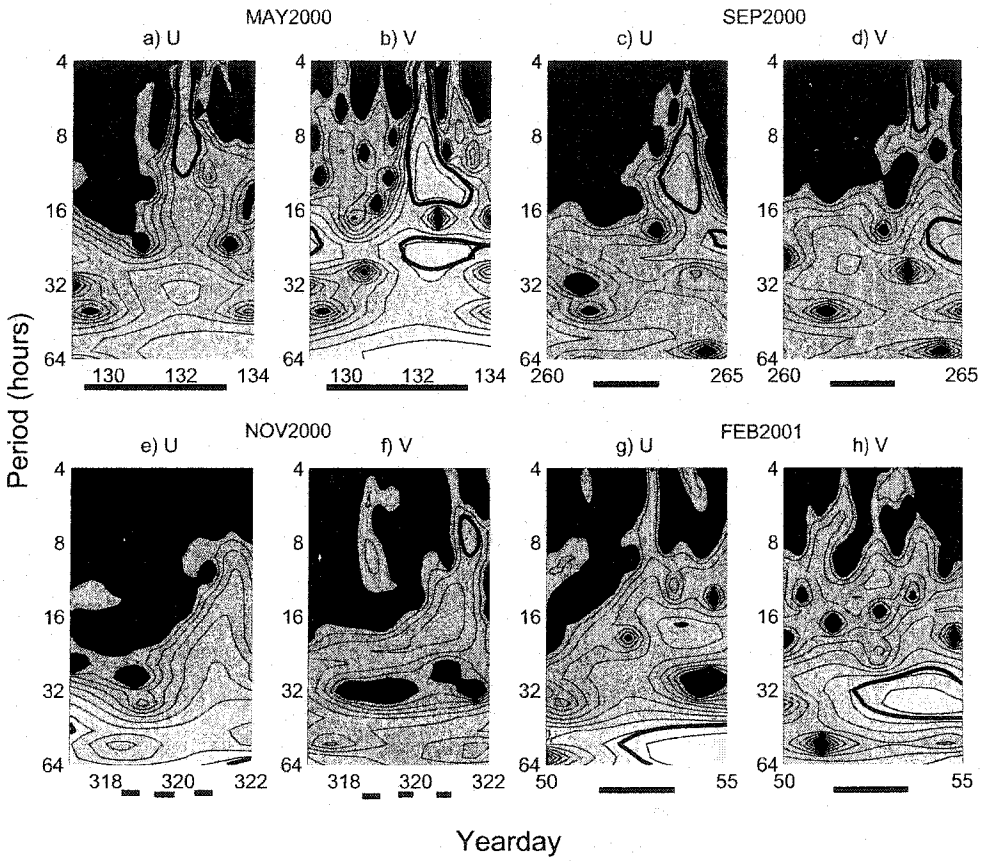

Fig. 4. Wavelet Power Spectral Analysis of Wind. Data from Chesapeake Light Tower. Wind components are rotated, so U corresponds to the along shore direction, and V to the across shore direction. Solid bars indicate when ADCP data were collected. The darker shades indicate a lower power and the lighter shades a higher power. The thick contour is the 95% confidence level for the corresponding red–noise spectrum. The length of the time series analyzed was longer than the interval shown and is located inside the cone of influence, so there are no edge effects on the results.

Reproduced with permission of the copyright owner. Further reproduction prohibited without permission.

2.3 DATA PROCESSING

The following section shows the results of a preliminary analysis of the hydrographic and current velocity data. The analysis highlights some of the hydrographic characteristics of the area that will be compared with the results obtained from the data assimilation and dynamic assumptions of the numerical model such as the two dimensional characteristics of the flow.

Hydrographic Data

Vertical Stratification

Hydrographic stations from all cruises were analyzed to study the strength of the vertical stratification in the area. The buoyancy frequency, defined as

$$N^2 = -\frac{g}{\rho_o}\frac{\partial \rho}{\partial z} \tag{1}$$

(Pedlosky, 1987), with g the gravity acceleration, ρ_o the mean density and $\frac{\partial \rho}{\partial z}$ the vertical gradient in density. As a reference, strong stratification would represent a $\Delta\rho$ of 10 Kg m^{-3} in water 10 m deep ($\Delta z = -10$ m), which implies

$$N^2 = -\frac{g}{\rho_o}\frac{\partial \rho}{\partial z} \approx -\left(\frac{10}{1000}\right)\left(\frac{10}{-10}\right) = 10^{-2}\mathrm{s}^{-2} \tag{2}$$

i.e.

$$N = 10^{-1}\mathrm{s}^{-1}$$

Maximum and mean values of N were calculated at each cast as a measure of the strength of stratification during the surveys (Fig. 6). N values calculated using subtidal σ_θ values at the Chesapeake Bay mouth during several spring and neap conditions (Reyes-Hernandez, 2001) ranged between 0.05 and 0.08 s^{-1}. The last part of the MAY2000 and FEB2001 cruises showed a buoyancy frequency value close to zero. This corresponds to the part of the cruises closer to the coast. These values indicate weak stratification or vertical homogeneity typically present in the study site.

Surface Salinity and Density Gradients

The surface temperature and conductivity data obtained along the cruise track were used to derive maps of surface temperature, salinity and σ_θ (Fig. 7). The TSG data were interpolated into a regular grid using Delaunay triangulations (Fang and Piegl, 1992, 1993). The MAY2000 and FEB2001 cruises showed salinities greater than 31 over the northern

Reproduced with permission of the copyright owner. Further reproduction prohibited without permission.

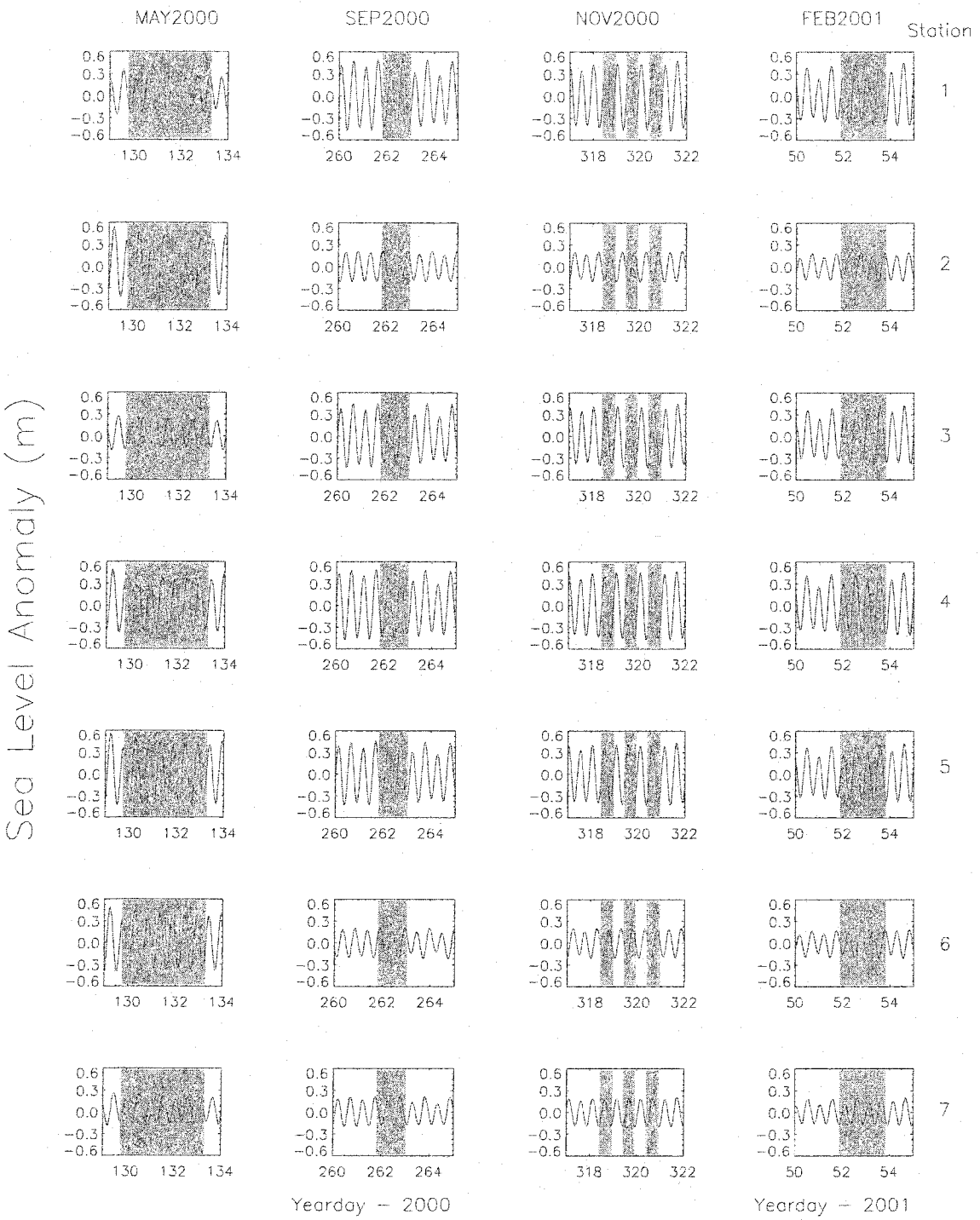

Fig. 5. Predicted sea level. Data from seven NOAA stations in Chesapeake Bay for MAY2000, SEP2000, NOV2000, and FEB2001 cruises. Shaded areas indicate the time when each survey was done. See Fig. 1 for the location of each station. The mean has been removed from each time series.

Reproduced with permission of the copyright owner. Further reproduction prohibited without permission.

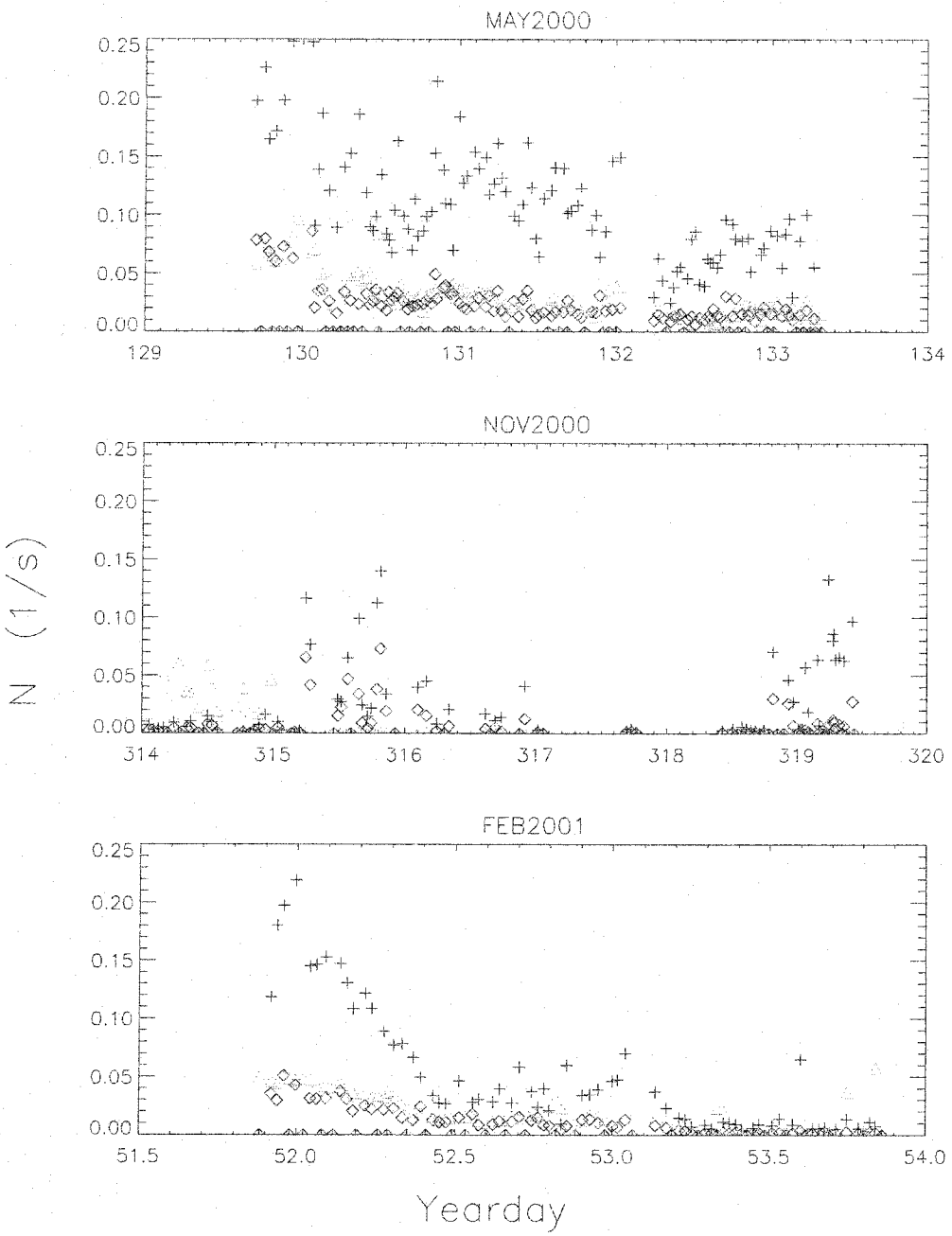

Fig. 6. Buoyancy frequency N. Results for MAY2000, NOV2000, and FEB2001 cruises. Maximum (+) and average (diamonds) values for each cast are represented. These values are calculated adjacent bins. Triangles represent N calculated using the top and bottom bins of the hydrographic profile.

Reproduced with permission of the copyright owner. Further reproduction prohibited without permission.

part of the study area. Wong and Münchow (1995) described the Delaware coastal current as having salinities less than 31. The SEP2000 survey showed salinities greater than 31 only in the outer portion of the north end of the survey. The MAY2000 and SEP2000 data show low salinities north of the Chesapeake Bay entrance because of SW winds. This is less marked in NOV2000 and FEB2001. The vertical density structure for the area was studied using hydrographic cast taken during MAY2000 and FEB2001. Every other transect measured during the northward tracks of MAY2000 (Fig. 8) was analyzed. The temperature and salinity contours for these transects (Fig. 9) show a thermocline located at 5 m depth and an increase in salinity gradient near the Chesapeake Bay entrance (lower panels). The derived $\sigma\theta$ (Fig. 9, right column) shows strong stratification near the Chesapeake Bay entrance. The information form every other transect measured during the northward track of FEB2001 (Fig. 10) only show a significant vertical gradient in salinity and σ_θ for the transect located south of the Chesapeake Bay entrance (Fig. 11, bottom right and bottom center panels). For the rest of the panels the vertical and horizontal variation of the hydrographic properties is less than one unit. This difference is due to the seasonal variations; MAY2000 reflecting spring conditions, and FEB2001, winter conditions.

Hydrographic Time Series

During MAY2000, a transect located near the southern area of the Delmarva peninsula was measured repeatedly for 24 hours. The hydrographic stations measured in this area were used to describe the temporal variation of salinity, temperature, and density (σ_θ). During the time series, the hydrographic structure showed little variation. The change in σ_θ during the time series was 0.8, while maximum change in salinity and temperature were 0.6 and 2.5 °C, respectively.

During NOV2000 two transects were measured repeatedly for 13 hours each. The hydrographic time series obtained also showed little variation (data not shown). The change in σ_θ during the two time series was 0.1, while maximum change in salinity was 0.15 and 0.3 °C in temperature.

ADCP

Spatial Scales

The across shelf and along shelf spatial scales of the ADCP velocities was studied to understand the inherent length scales in the data. First the ADCP velocity was vertically averaged and then temporally averaged every 5 min. The u and v components were rotated into along and across shelf components and then interpolated into a regular matrix with a

Reproduced with permission of the copyright owner. Further reproduction prohibited without permission.

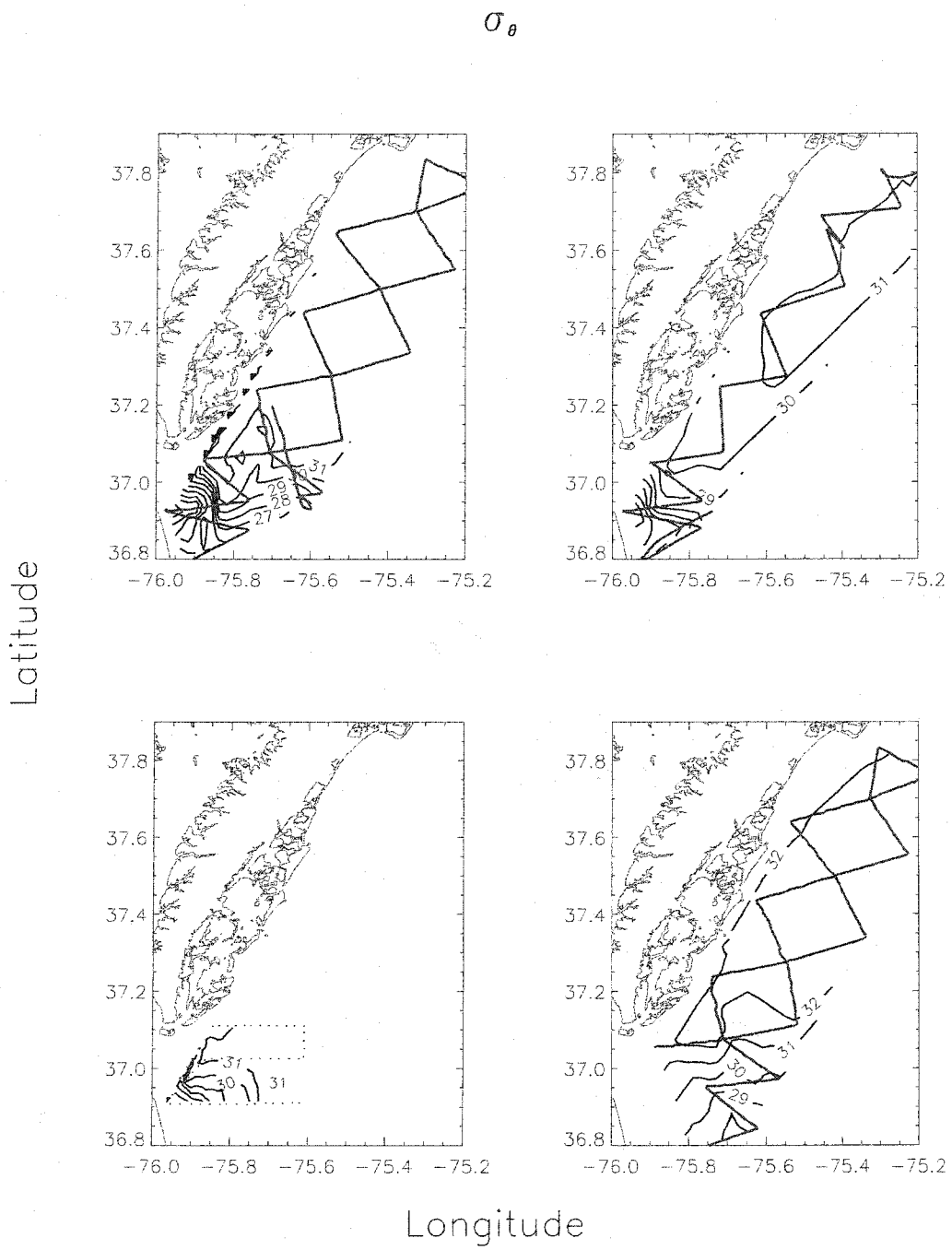

Fig. 7. Surface Density Anomaly (σ_θ) fields - MAY2000, SEP2000, NOV2000, and FEB2001 Cruises. Dots represent the cruise track. σ_θ is in kg m^{-3}. Isolines are every one unit.

Reproduced with permission of the copyright owner. Further reproduction prohibited without permission.

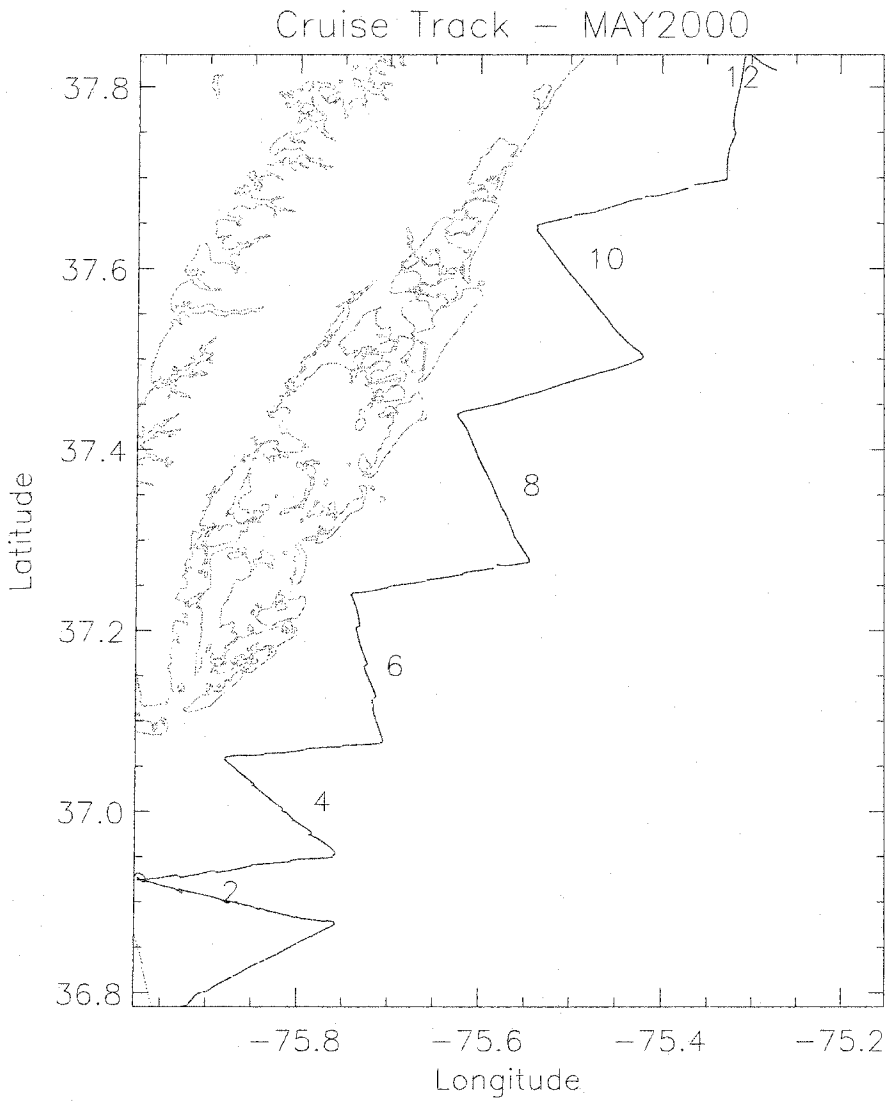

Fig. 8. MAY2000 Sections. The sections are sequentially numbered.

Reproduced with permission of the copyright owner. Further reproduction prohibited without permission.

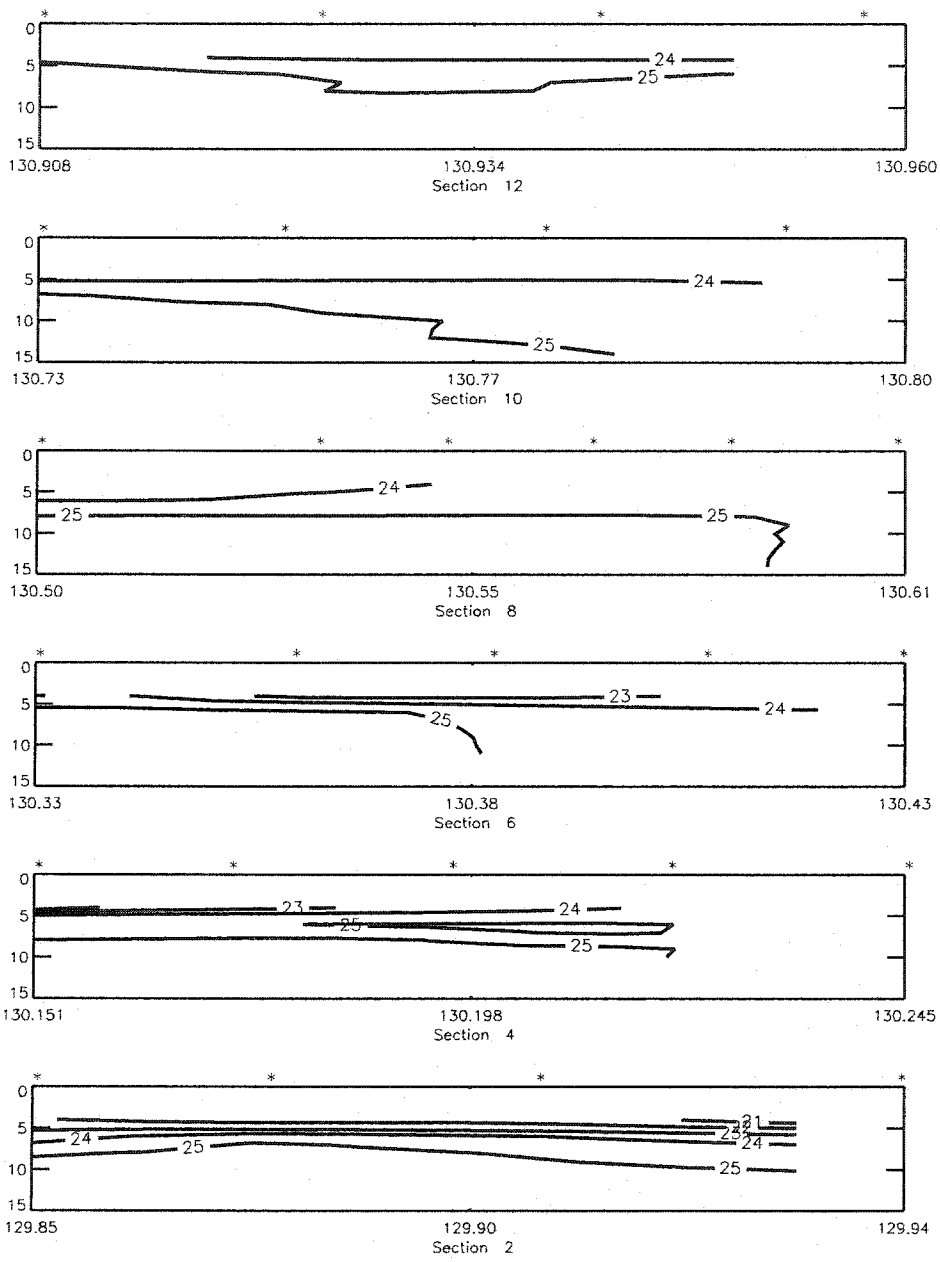

Fig. 9. Density Sections Contours - MAY2000. * represent the position of the casts. σ_θ is in kg m^{-3}. Isolines are every one unit. The location of each section is specified in Fig. 8.

Reproduced with permission of the copyright owner. Further reproduction prohibited without permission.

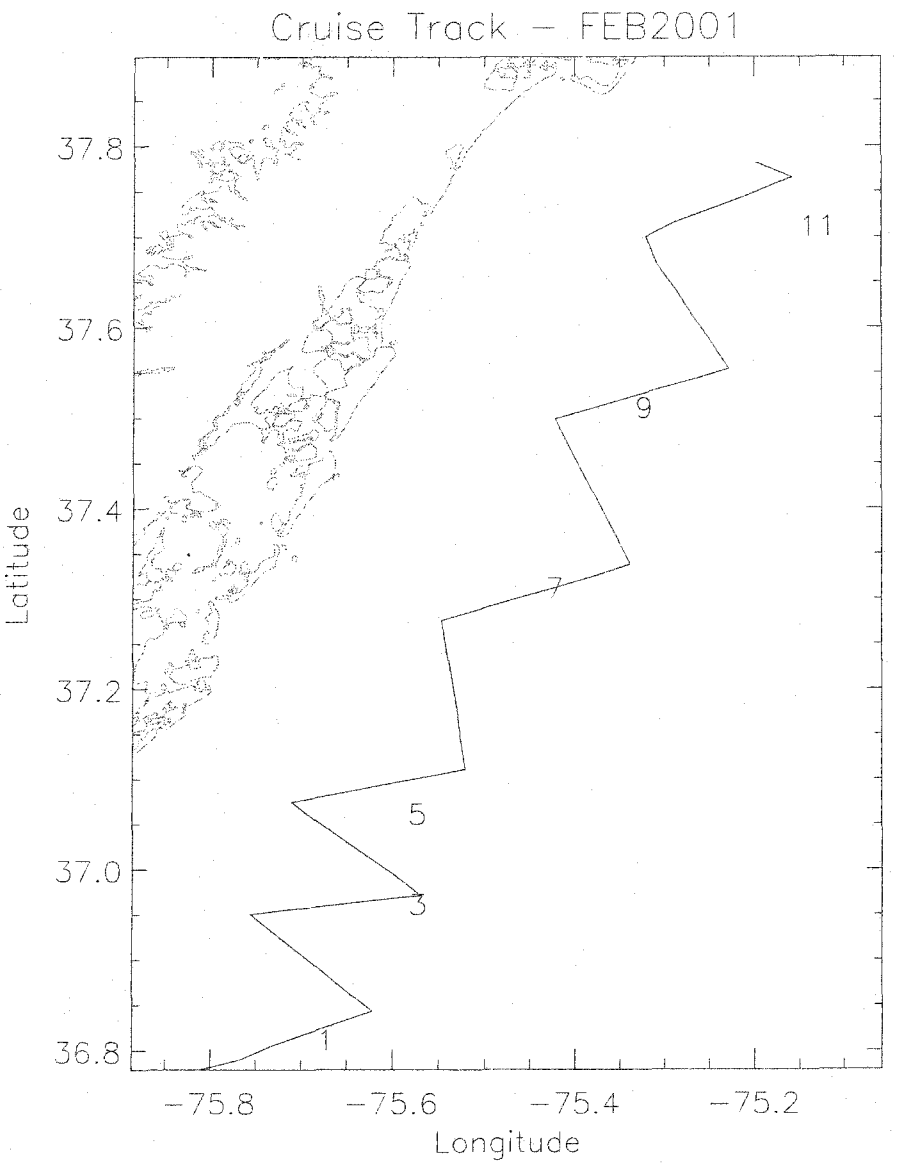

Fig. 10. FEB2001 Sections. The sections are sequentially numbered.

Reproduced with permission of the copyright owner. Further reproduction prohibited without permission.

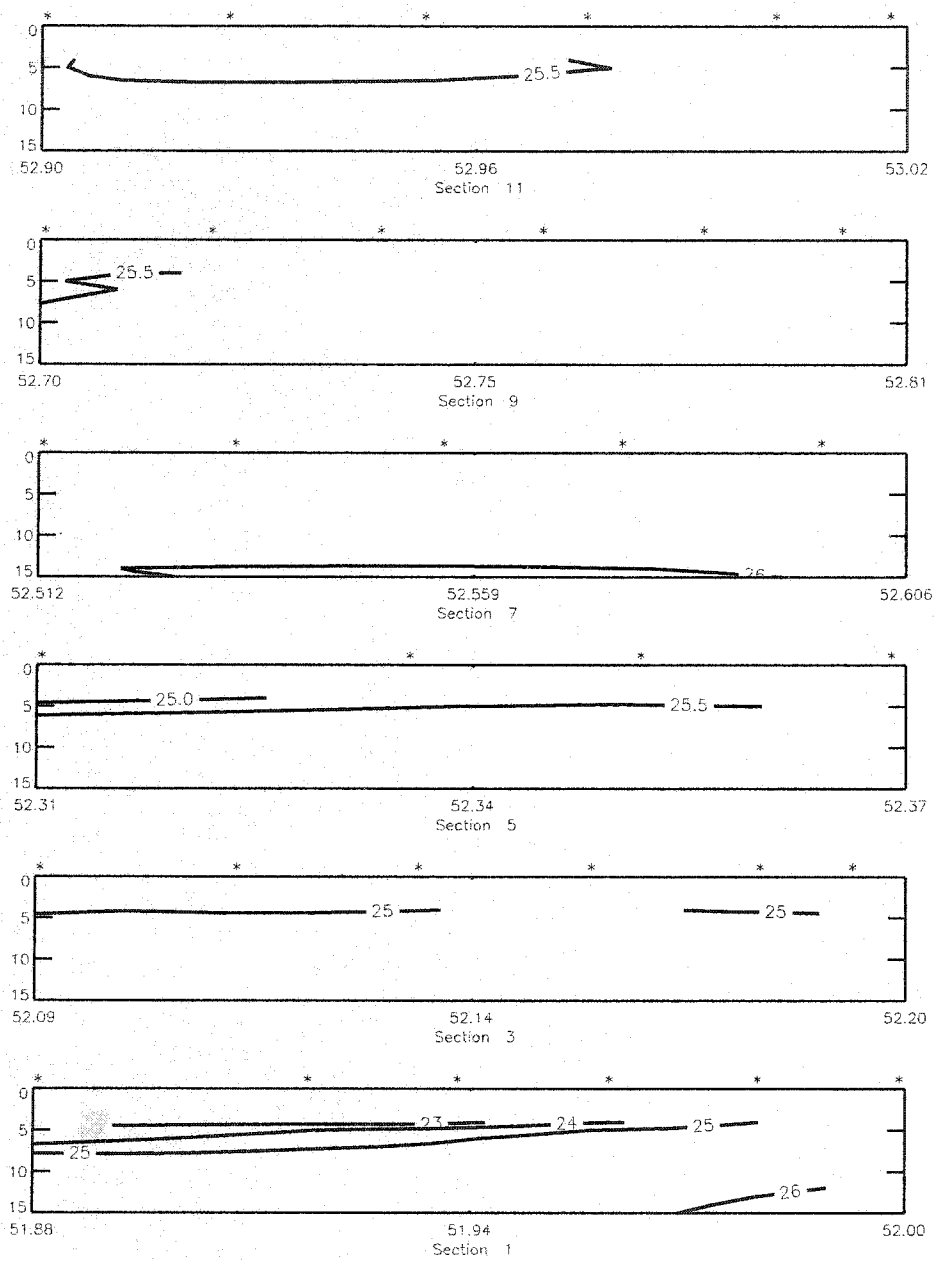

Fig. 11. Density Sections Contours - FEB2001. * represent the position of the casts. σ_θ is in kg m^{-3}. Isolines are every one unit. The location of each section is specified in Fig. 10.

Reproduced with permission of the copyright owner. Further reproduction prohibited without permission.

constant grid spacing of $\approx$ 2 km by using a minimum curvature surface algorithm (Franke, 1982). This approach does not separate the confounded spatial and temporal effects, but is a first approximation to the spatial scales of the area which will be compared with the results from the numerical model. The results were independent of changes in the spatial resolution of the interpolation, however there were dependent on the angle of rotation chosen to define the along and across shore component. These results represent the mean values for a rotation angle between 50–60 degrees. The row and columns of the interpolated matrix, representing the along shore and across shore direction, were then used to calculate the autocorrelation scale. The spatial scale was defined as the area under the autocorrelation curve, between the first lag interval and the first intersection with the zero autocorrelation value. The results show larger spatial scales in the along shelf direction than in the across shelf direction (Table 5).

Table 5
Data Spatial Autocorrelation Scales

Cruise	Across Shelf (km)		Along Shelf (km)	
	u	v	u	v
MAY2000	$\leq$4	$\leq$4	5–10	5–15
SEP2000	$\leq$5	$\leq$4	10	8
FEB2001	$\leq$5	$\leq$4	5–15	4–8

2.4 REPEATED TRANSECTS

In addition to survey transects, two of the cruises included repetitions of a transect. In MAY2000, the last track was repeatedly measured for 24 h. This transect, 14 km long, was located north of the Chesapeake Bay entrance and was oriented parallel to the coastline. In NOV2000 two transects located in front of the Chesapeake Bay entrance were repeated over 13 h. To analyze these repeated transects the approach of Simpson et al. (1990) was followed; a sinusoidal function was fitted to the velocity data, $u_{i,j}(t)$, at every grid point of the transect;

$$u_{i,j}(t) = u_{o(i,j)} + A_{i,j}\sin(\omega t) + B_{i,j}\cos(\omega t) \tag{3}$$

where $u_{o(i,j)}$ is the mean current at the grid point (i, j), t is time, and ω is the tidal frequency to be fitted. For each velocity component, the fit provides one parameter for the mean velocity, and two parameters for each tidal constituent (A, B) from which we can derive the amplitude and phase of that constituent. This method has been widely used when a transect is measured repeatedly with a towed or vessel mounted ADCP. Li

Reproduced with permission of the copyright owner. Further reproduction prohibited without permission.

et al. (2000) used a similar approach to study the elevation measured by the ADCP on each transect. The repeated measurements of the elevation provide information of the mean depth and the amplitude and phase of the tidal elevation signal. The advantage of this approach over moored ADCPs is that gives a more detailed spatial structure along a transect. A disadvantage is that the average time spent measuring the transect is usually short, from 13 hours to the order of days, limiting the tidal constituents that can be separated. These short time series allow only the separation of the tidal constituents in harmonics that are representative of semidiurnal and diurnal components. This method also gives a detailed vertical and along transect structure of the mean current and tidal parameters. However, for the purpose of this study the velocities will be vertically averaged to facilitate comparison with the results from the numerical model.

Reproduced with permission of the copyright owner. Further reproduction prohibited without permission.

CHAPTER 3

DATA ASSIMILATION APPROACH

The advent of ship-board ADCP data has brought about the implementation of several methods to separate the tidal and the subtidal signal in the measured profiles of water velocity. Some of these methods involve the use of a numerical model (Foreman and Freeland, 1991; Foreman and Thomson, 1997). However, setting up a model to hindcast the circulation in an area faces several difficulties, as it requires considerable previous knowledge of the area, to make sure the model appropriately represents the tides. Also, if the model has open boundaries, the definition of such boundaries can become a case to study by itself (e.g. Palma and Matano, 1998). The definition of open boundary conditions is an issue that complicates the use of numerical models, but can be addressed with a data assimilation approach. Data assimilation techniques have been used previously in oceanography to study oceanic tides (Egbert, 1997), estimate parameters for numerical models (Das and Lardner, 1991; Lardner et al., 1993), and to obtain open boundary conditions. For the open boundary condition problem, different methods have been used, such as the representer method (Bennett and McIntosh, 1982; Bogden et al., 1996), variational adjoint technique (Griffin and Thompson, 1996; Thompson and Griffin, 1998; Bogden and O'Donnell, 1998; Zhang et al., 2003), inverse methods (Lynch et al., 1998), and statistical methods (Dowd and Thompson, 1996). These methods search for open boundary conditions which minimize a predefined measure of the model error, the cost function.

This analysis uses a numerical model with a variational adjoint technique, based on the work of Thompson and Griffin (1998) and Griffin and Thompson (1996), assimilating vertically averaged velocities and predicted sea level as the input data. This method is best described as a least-square fit of the dynamic equations to the data. By using this method, the tidal and subtidal information contained in the data propagates into the rest of the domain, allowing the study of the tidal and subtidal distribution in areas were no direct measurements are available. The propagation of the information has a dynamic consistency defined by the model equations.

3.1 NUMERICAL MODEL - SHALLOW WATER EQUATION

In order to obtain a better understanding of the dynamics of the area, a numerical model was adapted for the study area. The 2-D shallow water equations were linearized and simplified to

Reproduced with permission of the copyright owner. Further reproduction prohibited without permission.

$$\frac{\partial u}{\partial t} = -\frac{r}{h}u + fv - g\frac{\partial \eta}{\partial x} \quad (4)$$

$$\frac{\partial v}{\partial t} = -\frac{r}{h}v - fu - g\frac{\partial \eta}{\partial y} \quad (5)$$

$$\frac{\partial \eta}{\partial t} = -\frac{\partial hv}{\partial y} - \frac{\partial hu}{\partial x} \quad (6)$$

where h is the water depth, r is the linear bottom friction coefficient, where f is the Coriolis parameter, u and v are the velocity components and η is elevation. The model was spin up from rest, u, v, η initially zero across the model domain, for three days before the data assimilations started. This was chosen instead of defining arbitrary initial conditions, as it decreases the number of parameters that have to be adjusted (the initial conditions) by the data assimilation process. For a more complete discussion on the difference between selecting initial conditions and spinning up from rest, see Griffin and Thompson (1996).

The bathymetry was constructed from an existing file with a resolution of 15×15 seconds of a degree, compiled from different sources. This bathymetry was interpolated into a 1×1 km grid. Other sources of bathymetry from NOAA with a greater resolution were available, however they covered primarily the interior of the Chesapeake Bay. The linear bottom drag coefficient initially used was $r = 0.15$ m s^{-1}. Previous studies (Spitz and Klinck, 1998; Ullman and Wilson, 1998) have found a fortnightly variability in the bottom drag coefficient, however, given the time scale of our measurements, 1–3 days, is safe to assume a constant value for our model.

The ADCP measurements were taken on the inner continental shelf in front of the Delmarva Peninsula. However, in the numerical model, a large portion of the Chesapeake Bay was included in order to use the sea level records available from NOAA stations and remove the need of another open boundary at the Bay mouth. The orientation of the model grid was rotated 50° counterclockwise, with respect to the East-West direction, in order to orient the u velocity component in the along shelf direction (relative to the Delmarva Peninsula coastline) and v in the across shore direction. The horizontal and vertical grid spacing of the model was chosen as 2 km. The computational matrix had a size of 128×135. A more detailed description of the characteristics of the numerical model is given in Appendix B.

3.2 VARIATIONAL ADJOINT TECHNIQUE

The data assimilation technique used in this investigation is a gradient-descent or variational adjoint technique. This method consist of iterating the calculations of a numerical

Reproduced with permission of the copyright owner. Further reproduction prohibited without permission.

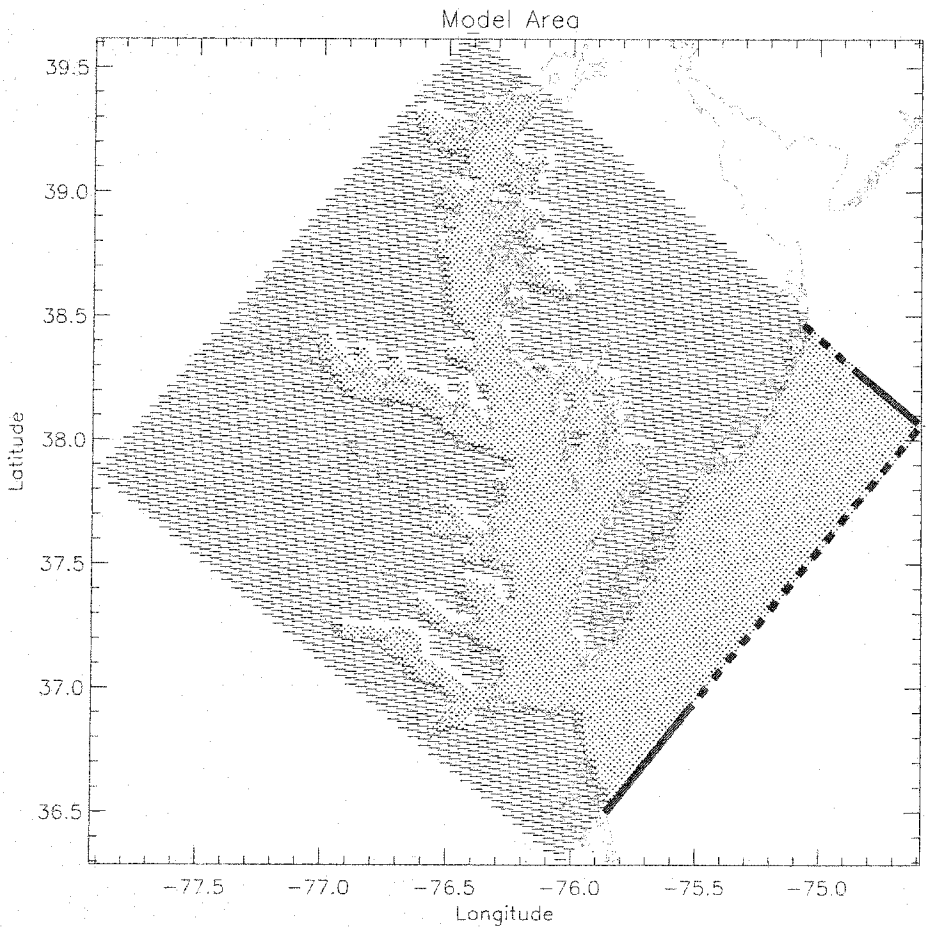

Fig. 12. Orientation and coverage of the numerical model grid. Dots represent water, dashes represent land. The solid line and the dashed lines on the oceanic edges of the model represent the location and length of the first and second structure functions of each open boundary.

Reproduced with permission of the copyright owner. Further reproduction prohibited without permission.

model, also called a forward model, and an adjoint code derived from the numerical model. Both models are iterated until a convergence criterion, based on a cost or error function, J, is met. Between each iteration, a certain parameter of the model is optimized, in this case the open boundaries, in a way that reduces the magnitude of J. The convergence criterion is based on the minimization of a cost function that measures the misfit between the data being assimilated and the output from the model. The convergence of all the components of the cost function is expected. Each component of the cost function has a relative weight that depends on the relative importance of the measurements quantified in that component, or the confidence that we have in the data sources, e.g. measurements with a higher or lower error. The correctness in the construction of the adjoint code is critical for the method. To verify this, the adjoint is calculated by two different methods. The difference between them should be less than machine precision, with the calculations done in double precision.

In this study, the model is considered a strong constraint, as defined by Sasaki (1970). This means the physics of the model are taken as perfect and are not modified. Instead, the open boundary conditions, hereafter OBC, are adjusted to minimize the cost function. The open boundary conditions for this model represents the superposition of an incoming and outgoing gravity wave. The incoming wave is the forcing imposed on the model and the outgoing wave is used to radiate energy from the model domain. The normal flow at the boundary is defined then as

$$u(t) - u_p(t) = \sqrt{\frac{g}{h}}\left(\eta(t) - \eta_p(t)\right) \tag{7}$$

$$u(t) = \sqrt{\frac{g}{h}}\eta(t) + \left(u_p(t) - \sqrt{\frac{g}{h}}\eta_p(t)\right) \tag{8}$$

$$u(t) = \sqrt{\frac{g}{h}}\eta(t) + \chi(t) \tag{9}$$

The first right hand term of this boundary condition allows the radiation of normally incident gravity waves. The second term, $\chi(t)$, represents the boundary condition forcing that is obtained through the data assimilation approach. The gravity wave radiation condition in the OBC prevents basin-scale oscillations. It may reflect other kind of waves but the effect has been described as local (Bogden et al., 1996), keeping the interior circulation robust. The two open boundaries, north and east, were divide in two segments each. Each segment was allowed to vary in time but is kept constant along the segment. The choice in the number of structure functions and their location is arbitrary and is done considering previous knowledge of the area and practical computational issues. In this application, one segment of the east open boundary was placed in front of the entrance to

Reproduced with permission of the copyright owner. Further reproduction prohibited without permission.

the Chesapeake Bay (Fig. 12, bottom solid line) to cover the area of interaction between the estuary and the self area. The second segment covered the rest of the east open boundary parallel to the Delmarva Peninsula. The north open boundary was also divided in two segments to allow for an across shore variation in the forcing.

3.2.1 Cost Function

The cost function, J, is defined by:

$$J = J_p + J_a + J_v + J_t, \tag{10}$$

where J_p is proportional to the square of difference between the numerical sea level predictions, s_p, and the assimilated sea level, s_a,

$$J_p \propto (s_p - s_a)^2 \tag{11}$$

Similarly, J_a penalizes the difference between the current predicted by the model and the ADCP measurements , J_v penalizes the total vorticity of the model, and J_t penalizes non–tidal motions. Cost function terms like J_v and J_t are added to the cost function based on prior knowledge of the system. The use of such terms is equivalent to adding bogus data (Thacker, 1988). The data assimilation procedure will iteratively search for the minimum of the cost function (Eq. 10).

Each of the terms term of this function, penalization of ADCP misfit, penalization of sea level misfit, penalization of vorticity and penalization of non–tidal motions, has a numeric weight that considers the importance of that particular term, e.g.,

$$J_p = \frac{1}{2\sigma_p}(s_p - s_a))^2 \tag{12}$$

These numeric weights, $\sigma_p, \sigma_a, \sigma_v$, and σ_t respectively, will restrict the search of the minimum of the cost function and affect on how fast the minimum can be achieved. The weight ratios, e.g. σ_a/σ_p, can be established depending on factors like the quality of error level of a particular data set, the importance of a particular physical phenomena, e.g. Panteleev et al. (2000) proposed the minimization of advective terms in order to efficiently distinguish narrow jet streams in a velocity field. In this study, the numeric weights were obtained using a sensitivity analysis by comparing the value of the numeric weights of the cost function and the root mean square error of predicted and withheld (non–assimilated) data, as described in the following chapter. The minimization of the cost function will adjust the structure functions of the boundary conditions in order to detide the ADCP data. The tidal elevations (η) enter as background information of the area. The search for

Reproduced with permission of the copyright owner. Further reproduction prohibited without permission.

minimum value of this function was done in this case with the conjugate–gradient method described in Gill et al. (1981).

3.2.2 Mean Current and Residual Dispersion

The numerical model produced an output of u, v, and η matrices every hour. The matrices from the selected final runs were used to calculate tidal and subtidal circulation in the model area. For this, a least squares fit to a sinusoidal function was done at every grid point for u, v, and η. The least squares fit were done when ADCP data were being assimilated into the model, without including the 3 days of spin-up time. The function to be fitted included a semidiurnal and a diurnal constituent

$$u_{i,j}(t) = u_{o(i,j)} + A_{i,j}\sin(\omega_1 t) + B_{i,j}\cos(\omega_1 t) + C_{i,j}\sin(\omega_2 t) + D_{i,j}\cos(\omega_2 t) \qquad (13)$$

where u_o is the mean current at the grid point (i,j), t is time, and $\omega_{1,2}$ are the tidal frequencies to be fitted. The fit provides five parameters for each component (u and v): the mean or subtidal flow and the amplitude and phase of each of the two tidal constituents. The difference between the velocity reconstructed using Eq. 13 and the model output at each time step will be called residual velocity. The u and v residual velocities were analyzed using principal–component analysis (PCA), also known as empirical orthogonal functions (EOF, Lorenz (1956)), in order to construct the confidence ellipses that best represent the dispersion of the data set. Notice this method assumes a bivariate normal distribution of the data. The first eigenvector of each set of residuals was used to find the orientation of the principal axes

$$\theta = \cos^{-1}\left(\frac{x_1}{\sqrt{x_1^2 + y_1^2}}\right) \qquad (14)$$

where x_1 and y_1 are the components of the first eigenvector. The orientation of the second eigenvector is orthogonal to the first one, by construction. The eigenvalues obtained in the analysis are the sample variances of the principal components, and are used to represent the length of each axis of the ellipses, given by

$$L_{1,2} = \sqrt{\chi_2^2(F)\lambda_{1,2}} \qquad (15)$$

where $\chi_2^2(F)$ is the chi–square value for a cumulative probability F and two degrees of freedom , and $\lambda_{1,2}$ are the first and second eigenvalues. The values for $\chi_2^2(0.5)$ and $\chi_2^2(0.9)$ are 1.39 and 4.60, respectively (Wilks, 1995). Maps for these residual velocities were done for each model run. These maps were visually inspected in order to evaluate the quality of the least squares fit.

Reproduced with permission of the copyright owner. Further reproduction prohibited without permission.

CHAPTER 4

RESULTS

This chapter presents and validates the results from the data assimilation study. The first section shows the results of a sensitivity analysis of the data assimilation method. It describes changes in the results produced by the following parameters

- Linear bottom drag coefficient r
- Relative weight between:
  - Assimilated sea level
  - ADCP data
  - Vorticity
  - Tidal regularization term

The characteristics of the model runs that study these options are described in Tables 8–17 (Appendix C). Hereafter model runs will be referred by the number in the first column of each table. This sensitivity analysis was used to select the best combination of parameters. The effect of the change in the parameters will be described for selected model runs of each cruise. The assimilation results obtained with the best set of parameters are used to understand the tidal and subtidal field. The repeated transects measured during MAY2000 and NOV2000 were analyzed again using the method of Simpson et al. (1990), described in the previous chapter, to compare them with the model results. Finally, the dynamic characteristics of the area are studied with the obtained subtidal field.

4.1 SENSITIVITY ANALYSIS

4.1.1 Bottom drag coefficient

To investigate the sensitivity of the model to the bottom drag coefficient, data from cruise FEB2001 were used to repeat model runs, here the only variable changed was r. The relative weight of the cost function terms was kept constant. The reduction of the cost function for each case is represented in Table 17. The minimum in the cost function was found for a r value of .12–.17 m s^{-1} (Fig. 13). A second, less extensive, study was done with the SEP2000 data set. For this case, the minimum value of the cost function was located for r = 0.007–.17 m s^{-1} (Table 15, runs 43–49).

Reproduced with permission of the copyright owner. Further reproduction prohibited without permission.

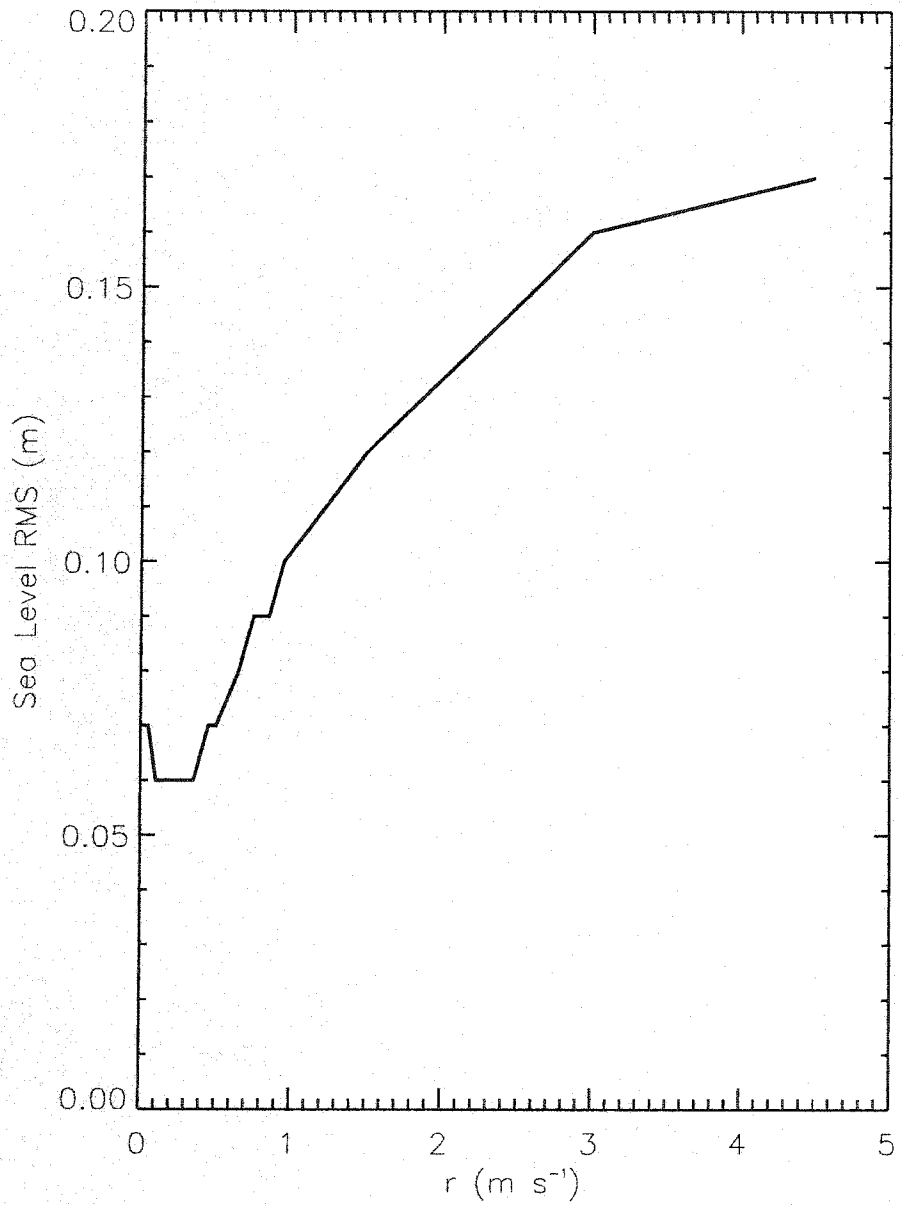

Fig. 13. Sensitivity of Cost Function to the linear drag coefficient r. Data from FEB2001 Cruise, Table 17, runs 63–65,67–82.

Reproduced with permission of the copyright owner. Further reproduction prohibited without permission.

4.1.2 Cost function weight

The relative weight of the ADCP, sea level, and vorticity terms were defined according to the criteria described below. First, the relative weight between the ADCP and sea level was established considering the reduction of the cost function after 10 iterations. Once this relative weight was defined, the weight of the vorticity term was defined considering the standard deviation of the reconstruction of withheld data sets. The weight of the tidal term was studied in a similar way, independently of the vorticity term. The data sets used for validation consisted on sea level stations and portions of the ADCP record.

ADCP and sea level relative weight

Using the information from MAY2000 and up to 4 sea level stations, the weight of the sea level and ADCP was changed to observe the effect on the reduction of the cost function (Table 13). This represents an approximation to define the covariance matrix for these two data sets, as the runs described in Table 13 study the sensitivity of the model to both data sources.

The weights defined for ADCP and sea level are shown in Table 13. For a large combination of weights the cost function only was reduced to a 15% of its value (Fig. 14). When the ratio between the sea level and the ADCP weight was reduced, the cost function was minimized, probably because the noise level of the ADCP data set. Using equal weights for the ADCP and sea level data the cost function was reduced to a 15%. The reduction of the cost function to a 5% of the original value, was obtained by defining a weight ratio of 20 for the ADCP/Sea Level.

Vorticity weight

Using an ADCP/sea level relative weight of 10, the value of the vorticity weight was evaluated for several model runs. The SEP2000 data was used to calculate the standard deviation of model results versus withheld data, i.e. data that was not assimilated in the model (Fig. 15). Data from four sea level stations and selected ADCP measurements were used for this purpose. The length of the withheld ADCP record was 5 hours usually, but it was longer in some cases. The location of the withheld ADCP record was chosen arbitrarily.

The standard deviation of the ADCP record was minimized with a vorticity weight of 250–500, relative to a ADCP weight of 1 and a sea level weight of 0.1. The sea level standard deviation was minimized at a vorticity weight value of 750-1000 and higher. The higher values increase the ADCP error and the lower valued of the vorticity weight decrease the sea level error by decreasing the amplitude of the tidal signal. As a compromise between

Reproduced with permission of the copyright owner. Further reproduction prohibited without permission.

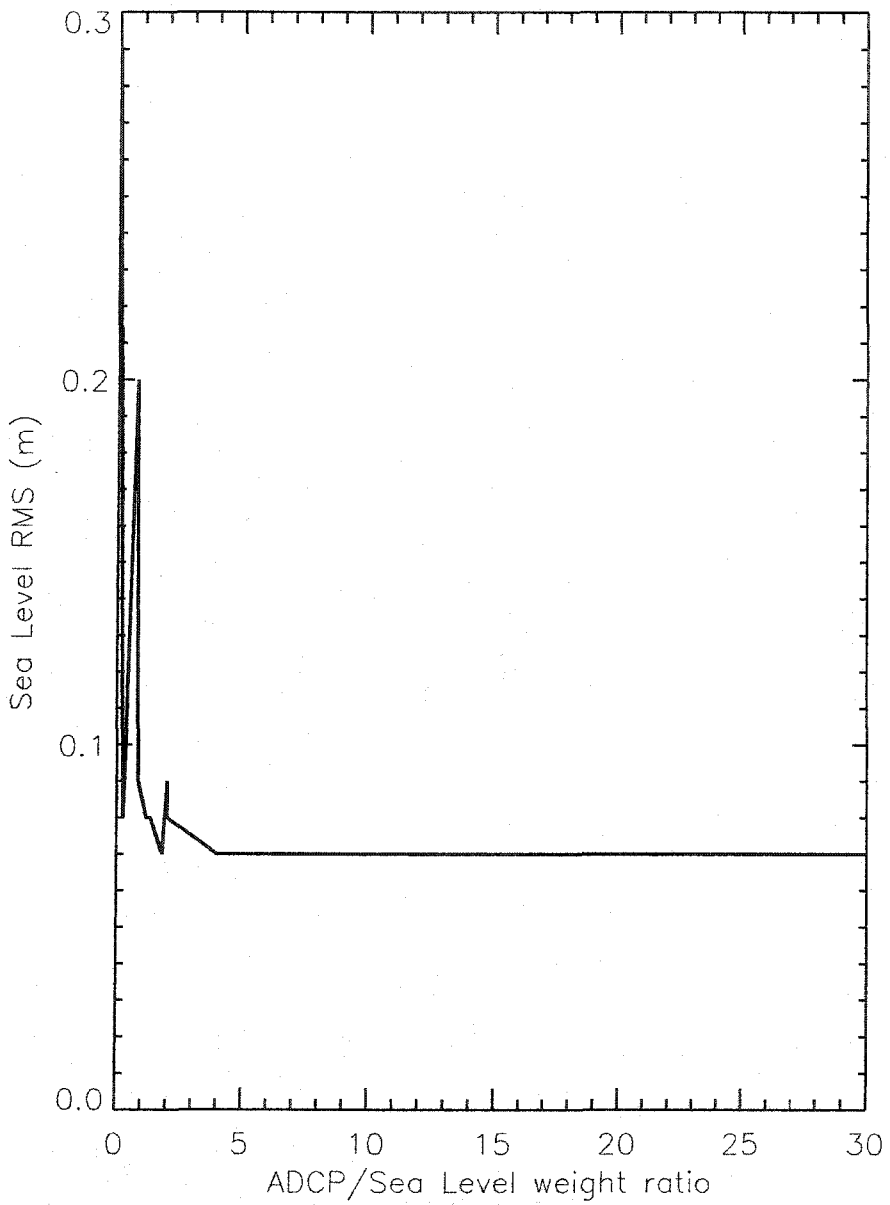

Fig. 14. Sensitivity of Cost Function to the ADCP/Sea Level weight ratio. ADCP weight has been set to 1 and the Sea Level weight has been renormalized accordingly. Data from MAY2000 Cruise, Table 13.

Reproduced with permission of the copyright owner. Further reproduction prohibited without permission.

these two results, a value of 500 or 1000 was used.

Tidal weight

Using an ADCP/sea level/vorticity relative weight of $1/.1/\infty$, the value of the tidal term weight was evaluated for several model runs. The SEP2000 data was used to find the optimal value of the tidal weight by calculating the standard deviation of model results versus withheld data (Table 10, runs t1–t10). It was found that the model performed better for a tidal regularization term of .0001. However, for the SEP2000 data set, the results obtained with this weight were not satisfactory. For the FEB2001 dataset the model run fh5 achieved satisfactory results with a tidal weight of .0001. The analysis of that model run will be described in the FEB2001 section of this chapter.

4.2 MAY2000 RUNS

On MAY2000 cruise, a northward transect covered for 24 hours, the returning southward transect, and a single track, parallel to the Delmarva peninsula, repeated for 24 hours. The model runs that assimilated the whole ADCP record (runs m4 and m6, Table 8) did not result in a coherent mean circulation pattern or showed a high dispersion of residuals. Other model runs studied the effect of assimilation 24 h periods of ADCP data at different locations. The sole assimilation of the ADCP data from the repeated transect was not successful (run m2, Table 8) , as well as the combination of north and southward transects (runs m1 and m5, Table 8). Reasonable results were obtained for the northward moving transect (runs m7 and m9, Table 8), but not so for the southward moving (runs m8, m11 and m12, Table 8). These results require further study since the model should be resilient to a bias in the ADCP record that may depends on the direction of the travel, relative to the preferential direction of current movement, or the direction of propagation of tidal information should be. A model run was done with the measurements done in a 24 hour period at the upper part of the model domain (run m3, Table 8). However the results were not satisfactory in recovering the ADCP record for the rest of the data set. This indicates a limitation on the temporal or spatial ability of the model to hindcast the circulation.

4.3 SEP2000 RUNS

The SEP2000 data set consisted in a single southward moving transect measured for 24 hours. This data set was used to find the best value for the vorticity and tidal regularization terms. The RMSE of the withheld ADCP and sea level data (aRMS and sRMS, in Tables 9, 10) was used as a first indicator of the quality of the assimilation. However, a second analysis was done by looking at the physical consistency of the resulting mean circulation

Reproduced with permission of the copyright owner. Further reproduction prohibited without permission.

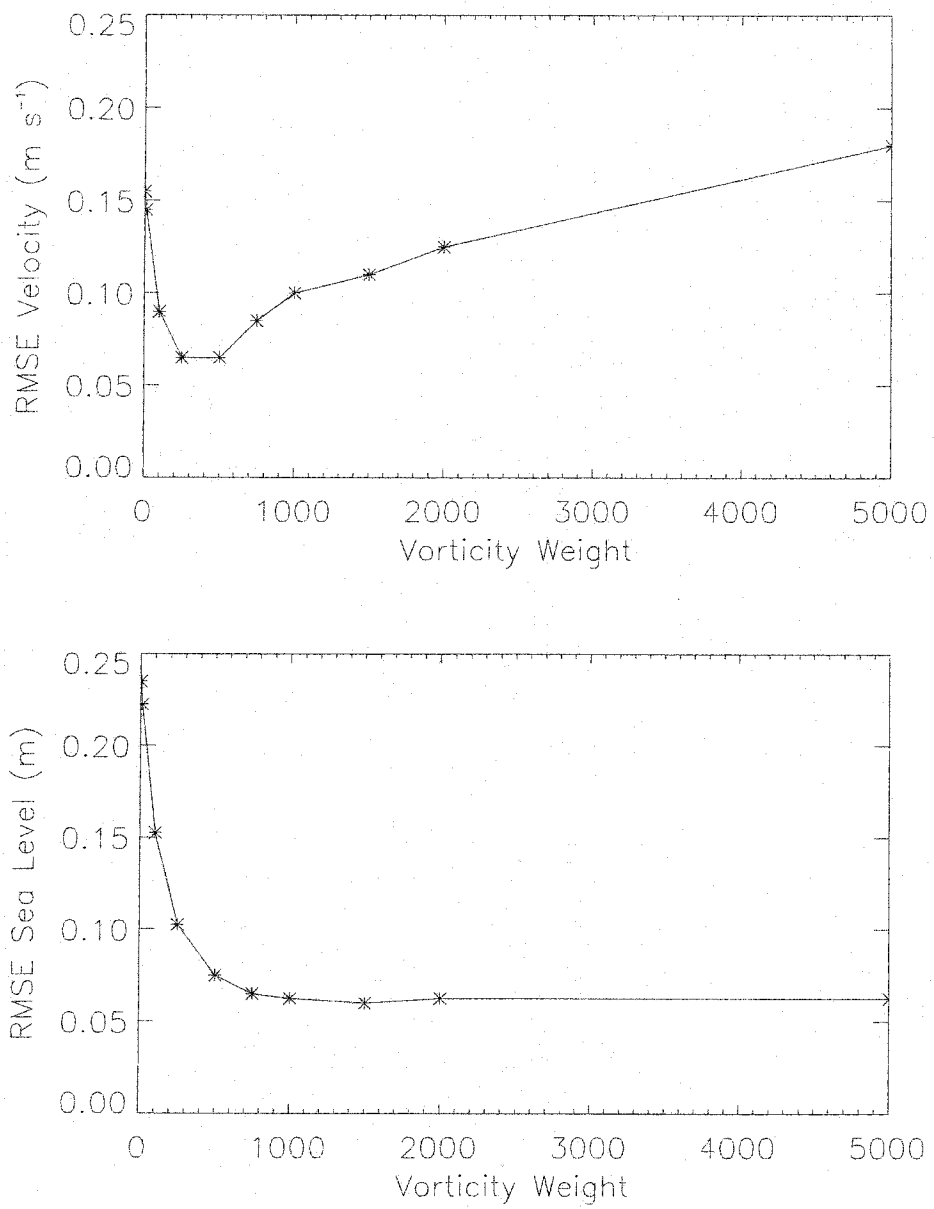

Fig. 15. Hindcast skill of Vorticity Term. Standard deviation as a function of the weight of the regularization term. The ADCP RMSE (upper panel) is an average of the u and v components, $.5\times(\sigma_u + \sigma_v)$. The sea level RMSE is the average RMSE of sea level stations 1, 2, 4, and 7.

Reproduced with permission of the copyright owner. Further reproduction prohibited without permission.

and the dispersion of the residuals. This was used to reject run s4, even it had the lowest aRMS and sRMS. Using these two criteria for runs s1–s12, the value chosen for the vorticity term was 500. The model runs t1–t10 and s001-s004 were used to obtain the optimal value for the tidal regularization term. Although none of the runs gave a low aRMS and sRMS, the best case was obtained with a tidal regularization factor of 0.0001. The high sRMS in most runs was mainly due to the recover of sea level station 2. This may be due to its particular location, given that is in a branch of the Chesapeake Bay (Fig. 1). Model runs s6a–s6e were done to study the effect of changing the location and length of record of the withheld ADCP data. The results indicate a large sensitivity in the location. An ADCP gap of 5 hours was found to be long enough to be used for validation. The aRMS is the mean value of the RMSE for the u and v component. In most cases, the v-RMS was much lower than the u-RMS and less sensitive to the changes in both regularization terms. This indicates the across shelf component is well represented by the dynamics included in the numerical model used and the data set obtained.

4.4 NOV2000 RUNS

The NOV2000 data set was concentrated to the east of the Chesapeake Bay mouth and consisted in three 13-hour measurements, separated by a 13 hour periods. The first and third set of measurements were repeated measurements of a transect, and the second set of measurements was a survey of the area. The results observed from runs n1–n2 (Table 11) indicate that these should be treated as independent records, or sub-cruises. Although the aRMS is high for all runs, in most cases, the trend in the ADCP record was recovered, but out of phase. The best results for the sRMS were obtained with a vorticity value of 1000, since the vorticity term tends to reduce the amplitude of the recovered sea level signal. These results indicate that the mean, vertically averaged flow in the Chesapeake Bay mouth is tidally dominated. The mean flow obtained for the rest of the shelf area is less coherent, particularly at the northern end. These results could be used to propose an area of influence for the Chesapeake Bay, in the context of shelf–estuary interactions. Runs n001-n006 were done to explore the effect of the tidal regularization parameter in this data set. A value of .001 and .0001 was used for runs considering each of the separate transects. None of these runs was able to recover the ADCP record. The recovery of the sea level stations was also poor. The current setup of the numerical model is inadequate to use such localized surveys. A different setup, with the open boundaries located much closer to the survey area, could be more successful to extract the tidal and subtidal information contained in these velocity records.

Reproduced with permission of the copyright owner. Further reproduction prohibited without permission.

4.5 FEB2001 RUNS

During the FEB2001 cruise the shelf area was surveyed by a northward and a southward transect of about 24 hour each. The lowest aRMS and sRMS were obtained when only the northward transect was assimilated; runs fh4, fh5 of Table 12). The difference between these runs is that run fh4 considers the optimal vorticity regularization value obtained in the previous studies (500) and run fh5 uses the optimal tidal regularization value (.0001). The same numerical experiment was done for the southward transect of FEB2001 (runs f001 and f002) but neither runs were successful in recovering the withheld ADCP record. The mean circulation and tidal ellipses derived from runs fh4 and fh5 are considerably different. The tidal ellipses have smaller amplitudes when the regularization term is used, and also the mean circulation is much weaker. The semidiurnal cotidal maps are also different. The case with the vorticity term shows an uniform amplitude in the whole area while the case with the tidal regularization term can be interpreted as a coastal trapped Kelvin wave propagating into the Chesapeake Bay from the north. At the northern end of the model area the semidiurnal cotidal map shows an uniform amplitude of the sea level in the across shore direction. This may be an artifact of the way the boundary conditions were defined, as the right (northern) boundary was divided only into two independent segments, previously called structure functions. This may not be enough to allow for the across shelf decrease of amplitude characteristic of a coastal trapped Kelvin wave.

4.6 OPTIMAL RUNS

Based on the previous observations the following configuration for the optimal model runs was chosen as:

- $r = 0.15$ m s^{-1}.
- ADCP/sea level/vorticity weights of 1/0.1/500-1000. or
- ADCP/sea level/tidal weights of 1/0.1/.0001

These parameters were used for the optimal runs from which the dynamic parameters are derived. The optimal model runs were also selected by visually inspecting the maps of the residual dispersion at the inner shelf for all runs in Tables 8–12, 13, 15, and 17. In these inspections, the model runs with a large dispersion of the residual values were discarded.

The optimal runs were run m9 for MAY2000, s5 for SEP2000, and run f003 for FEB2001. The current model setup was considered inadequate to analyze the inner shelf circulation using the NOV2000 dataset. The three optimal runs were obtained from data

Reproduced with permission of the copyright owner. Further reproduction prohibited without permission.

collected when the ships were traveling in a single direction, either northward or southward along the Delmarva shelf, and cover about one day of measurements only. The lowest RMSE for the withheld ADCP data was obtained in MAY2000 and FEB2001, 4 cm s^{-1}. These values represent the average of the u and v components. In most runs, the v (across shore) component had a lower RSME than u, the along shore component (Fig. 16). In the optimal runs, 3 sea level stations, out of 7 available, were assimilated. The predicted sea level at the remaining stations was successfully recovered in most cases (Fig. 17), however the addition of the vorticity term reduced the amplitude of the tidal signal, noticeably in sea level station 1, at the mouth of the Chesapeake Bay. The amplitude and phase of the semidiurnal (A_{M_2}, P_{M_2}) and diurnal tidal constituents (A_{K_1}, P_{K_1}) were obtained for each withheld station using a least squares fit (Table 6). These parameters were calculated using both the data predicted by NOAA and the model results. In each case the length of the record used was defined by the length of the model run (1–3 days). The error of each parameter, $\epsilon_{A_{M_2}} \cdots \epsilon_{P_{M_2}}$, were obtained as the diagonal elements of the covariance matrix of the least squarest fit (Bevington and Robinson, 1992).

The open boundary conditions were also obtained for the four optimal model runs. The right open boundary condition was located perpendicular, or across shore, to the coastline of the Delmarva Peninsula, the bottom boundary condition was oriented along shore or parallel to the coastline (Fig. 19). The along shore open boundary condition shows a more periodic structure than the across shore boundary. All runs were started three days before the data were assimilated in order to allow the model to spin up from an initial state of rest. In most cases, the boundary conditions only became active after the first day and a half (Fig. 19). Each boundary was composed by two structure functions. The wavelet power spectra was calculated for both structure functions in each boundary. The spin up part of each model (first 3 days) run was not considered in the wavelet analysis. After the spin up period, the boundary conditions had a different time length for each cruise as the model was run to assimilate data during the period when ADCP data was collected.

For the three optimal runs the bottom structure functions show a near semidiurnal periodicity. The bottom boundary runs parallel to the coastline of the Delmarva peninsula and represents the forcing coming from the open ocean. Both MAY2000 and SEP2000 (Fig. 20) show a semidiurnal periodicity in the first boundary structure function but not significant periodicity in the second across shelf (or right) boundary structure. The diurnal periodicity observed in the second right OBC during SEP2000 is questionable due to edge effects in the analysis, and because it does not show a 95% confidence level, compared with a red–noise spectrum. These results may be due to the short length of record of the optimal runs, one day of ADCP data.

Reproduced with permission of the copyright owner. Further reproduction prohibited without permission.

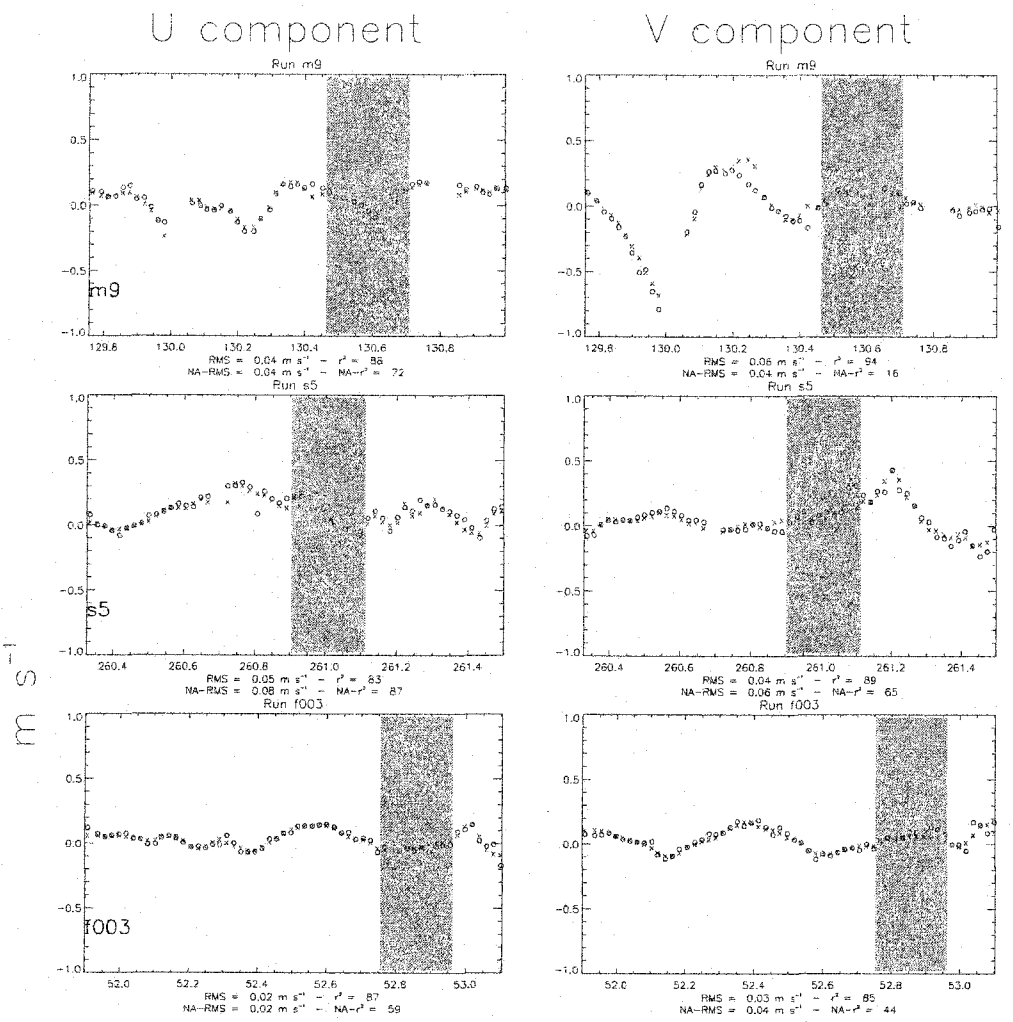

Fig. 16. Predicted and Assimilated ADCP - MAY2000, SEP2000, and FEB2001. Solid line represents the assimilated data and dotted line the predicted data. Shaded area marks the withheld ADCP data. Each panel shows statistics of the data included in the model (RMSE and r^2) and of the withheld data (NA-RMSE and NA-r^2). Every 3rd data point is plotted.

Reproduced with permission of the copyright owner. Further reproduction prohibited without permission.

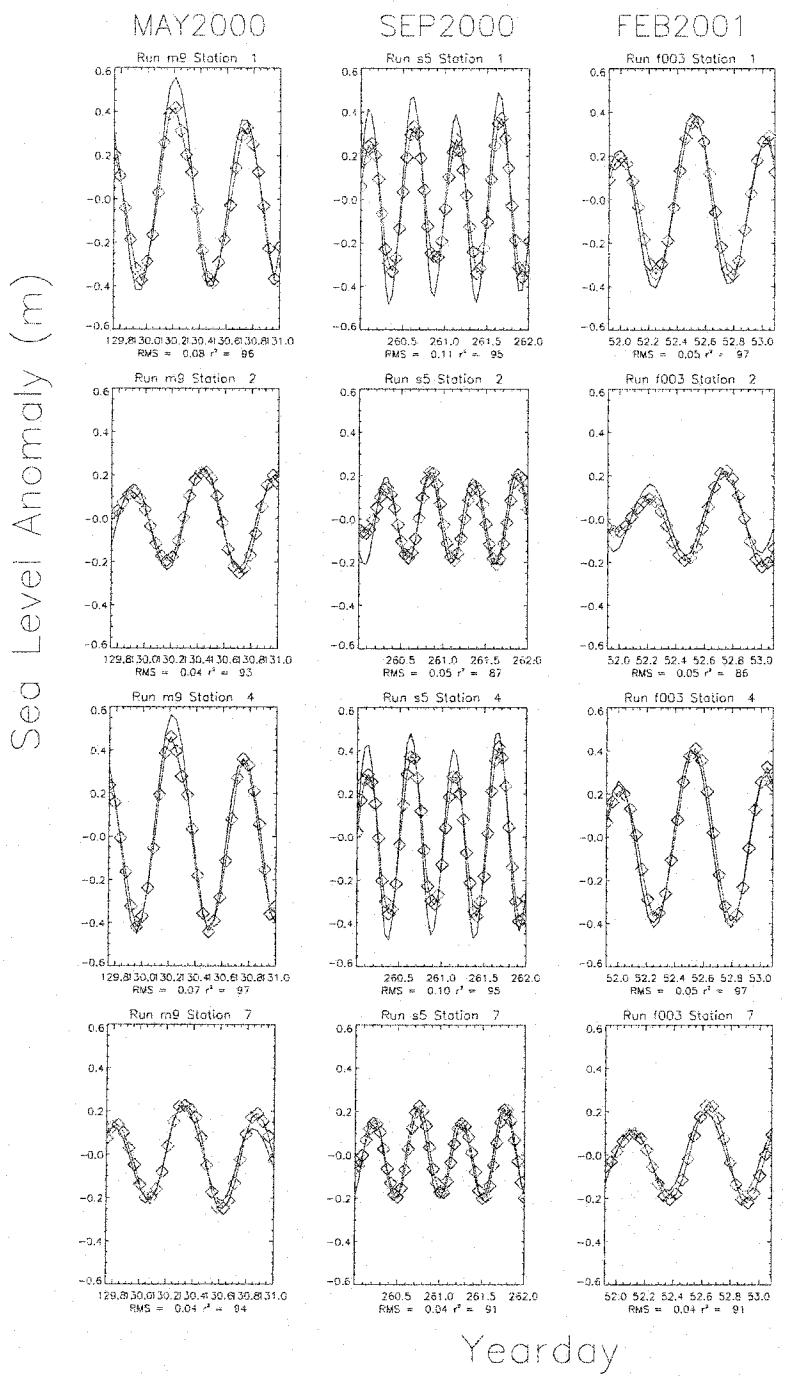

Fig. 17. Model Sea Level Validation. The sea level predicted by the model (diamonds) is compared with the sea level predicted by NOAA at stations that were not assimilated during the model run. See Table 6 for the results of a least squares analysis.

Reproduced with permission of the copyright owner. Further reproduction prohibited without permission.

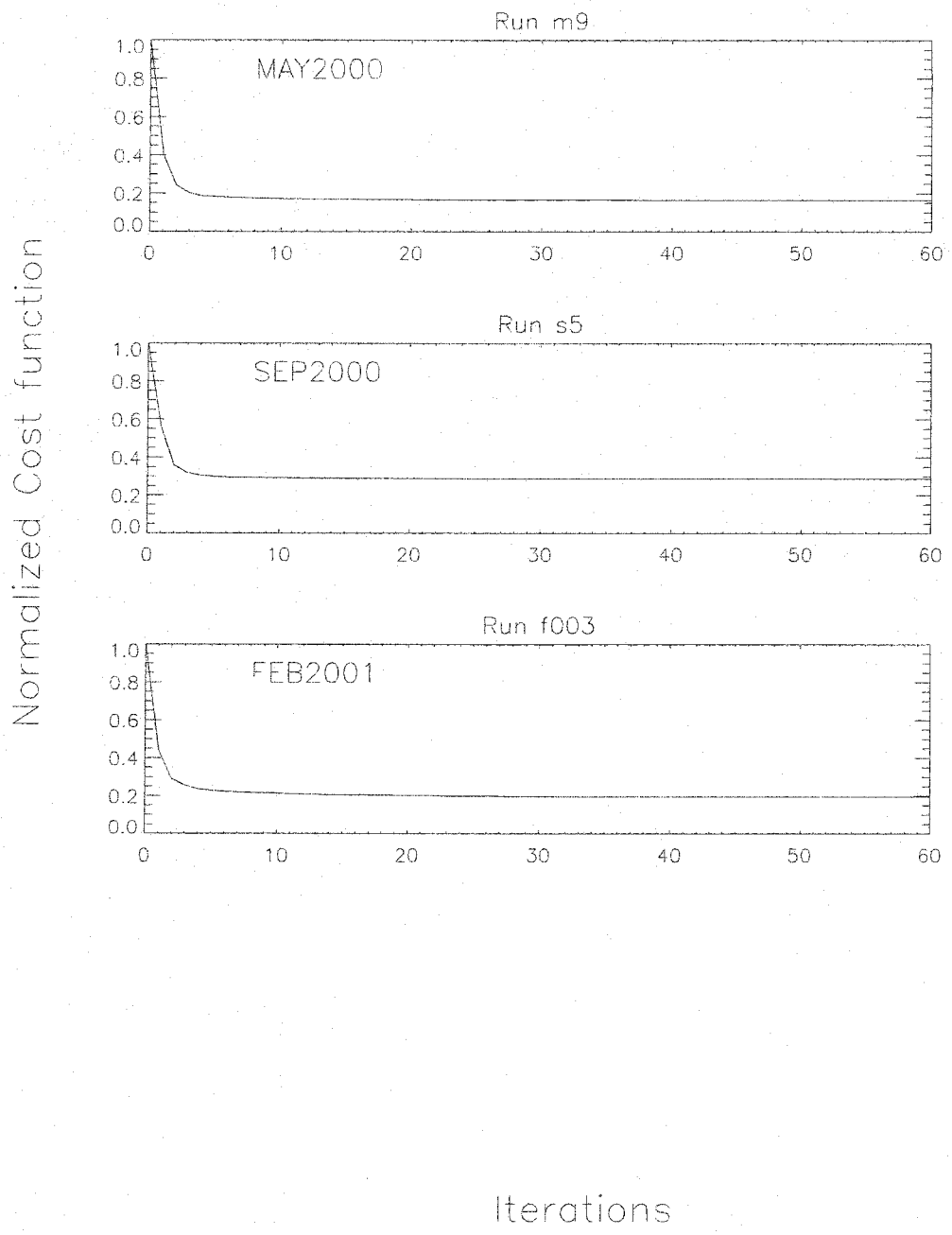

Fig. 18. Final Cost Function Value. The panel shows the decrease of the total cost function after each iteration for the optimal runs. The results are normalized by the maximum value.

Reproduced with permission of the copyright owner. Further reproduction prohibited without permission.

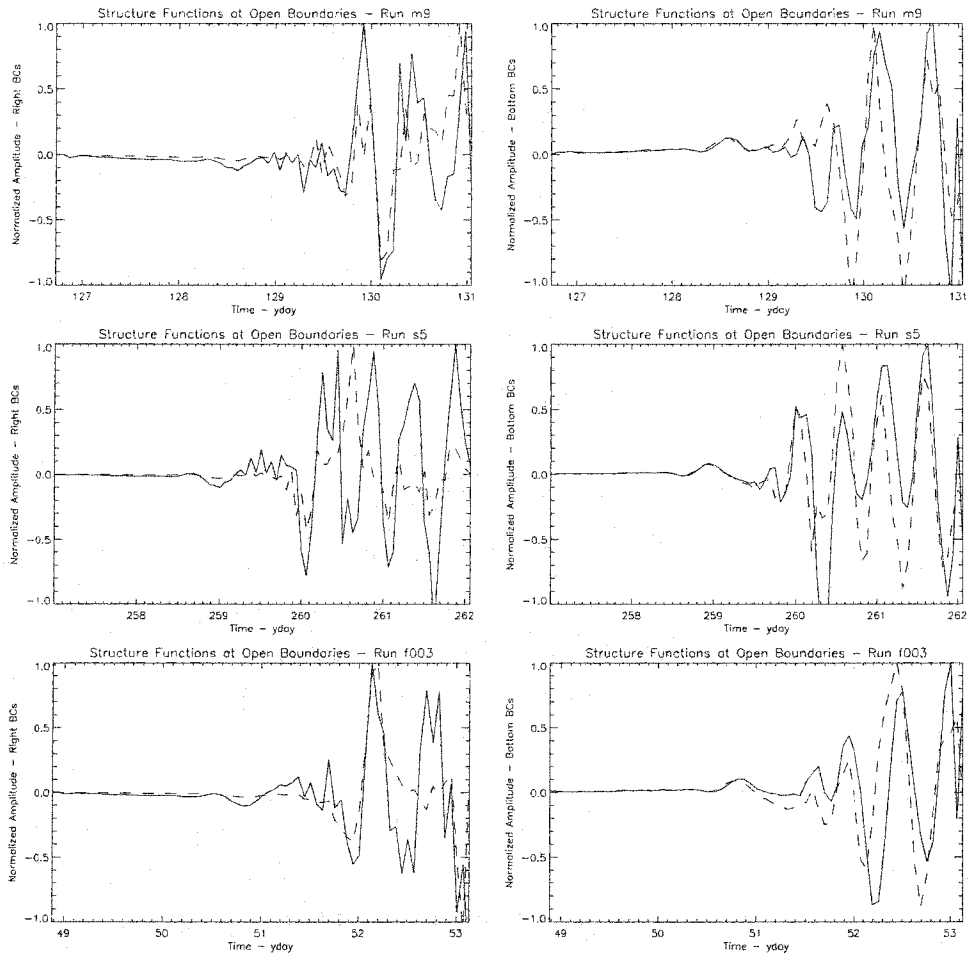

Fig. 19. Optimal Boundary Conditions - MAY2000, SEP2000, FEB2001. The across shelf and along shelf boundaries of the numerical model were partially open. Each boundary was represented by two structure functions that were obtained by the data assimilation procedure. Solid line represent the temporal evolution of the first structure function and the dotted line represent the second structure function.

Reproduced with permission of the copyright owner. Further reproduction prohibited without permission.

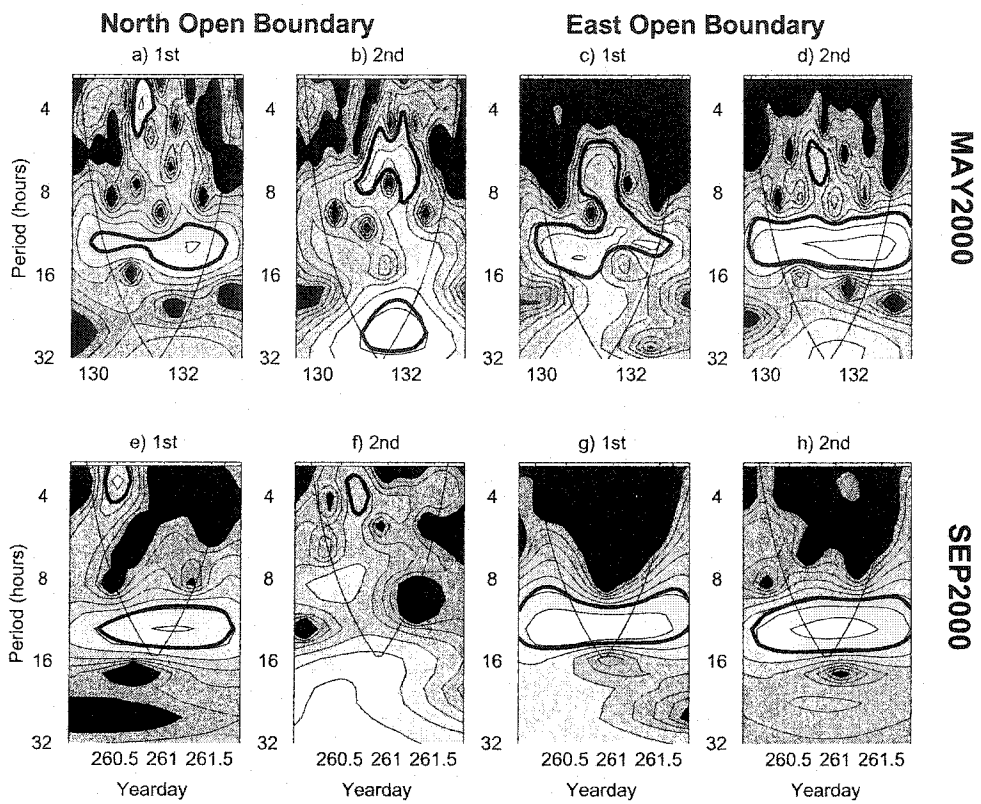

Fig. 20. Wavelet Analysis of Boundary Conditions - MAY2000 and SEP2000. The upper panel shows the Wavelet Power Spectrum of the elevation during MAY2000 and the lower panels during SEP2000. Panels a), b), e), and f) represent the right open boundary and panels c), d), g), and h) represent the bottom boundary condition. The open boundary conditions were obtained with the data assimilation process. The darker shades indicate a lower power and the lighter shades a higher power. The V-shaped contour separates the areas where edge effects become important. The thick contour is the 95% confidence level for the corresponding red–noise spectrum.

The result of data assimilation approach used was to obtain the open boundary conditions that minimize the cost function. This wavelet analysis helps to understand the physical dynamics implicit in the open boundary forcing. In this case, the semidiurnal variability was forced in the model with the bottom boundary in all four cases. The right boundary forcing presented also semidiurnal periodicities but also non periodic events.

4.6.1 Results Repeated Transects

For MAY2000 the transect was measured for 24 h. Therefore M_2 (12.42 h) and K_1 (23.93 h) were used as tidal constituents in the least square fit. The mean vertically averaged velocity along the transect was 15 cm s^{-1}, oriented southward (Fig. 22a). The across shore component of this velocity was up to 7 cm s^{-1}. The magnitude of the semidiurnal

Reproduced with permission of the copyright owner. Further reproduction prohibited without permission.

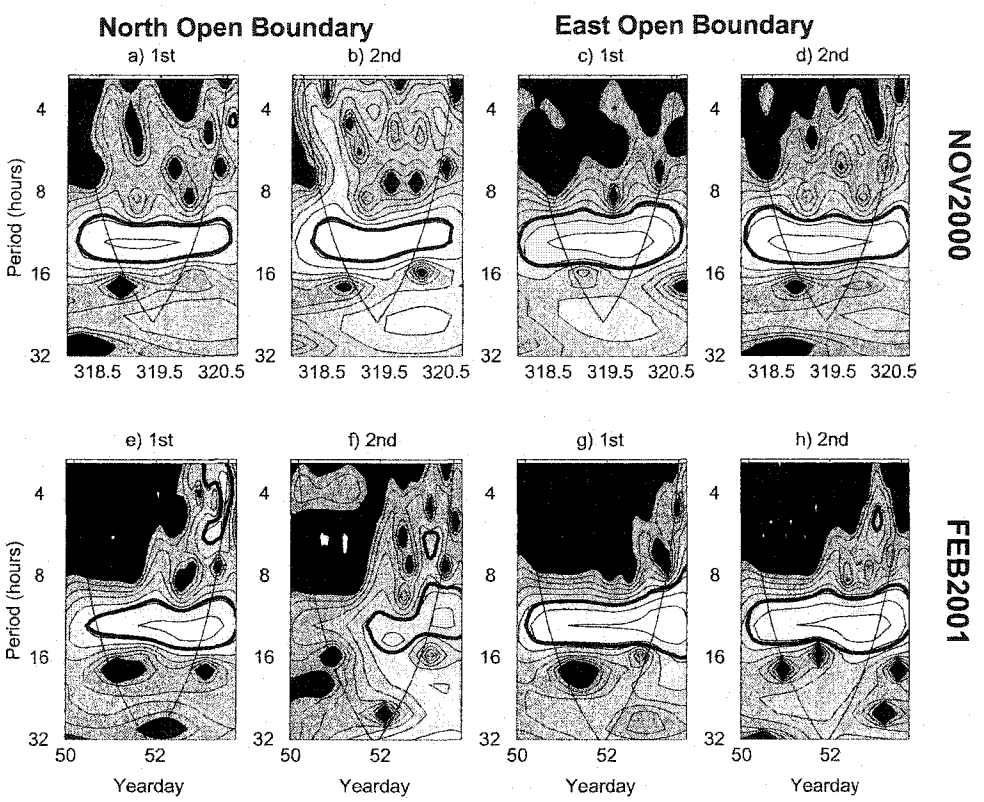

Fig. 21. Wavelet Analysis of Boundary Conditions - FEB2001. Same as in Fig. 20.

Reproduced with permission of the copyright owner. Further reproduction prohibited without permission.

tidal constituent was 15 cm s^{-1}, on average. The orientation and ellipticity of the tidal ellipses changes along transect but are generally parallel to the coastline (Fig. 22b). The diurnal tidal velocity had magnitudes comparable to the semidiurnal tide, 10–15 cm s^{-1}. The orientation of the diurnal ellipses is mostly north–south (Fig. 22c). The variance of the u and v velocities explained by this least squares fit was a 60–80 %. The tidal elevation deduced from these repetitions (Li et al., 2000) shows a semidiurnal elevation amplitude of 40–60 cm and a diurnal elevation amplitude of 10–20 cm.

During NOV2000, two transects oriented east–west were repeated for 13 hours, and the least squares fit only included a semidiurnal constituent. The first transect, located north of the Chesapeake Bay entrance, presented a weak mean circulation (Fig. 23a), with magnitudes less than 5 cm s^{-1}, oriented southward. The semidiurnal velocity amplitude decreased from about 35 cm s^{-1} near shore end of the transect, to 10 cm s^{-1} in the offshore end. The orientation of the semidiurnal ellipses presented little along–transect variation (Fig. 23b), although the ellipticity increases in the near shore end of the transect. The variance of the velocity explained by the least squares fit to the mean and semidiurnal terms was 90% for u (E–W component), but less than 60% for v (N–S). The semidiurnal tidal elevation throughout this 14 km long transect had a mean value of 80 cm. The least squares fit of the elevation had an average RMS error of 15 cm.

The second transect repeated during NOV2000 was also oriented East–West and located south of the Chesapeake Bay entrance. The mean velocity had an average magnitude of 10 cm s^{-1}, oriented to the S–W (Fig. 23c). The semidiurnal tidal velocity had amplitudes of 10 cm s^{-1}. Again, the orientation of the semidiurnal ellipses presented little along–transect variation (Fig. 23d). The major axes were in the SE-SW direction. For this transect, the variance of the velocity explained by a mean and a semidiurnal term was less than 40%, on average. This may be attributed to the short length of the time series, one semidiurnal cycle. The semidiurnal tidal elevation throughout the 11 km long transect had a mean value of 70 cm. The least squares fit of the elevation had an average RMS error of 15 cm.

4.7 PHYSICAL ANALYSIS OF OPTIMAL MODEL RUNS

The following section describes the tidal and subtidal field obtained with the optimized model runs, as well as the dynamic balance obtained for each data assimilation. First the semidiurnal and diurnal current fields will be described for each cruise. The mean flow will be then described, as well as the residual circulation, i.e. the remaining flow that is not explained by a combination of a tidal and a constant subtidal flow. The semidiurnal and diurnal cotidal fields will be presented, and finally, the dynamic balance of each cruise will be derived using the mean u, v, and η fields, as well as the spatial scale of these fields.

Reproduced with permission of the copyright owner. Further reproduction prohibited without permission.

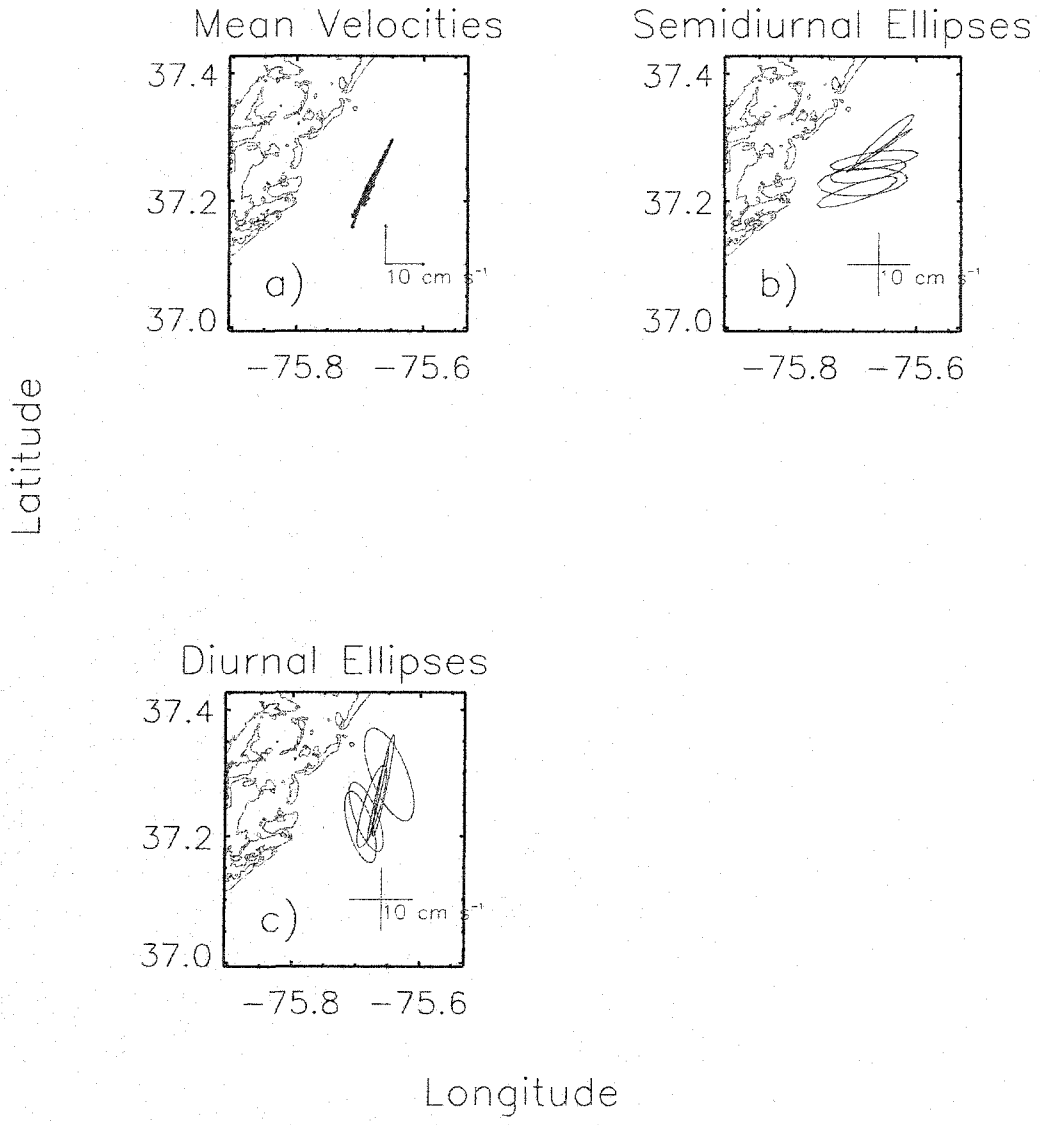

Fig. 22. Repeated Transect - MAY2000. Mean velocity, semidiurnal and diurnal tidal velocities. Transect was measured for 24 hours. Velocities are vertically averaged. Vectors and ellipses are plotted every 2 km.

Reproduced with permission of the copyright owner. Further reproduction prohibited without permission.

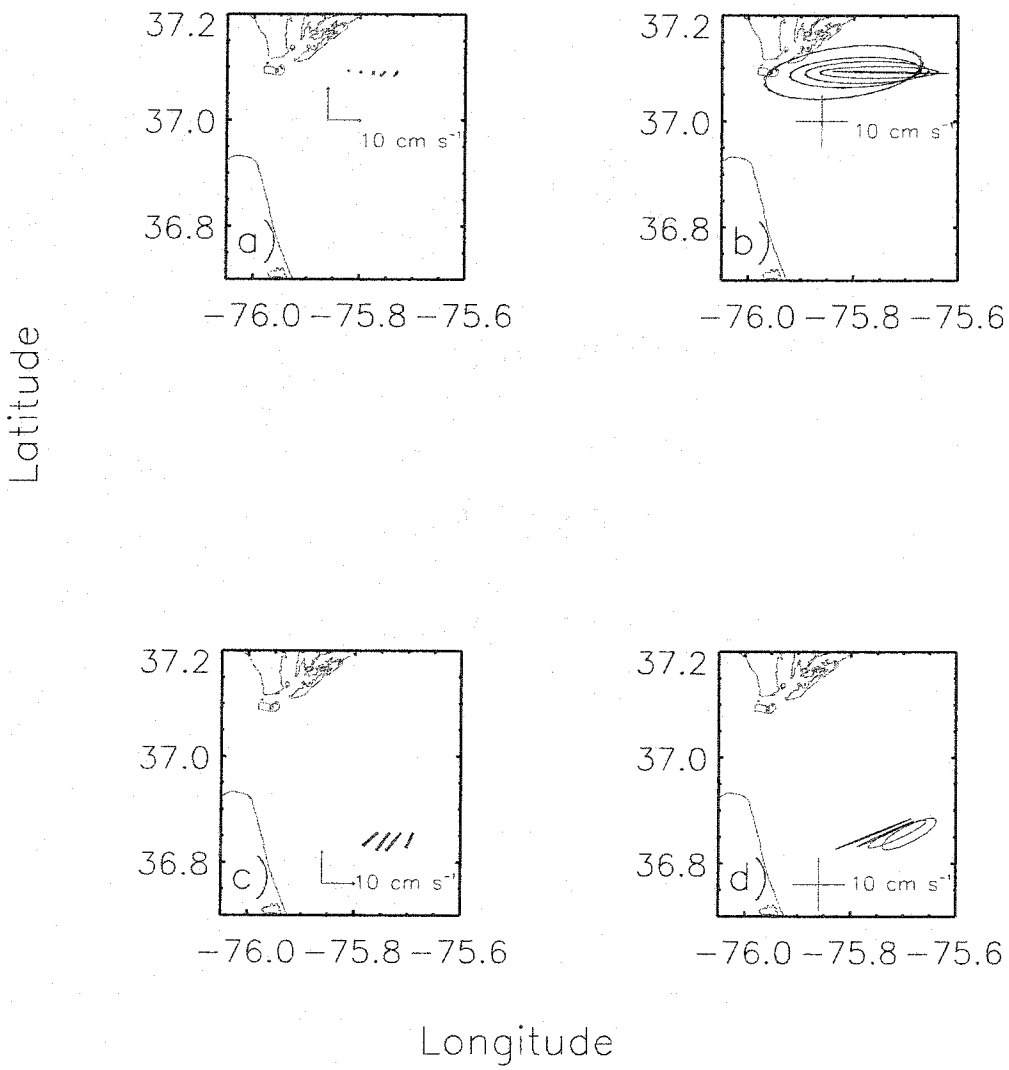

Fig. 23. Repeated Transects - NOV2000. Mean velocity and semidiurnal tidal velocities. Each transect was measured for 13 hours. Velocities are vertically averaged. Vectors and ellipses are plotted every 2 km.

Reproduced with permission of the copyright owner. Further reproduction prohibited without permission.

This is the first time that the tidal properties in the Delmarva inner shelf area have been described.

4.7.1 Semidiurnal and Diurnal Ellipses

The distribution of the semidiurnal ellipses obtained for the three optimal model runs show two areas with similar characteristics; at the Chesapeake Bay mouth (columns 20–45, Fig. 24), and between the Bay mouth and the Chincoteague area (columns 45–95, Fig. 24). The lower area is a result of the interaction between the Chesapeake Bay and the inner shelf, while the area north of the Chincoteague, may be more representative of the inner shelf itself. Notice that the survey tracks are all located south of the Chincoteague area (Fig. 2), and therefore there is no information available north of that area that could correct the behavior of the model. Therefore, the following analysis on semidiurnal and diurnal ellipses will be limited then to the area below the Chincoteague area.

The orientation of the semidiurnal ellipses near the Chesapeake Bay mouth, (columns 20–45, Fig. 24), is consistent for MAY2000, SEP2000, and FEB2001 results and reflects the flows that enter and leave the Chesapeake Bay. Similarly, the surface semidiurnal ellipses observed by Shay et al. (2001) were oriented towards the Bay mouth and rectilinear. The magnitude of has a minimum of 10 cm s^{-1} near the Chincoteague area in the Delmarva peninsula. The magnitude increases again near the Chesapeake Bay mouth to a mean of 20 cm s^{-1}, with amplitudes reaching 60–80 cm s^{-1}. The mean values are comparable with the surface semidiurnal amplitude for M_2 observed by Shay et al. (2001), 10-30 cm s^{-1}, 12 km from the Bay mouth. The major axis of the calculated semidiurnal ellipses have different orientation in the inner shelf for the three model results analyzed (columns 45–90, Fig. 24), but are primarily perpendicular to the coastline, becoming parallel to the coastline near the Chesapeake Bay entrance. SEP2000 results show more circular ellipses, while for SEP2000 and FEB2001 the semidiurnal ellipses are more rectilinear.

The calculated diurnal ellipses (Fig. 25) are generally oriented parallel to the coastline for the three assimilation runs. The are two distinct patterns; near the Chesapeake Bay entrance (columns 20–50, Fig. 25) and the area northward, (columns 50–95, Fig. 25). The magnitude of the major axis is much smaller than the semidiurnal ellipses, less than 10 cm s^{-1} for MAY2000 and SEP2000 results. These values are larger than those observed near the Bay mouth (Shay et al., 2001), where semidiurnal magnitudes are less than 10 cm s^{-1}. Mean values for FEB2001 have a larger amplitude, 10–20 cm s^{-1}.

4.7.2 Mean Circulation

The mean circulation during the MAY2000 cruise was along shelf, directed northeastward. The larger magnitudes were about 10 cm s^{-1}, located near the entrance to the Bay (Fig.

Reproduced with permission of the copyright owner. Further reproduction prohibited without permission.

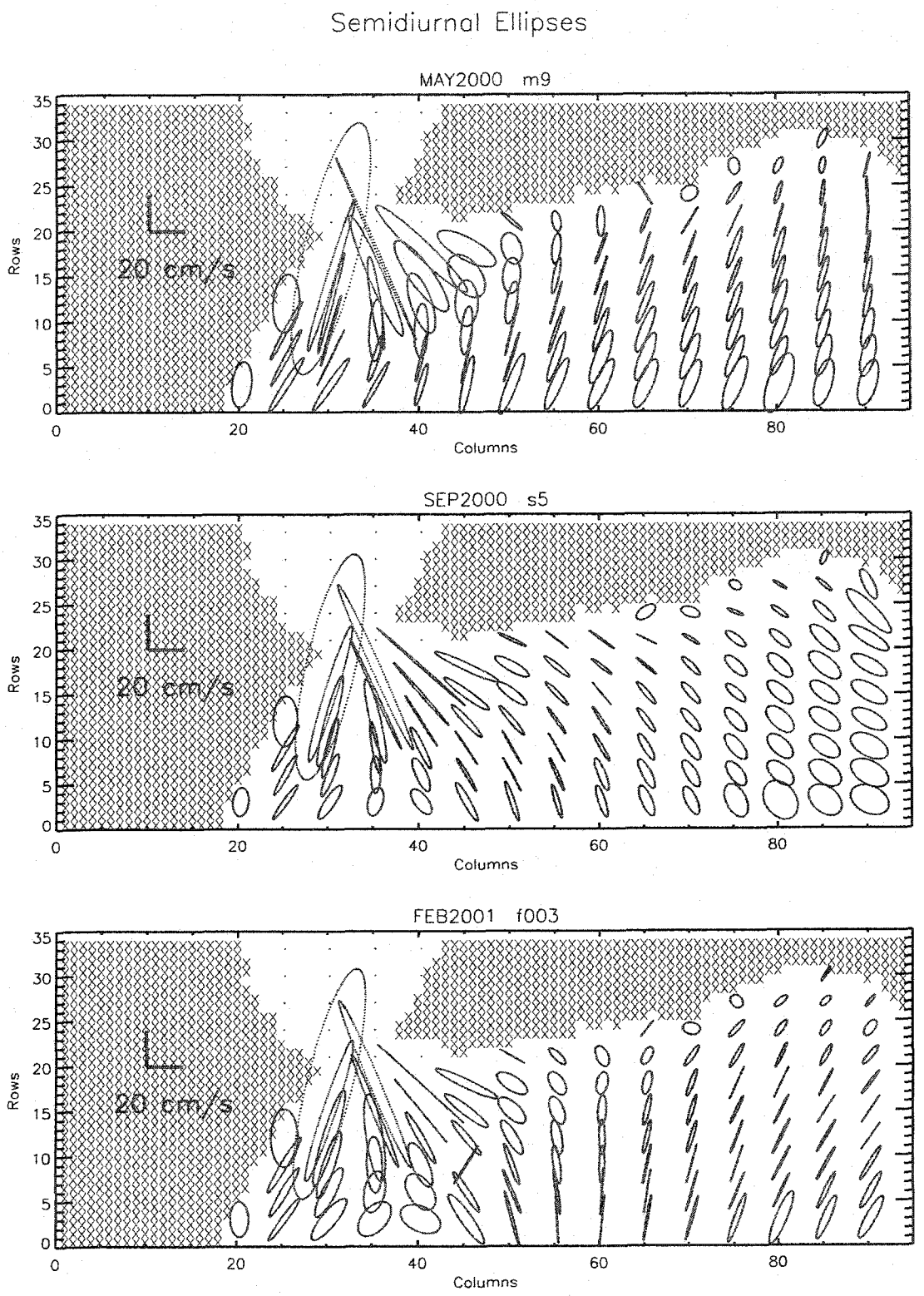

Fig. 24. Semidiurnal Ellipses - MAY2000, SEP2000, and FEB2001 optimal runs.

Reproduced with permission of the copyright owner. Further reproduction prohibited without permission.

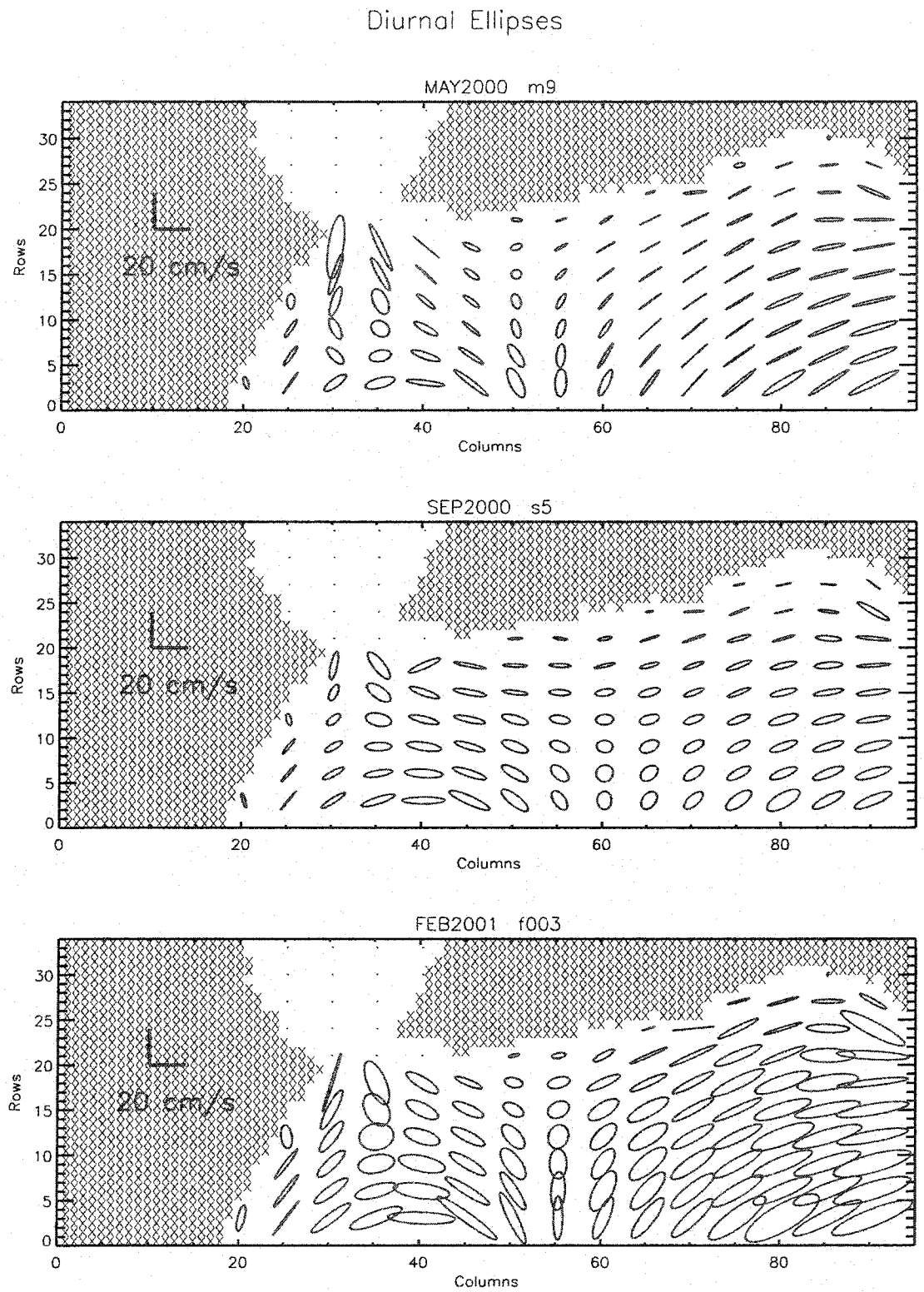

Fig. 25. Diurnal Ellipses - MAY2000, SEP2000, and FEB2001 optimal runs.

Reproduced with permission of the copyright owner. Further reproduction prohibited without permission.

26, upper panel). The area north of the Chesapeake Bay entrance shows a very weak mean circulation. The dispersion of the residuals (Fig. 27, upper panel) shows a major axis oriented along shelf toward the Bay entrance. The average magnitude of the major axis is 30 cm s^{-1}, with a minor axis of less than 10 cm s^{-1}. These values increase near the Chesapeake Bay entrance, where the dispersion of the residuals is high, but not isotropic. Wind measurements at the Chesapeake Light Tower during the first day of the MAY2000 cruise are oriented northeastward, which is consistent with the direction of the mean circulation shown.

During SEP2000, the mean circulation had a magnitude lesser or equal to 5 cm s^{-1}, directed northward along shelf (Fig. 26, middle panel). The dispersion of the residuals is almost isotropic north of the entrance to the Chesapeake Bay entrance, with a major axis of 10 cm s^{-1}, or less. Wind measured at the Chesapeake Light Tower shifted from a northeastward to northwestward direction, with a magnitude of $\approx$ 5 m s^{-1}. The observed weak mean circulation, relative to the MAY2000 and FEB2001 cases, reflects the general orientation of the wind and its reduced magnitude.

The mean flux after the assimilation of the FEB2001 northward data (Fig. 26, lower panel) shows a uniform field flowing northward, along the Delmarva coastline with velocities of about 10 cm s^{-1}. The residuals for this case are primarily oriented along shelf, with a major axis of approximately 15 cm s^{-1} (Fig. 27, lower panel). Wind conditions during the northward track of FEB2001 (data assimilated in the f003 run) changed from a N wind to a NE. This is consistent with the mean observed circulation north of the Chesapeake Bay entrance.

4.7.3 Cotidal Maps

The semidiurnal and diurnal cotidal maps were obtained using the η fields generated every hour by the numerical model. The RMSE for the η and the variance explained by the least-squares fit is also presented. These results were calculated doing a least squares of the data at each point of the elevation grid to a sinusoidal function with a semidiurnal and a diurnal constituent. The data from the first three days, used to spin up the model, were not considered for the least squares.

The results for MAY2000 show that the magnitude of the semidiurnal amplitude decreases from 60 cm to 45 cm at the Chesapeake Bay mouth (Fig. 28). The tidal elevation phase of less than half an hour between the right end of the model domain and the Chesapeake Bay entrance. The diurnal component, instead, shows a 1 hour phase difference between the right end of the domain and the Chesapeake Bay entrance. The diurnal tidal amplitude ranges from above 16 cm at the right side of the domain and then decreases to 8 cm at the Chesapeake Bay entrance. The highest RMSE of the elevation least squares,

Reproduced with permission of the copyright owner. Further reproduction prohibited without permission.

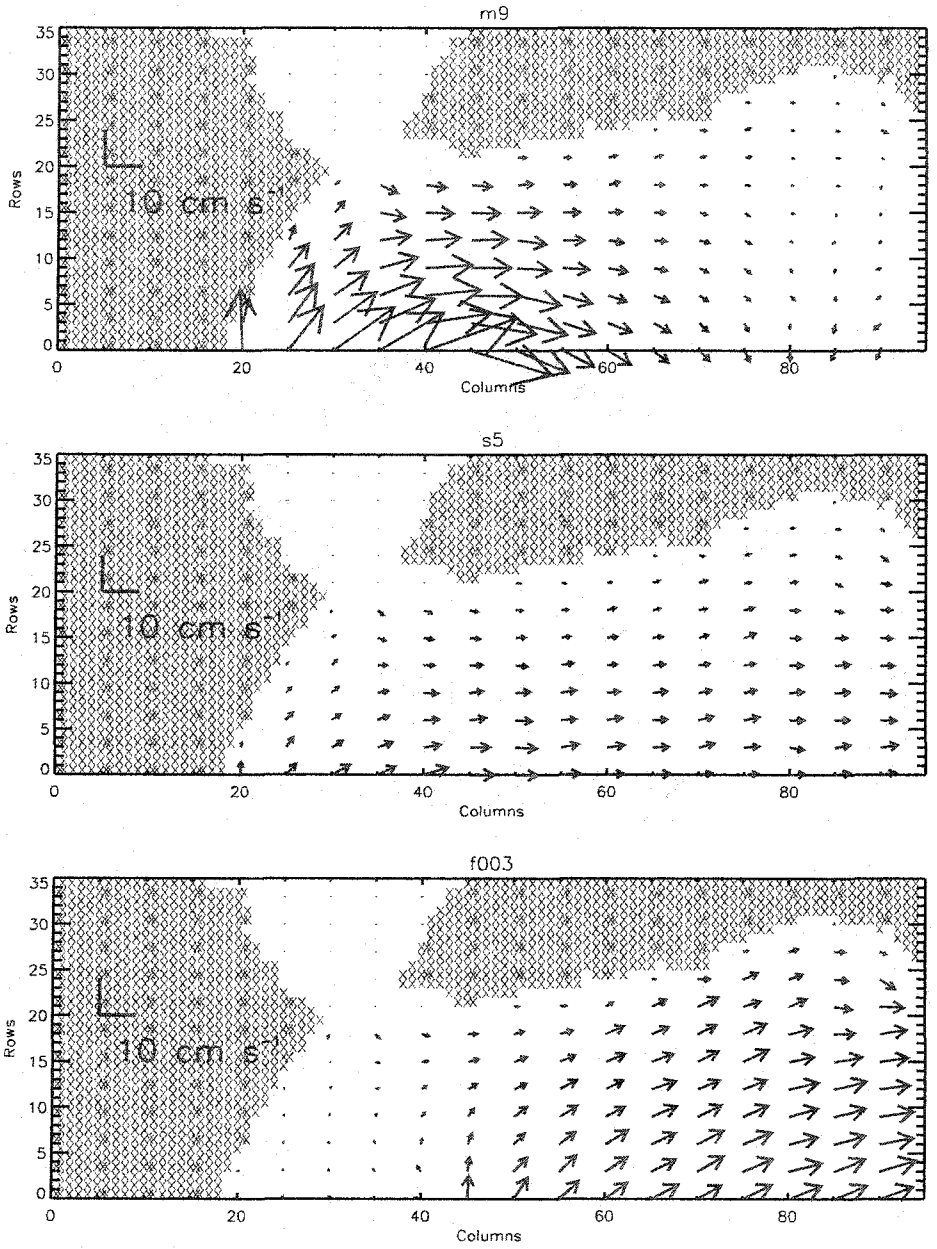

Fig. 26. Mean Velocities - MAY2000 (top panel), SEP2000 (middle panel) and FEB2001 (lower panel).

Reproduced with permission of the copyright owner. Further reproduction prohibited without permission.

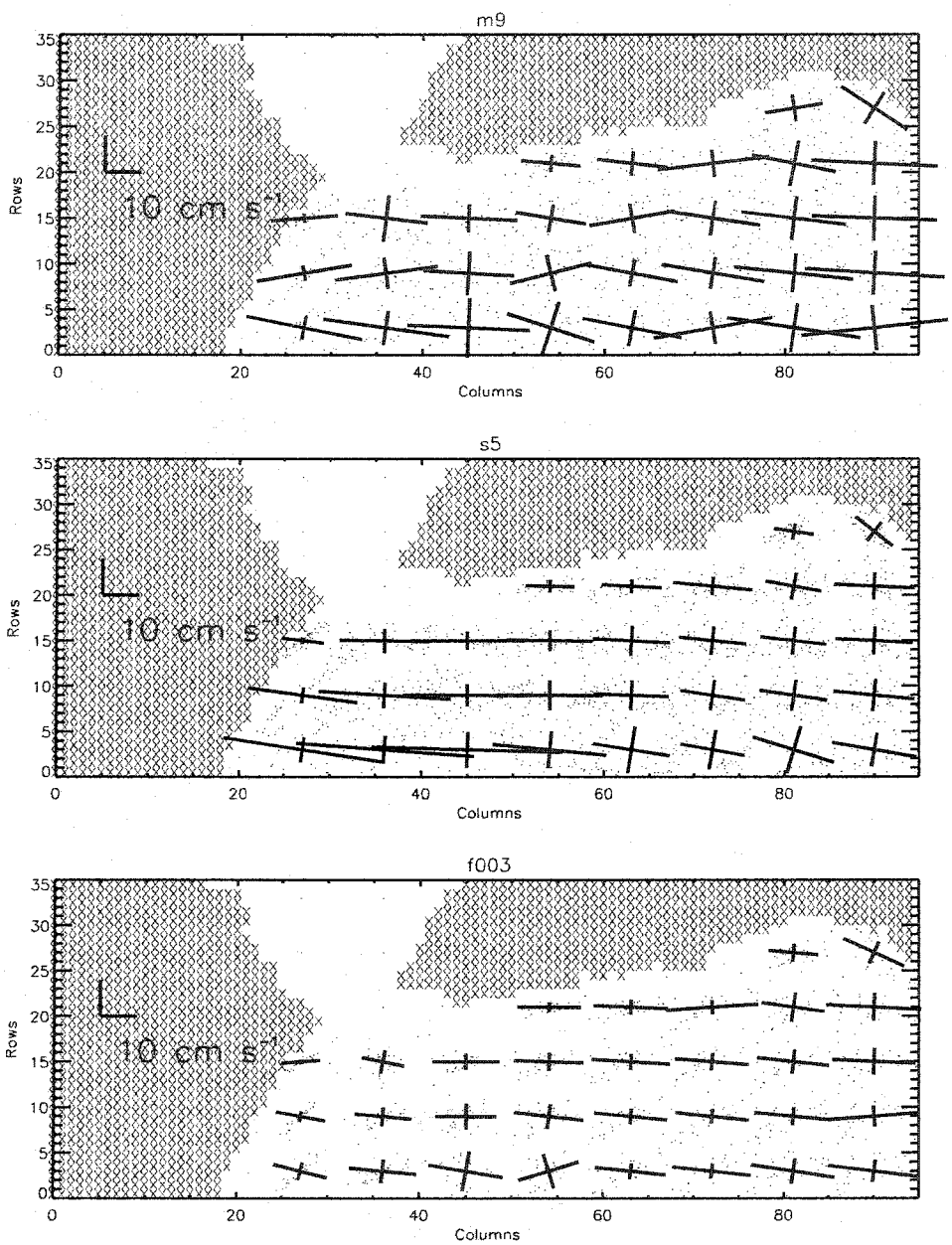

Fig. 27. Residuals - Dispersion of velocities not explained by the mean and tidal flow. Superimposed are the confidence ellipses of each group of residuals, calculated using EOF analysis. Panels show the MAY2000 (top), SEP2000 (middle), and FEB2001 (lower) results. The confidence interval shown is 50%.

Reproduced with permission of the copyright owner. Further reproduction prohibited without permission.

20–25 cm, is located near the Chincoteague area in the Delmarva peninsula, and close to the right boundary. This decreases to about 5 cm in the Chesapeake Bay mouth. The percentage of variance explained by the fit (represented by $r^2*100.$) increases from a 85% near the Chincoteague area to a 95% at the Chesapeake Bay entrance.

For the SEP2000 data, the semidiurnal cotidal map shows an increase in the magnitude of the elevation near the southern tip of the Delmarva Peninsula. Amplitude increases from 35 cm at the north end of the domain to 50 cm north of the Bay mouth, and then decreases into the Bay and to the east boundary (Fig. 29). The phase of the semidiurnal tide has a difference of less than half an hour between the right end of the domain and the Bay mouth. The diurnal tide shows a uniform amplitude of about 7 cm. The RMS error for this data assimilation experiment was less than 15 cm, the higher values concentrated near and north the Chincoteague area, decreasing to 4 cm near the Bay mouth. The tidal elevation variance explained in this run is greater than 90%, except north of the Chincoteague area where is 80–85%.

The FEB2001 data assimilation shows semidiurnal tidal amplitudes of 45–50 cm north of the Chesapeake Bay entrance, increasing to 55 cm at the right end and at the Bay mouth (Fig. 30). The semidiurnal phase is, again, with less than 0.5 hour change between the ends of the inner shelf area. The diurnal tidal signal has amplitudes of about 8 cm for the inner shelf, increasing to 16–18 cm at the lower left end of the domain. The maximum phase difference between two points is less than two hours. The RMS error decreases from the right end of the domain, from 20 cm to 6 cm at the Bay entrance. The variance explained increases accordingly form 60% at the right end to 95% at the Bay entrance.

4.7.4 Spatial Scales

The spatial scales from the model output were studied by doing the autocorrelation analysis of the mean elevation from the final model runs. The orientation of the model grid was such that the data along rows represent the along shelf orientation and the columns, across shelf (Fig. 31). The mean elevation along rows 1–25 was analyzed with an autocorrelation routine (IDL software). The spatial scale at each row was calculated by integrating the area under the autocorrelation function until the first zero intersect and multiplying this by 2 km, the model grid (Fig. 32, left panels). The same procedure was used to study the across shelf structure, by obtaining the autocorrelation function considering the data between rows 0–25 at each column (Fig. 32, right panels). The land grid points were excluded from the data being autocorrelated. The results show an spatial autocorrelation scale an order of magnitude larger ($\approx$ 30 km)in the along shelf direction than across shelf. The values obtained are also larger than those calculated for u and v, using only the ADCP data (Table 5). The low values of the across shelf spatial scales, comparable with the size

Reproduced with permission of the copyright owner. Further reproduction prohibited without permission.

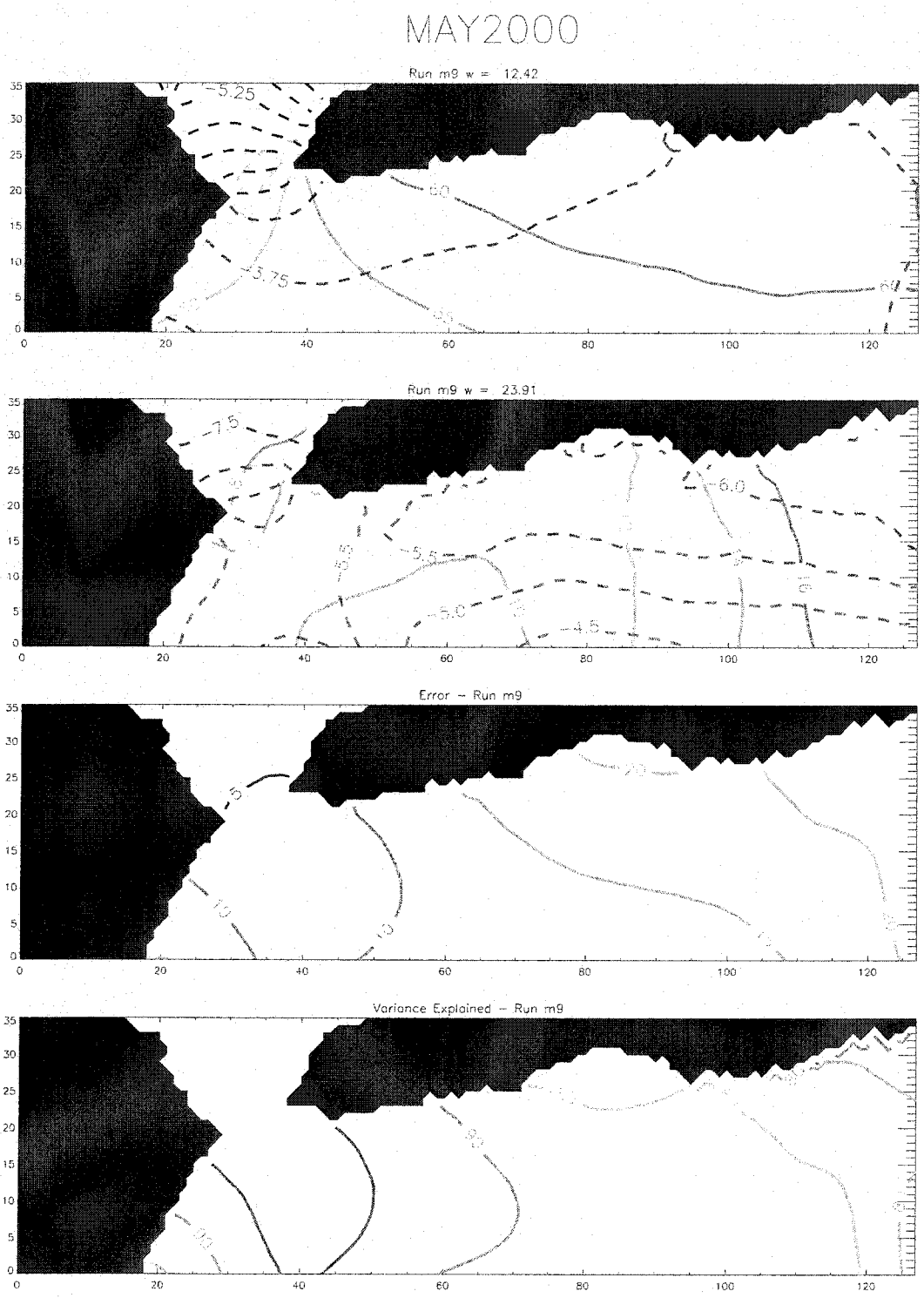

Fig. 28. Cotidal Elevation - MAY2000. The panels are (top to bottom) the semidiurnal and diurnal components, RMSE and map of variance explained. Phase is in hours, elevation in cm. Time reference for phase is GMT.

Reproduced with permission of the copyright owner. Further reproduction prohibited without permission.

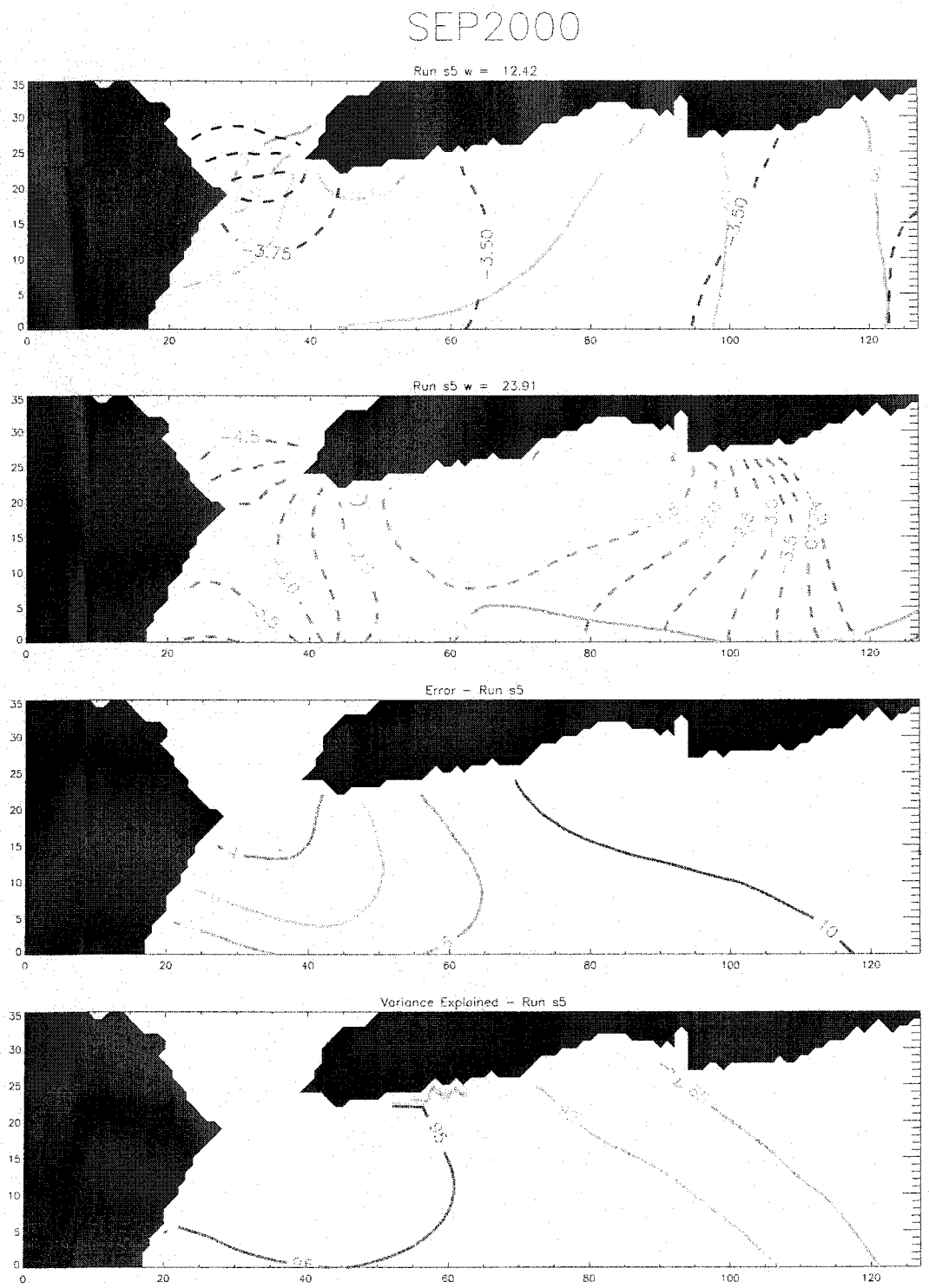

Fig. 29. Cotidal Elevation - SEP2000. Same as in Fig. 28.

Reproduced with permission of the copyright owner. Further reproduction prohibited without permission.

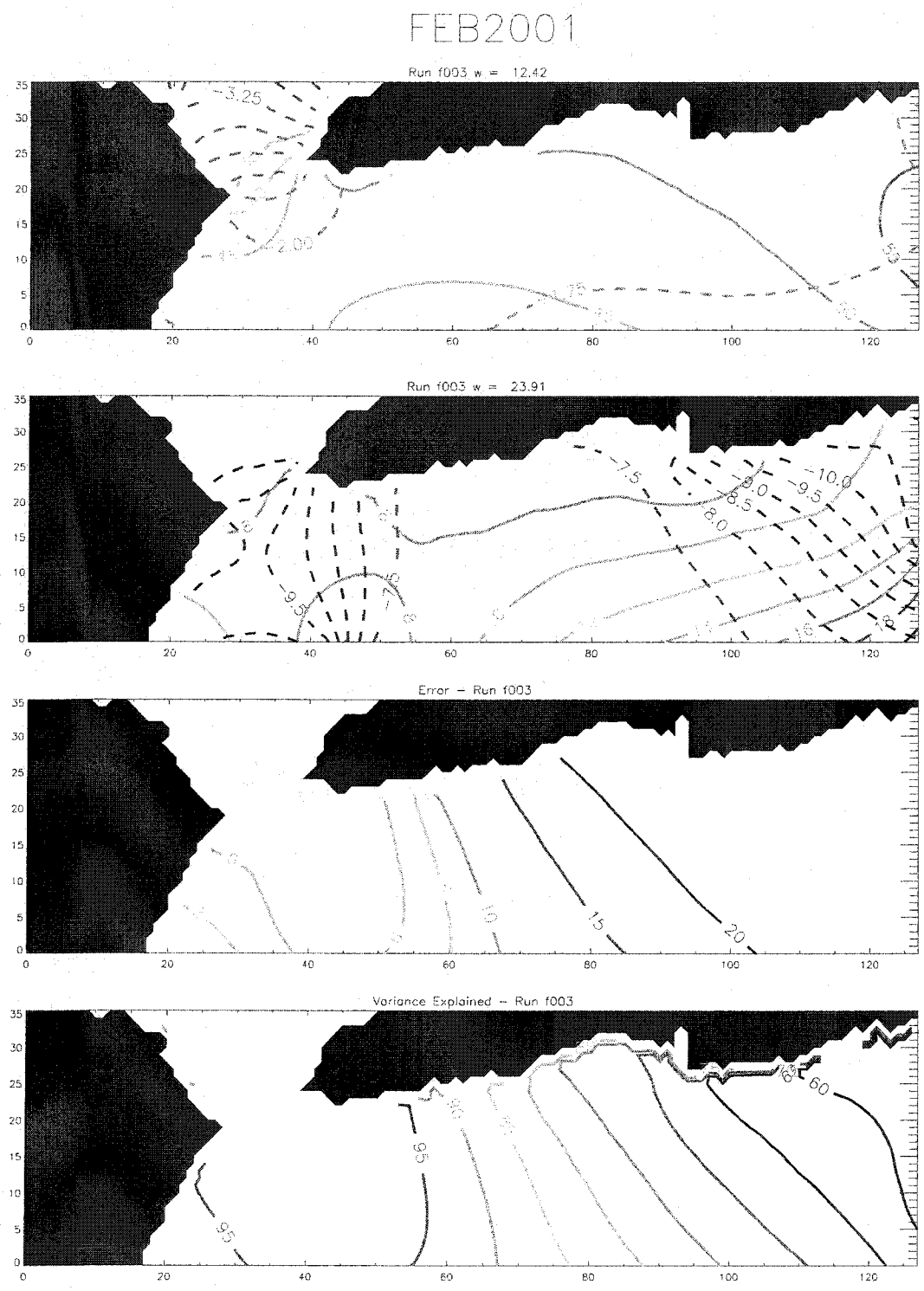

Fig. 30. Cotidal Elevation - FEB2001. Same as in Fig. 28.

Reproduced with permission of the copyright owner. Further reproduction prohibited without permission.

of the model grid, might as well indicate a lack of autocorrelation in this direction. Notice that alternative definitions of the autocorrelation scale can give results larger of smaller by a factor of 2. However, the anisotropy in the spatial scales is a more solid result.

4.7.5 Dynamic Balance

The model output was used to calculate the dynamic terms in the along shelf (u) and across shelf (v) component for the study area. The u and v mean were interpolated into the η points of the model grid prior to the analysis. The dynamic terms calculated were the Coriolis term,

$$u_f = fu \tag{16}$$

$$v_f = -fv \tag{17}$$

pressure gradient,

$$u_{pg} = g\frac{\partial \eta}{\partial y} \tag{18}$$

$$v_{pg} = g\frac{\partial \eta}{\partial x} \tag{19}$$

and frictional terms ($r = 0.15$ m s^{-1}),

$$u_{fr} = \frac{r}{h}u \tag{20}$$

$$v_{fr} = \frac{r}{h}v \tag{21}$$

For the MAY2000 results, the dynamic balance for the along shore component, u (Fig. 33) is divided in two main areas; one in front of the Chesapeake Bay mouth, and the Delmarva Peninsula shelf. In the first area the Coriolis term is balanced by the pressure gradient and the frictional term, while in the second area the dynamic balance is dominated by the pressure gradient and the frictional term. In the across shore component (v, Fig. 34), the dynamic balance is dominated in front of the Chesapeake Bay entrance by the frictional term, the Coriolis term, and the pressure gradient. In the Delmarva area, the Coriolis and pressure gradient terms dominate while the influence of the frictional term decreases away from the Bay entrance. The low value of the mean circulation obtained for the area north of the Bay entrance complicates the analysis of this area.

During SEP2000, the along shore dynamics is dominated by the pressure gradient and the frictional term in the whole region. The Coriolis term is strong at the Chesapeake Bay entrance (Fig. 35). The across shelf balance is geostrophic (dominated by the Coriolis

Reproduced with permission of the copyright owner. Further reproduction prohibited without permission.

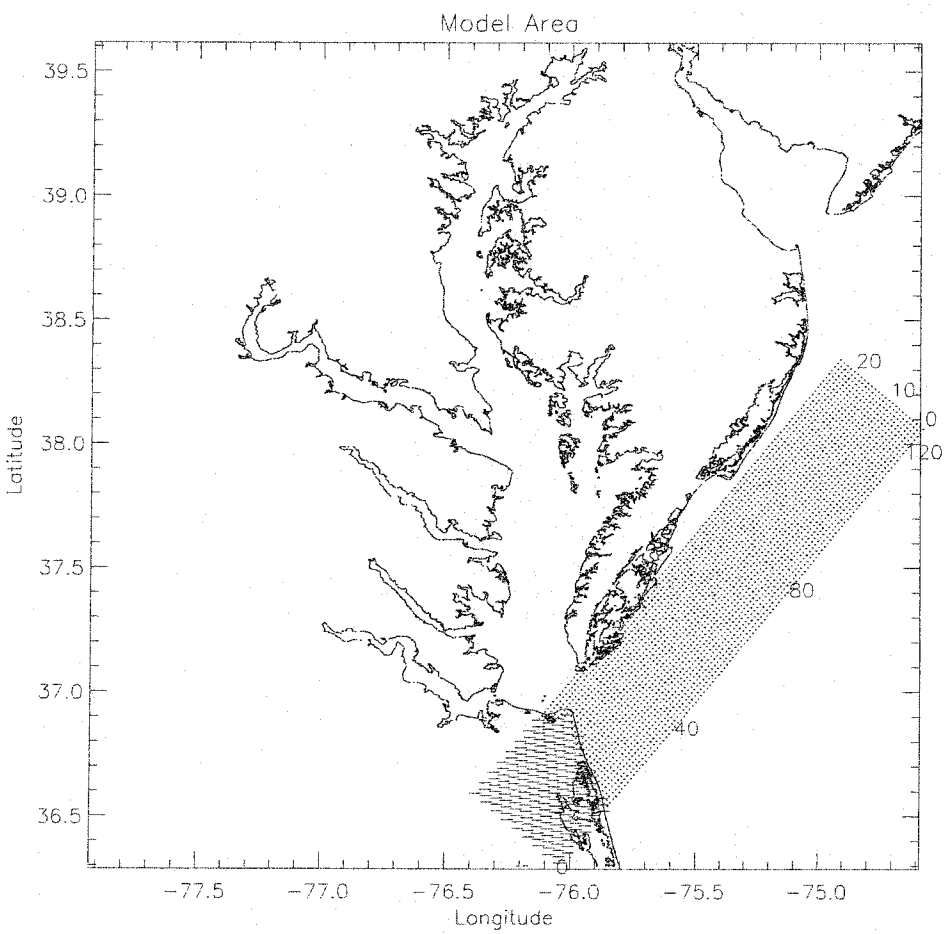

Fig. 31. Grid for spatial scales analysis.

Reproduced with permission of the copyright owner. Further reproduction prohibited without permission.

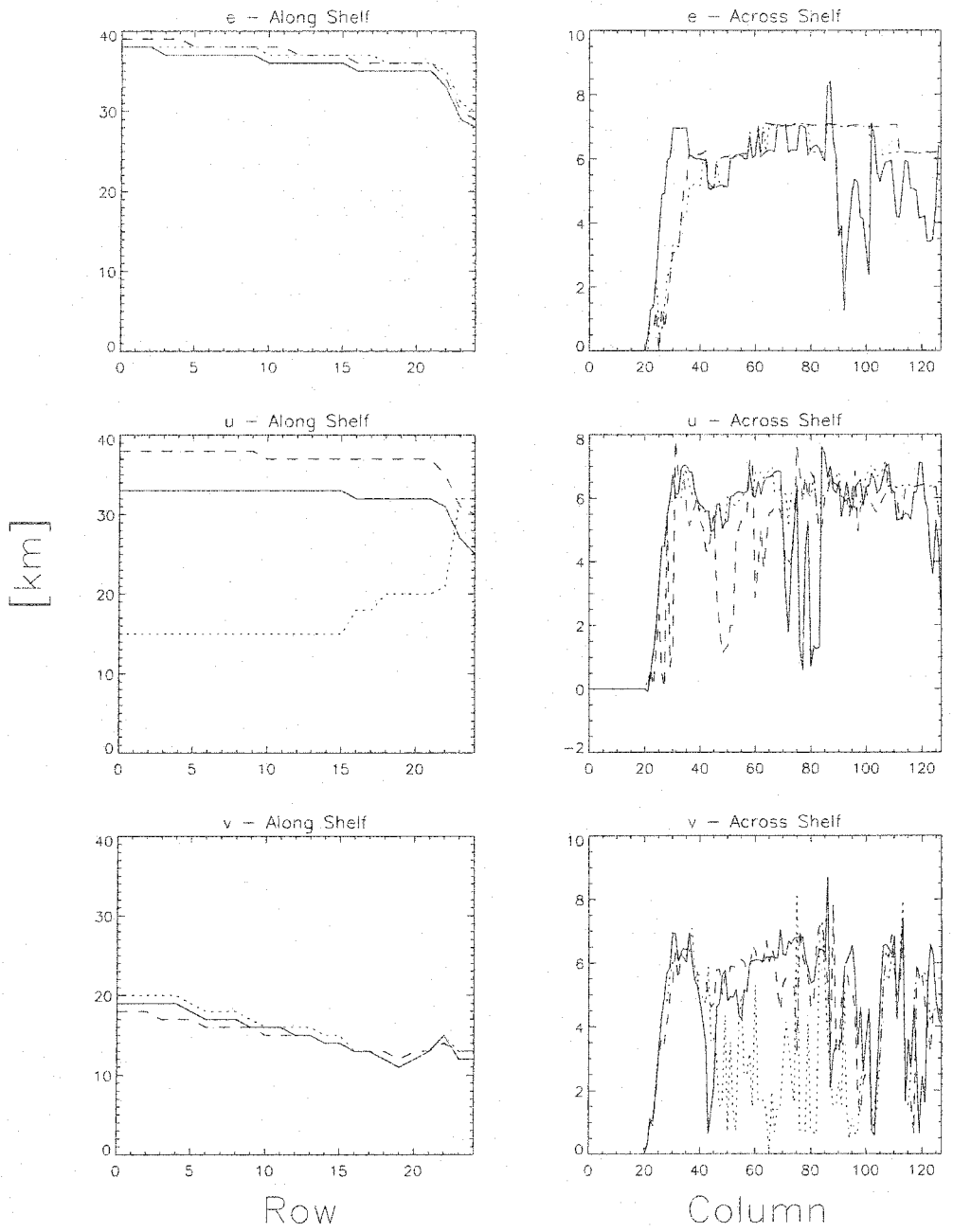

Fig. 32. Spatial Autocorrelation Scales of Model Results. MAY2000 (solid line), SEP2000 (dotted line), and FEB2001 (dashed line).

Reproduced with permission of the copyright owner. Further reproduction prohibited without permission.

term and the pressure gradient) in the Delmarva shelf, except near the right boundary were the frictional term increases. In front of the Chesapeake Bay entrance, the three terms are important (Fig. 36).

In FEB2001, the across shelf dynamic balance was again given by the pressure gradient and the frictional term (Fig. 37), with the area between the Chesapeake Bay and the right side of the model being influence by Coriolis. The across shore dynamic balance is ageostrophic for most of the area, being Coriolis and friction the dominant terms. The pressure gradient term has high values south of the Chincoteague area (Fig. 38).

Reproduced with permission of the copyright owner. Further reproduction prohibited without permission.

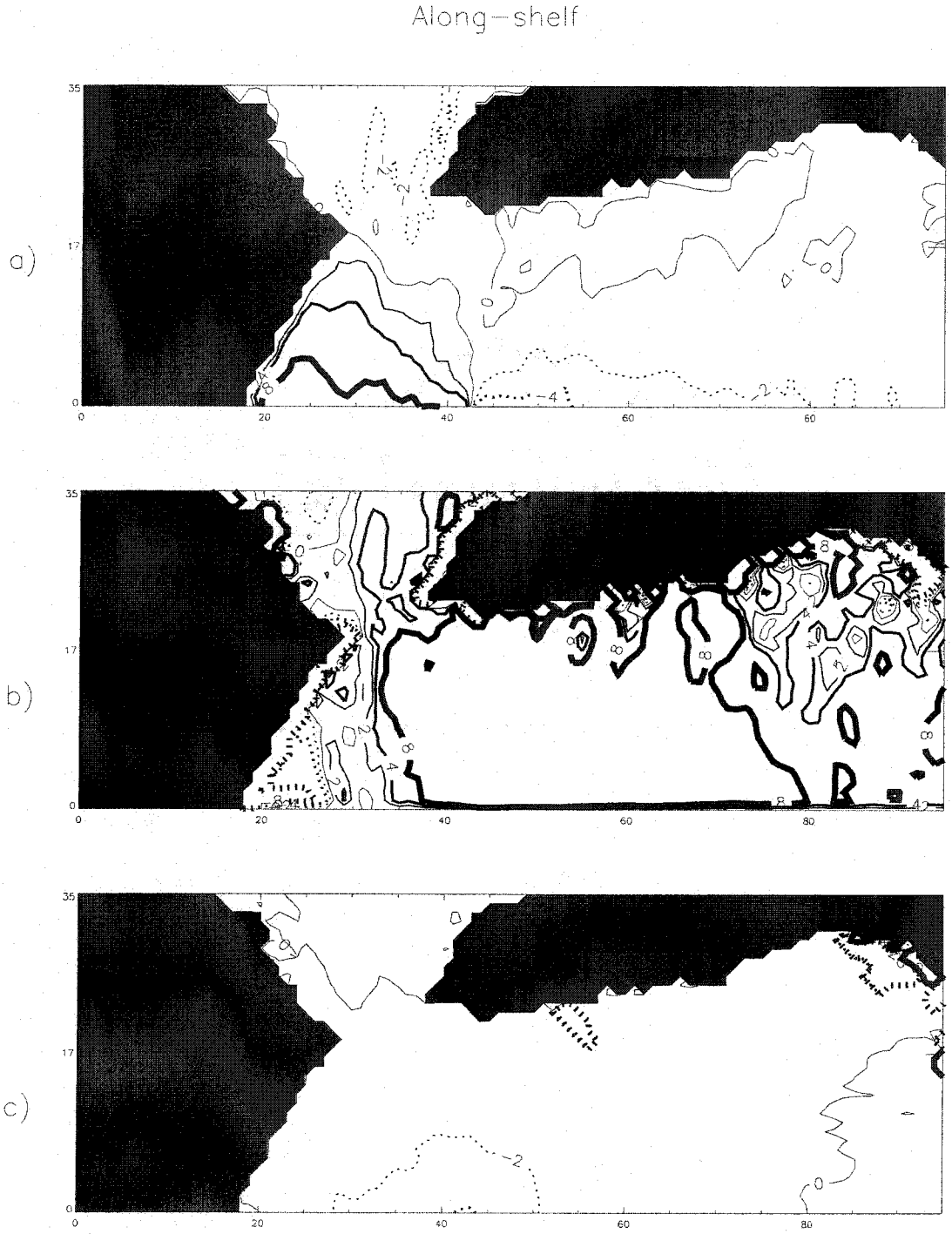

Fig. 33. Along Shore Dynamic Terms - MAY2000. The panels are, a) the Coriolis term, b) pressure gradient, and c) frictional term. Solid lines represent positive values; dotted lines negative values.

Reproduced with permission of the copyright owner. Further reproduction prohibited without permission.

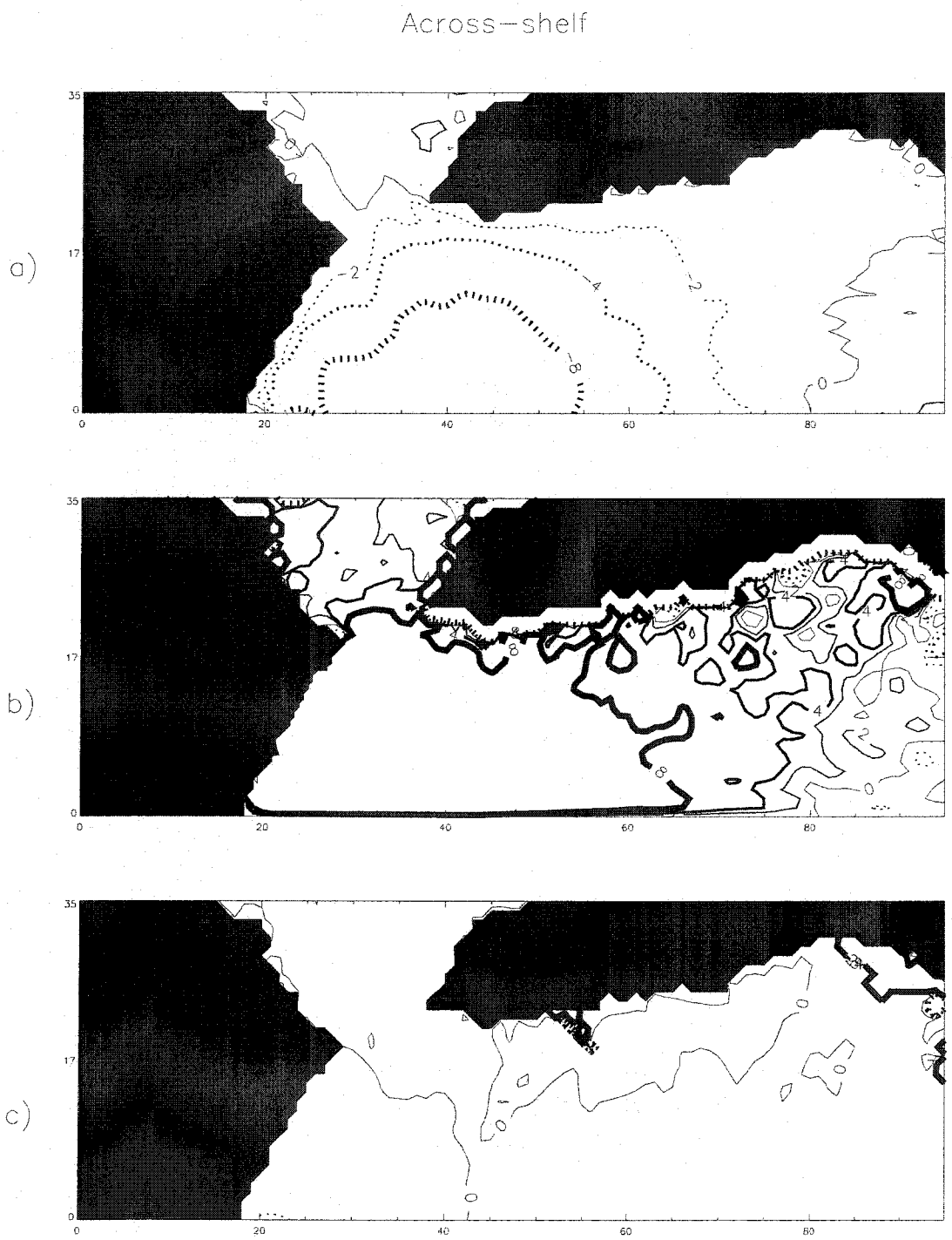

Fig. 34. Across Shore Dynamic Terms - MAY2000. Same as in Fig. 33.

Reproduced with permission of the copyright owner. Further reproduction prohibited without permission.

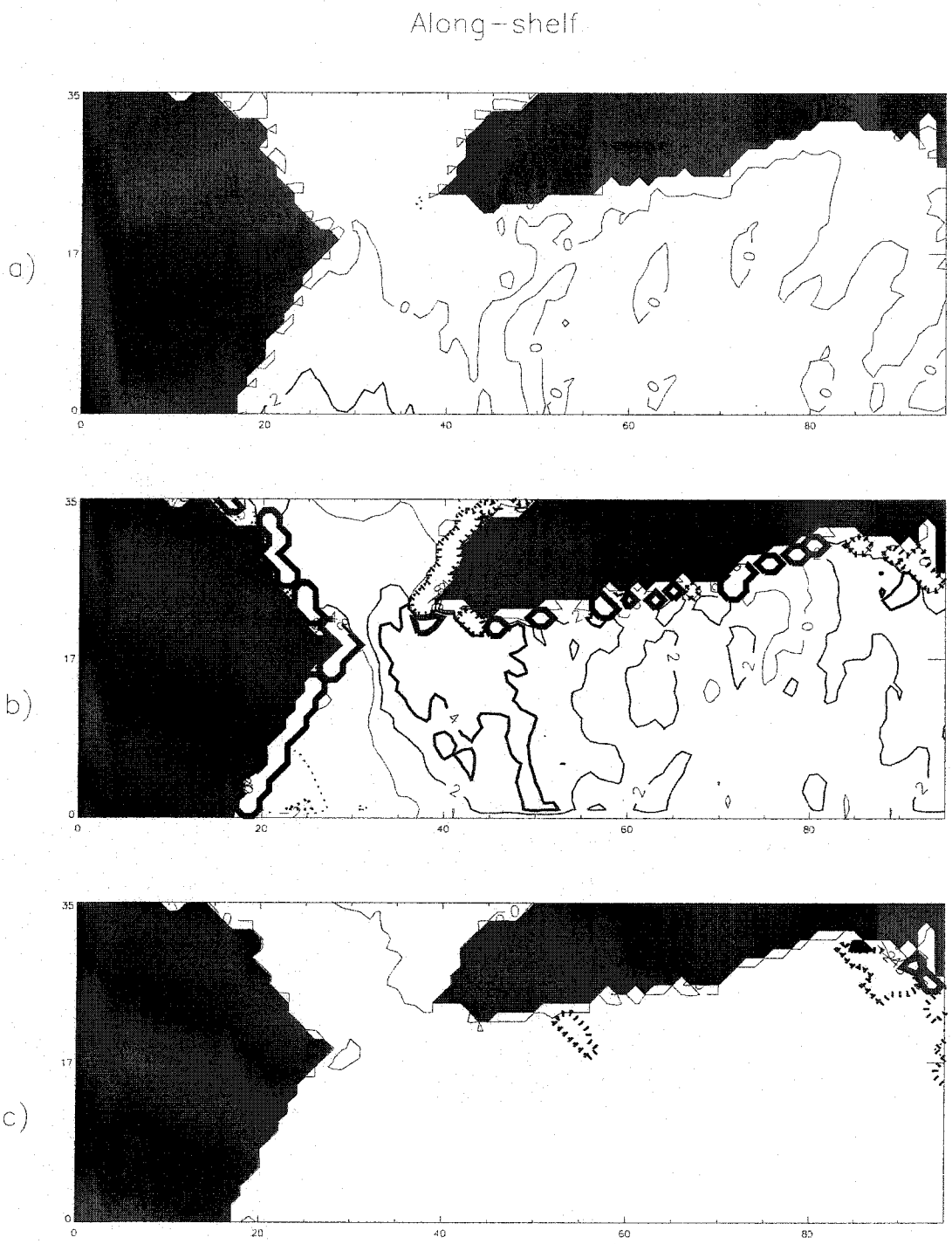

Fig. 35. Along Shore Dynamic Terms - SEP2000. Same as in Fig. 33.

Reproduced with permission of the copyright owner. Further reproduction prohibited without permission.

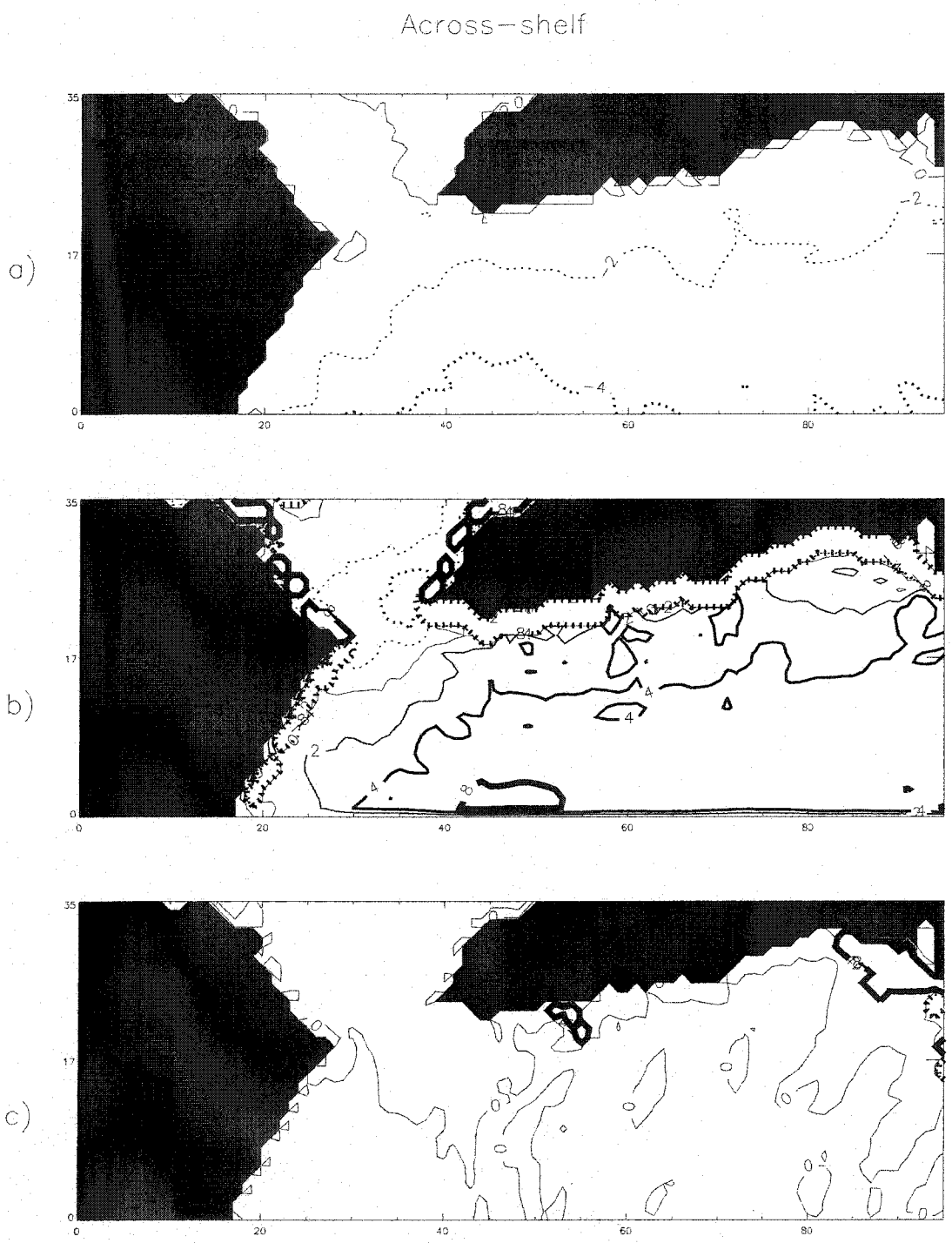

Fig. 36. Across Shore Dynamic Terms - SEP2000. Same as in Fig. 33.

Reproduced with permission of the copyright owner. Further reproduction prohibited without permission.

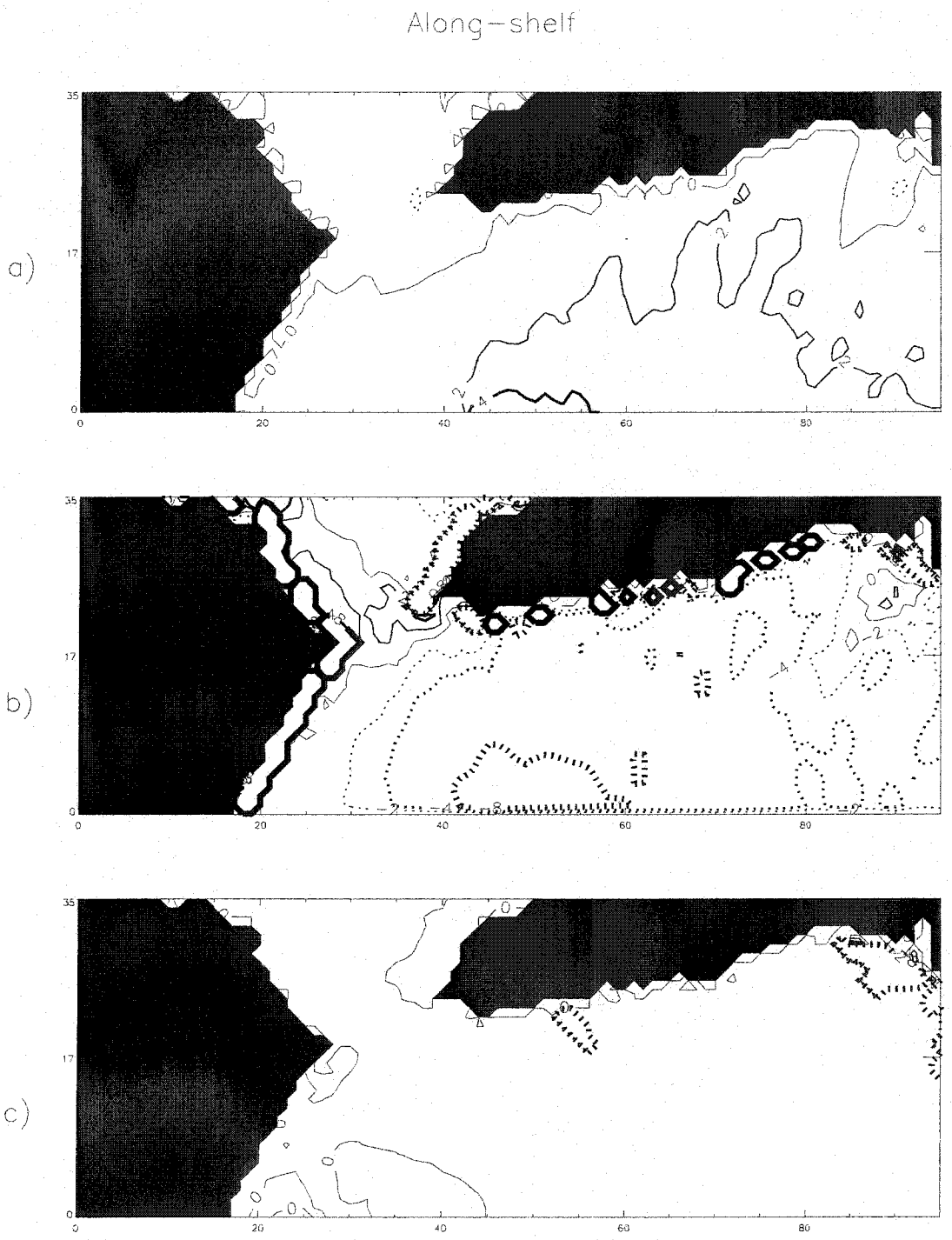

Fig. 37. Along Shore Dynamic Terms - FEB2001. Same as in Fig. 33.

Reproduced with permission of the copyright owner. Further reproduction prohibited without permission.

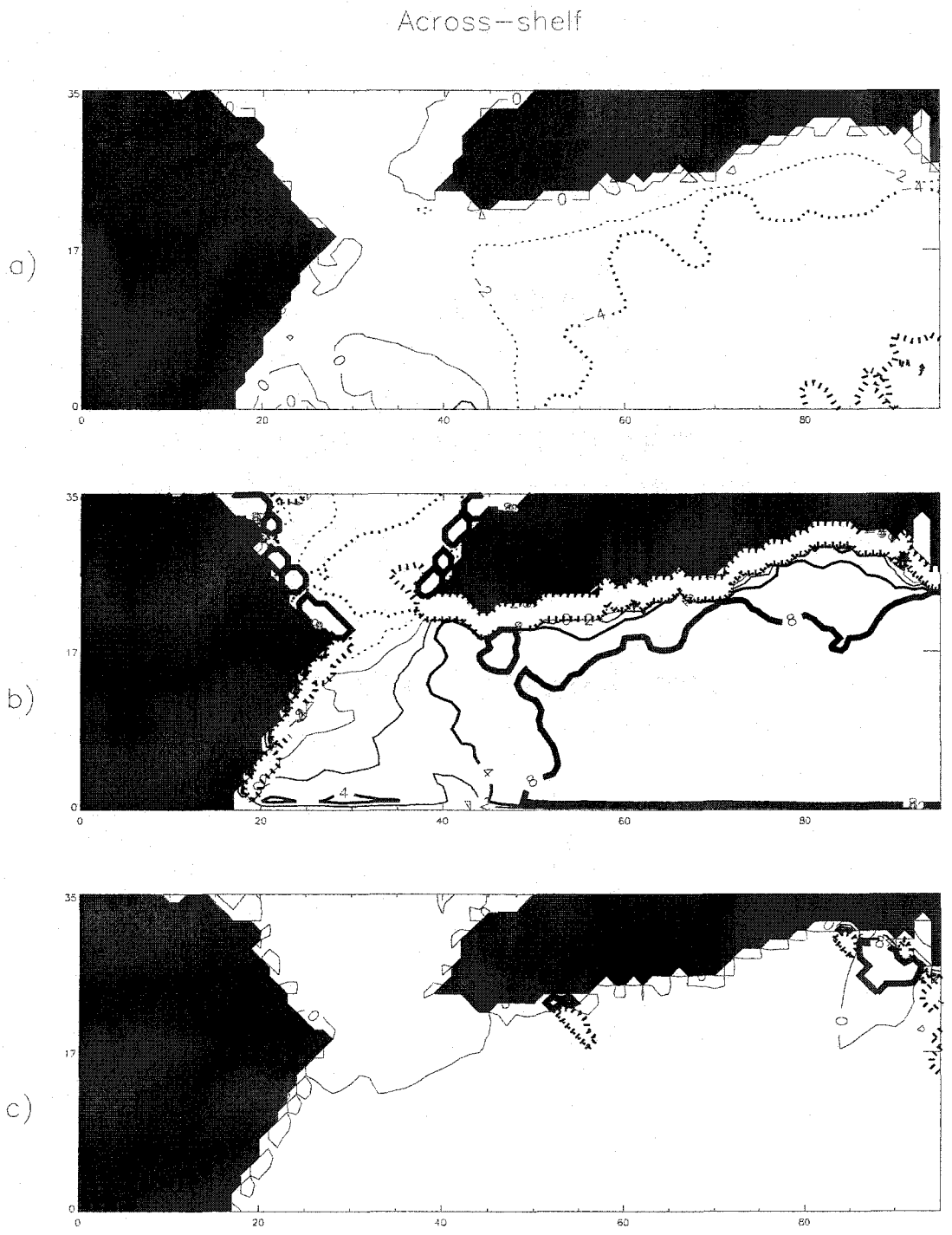

Fig. 38. Across Shore Dynamic Terms - FEB2001. Same as in Fig. 33.

Reproduced with permission of the copyright owner. Further reproduction prohibited without permission.

Table 6
Sea Level Validation. Data not assimilated in the model.

Station	NOAA Predicted				Model Predicted					
	A_{M_2} $\epsilon_{A_{M_2}}$ cm	P_{M_2} $\epsilon_{P_{M_2}}$ h	A_{K_1} $\epsilon_{A_{K_1}}$ cm	P_{K_1} $\epsilon_{P_{K_1}}$ h	A_{M_2} $\epsilon_{A_{M_2}}$ cm	P_{M_2} $\epsilon_{P_{M_2}}$ h	A_{K_1} $\epsilon_{A_{K_1}}$ cm	P_{K_1} $\epsilon_{P_{K_1}}$ h	RMS cm	r^2
				MAY2000						
1	.44	1.7	.09	-1.5	.35	1.6	.07	-1.3	.08	96
	.26	0.6	.27	2.8	.26	0.7	.27	3.6		
2	.21	-0.9	.04	3.1	.20	-1.0	.04	-2.8	.04	93
	.26	1.2	.26	6.5	.26	1.3	.25	6.1		
4	.45	1.5	.11	-1.6	.40	1.4	.08	-1.4	.07	97
	.26	0.6	.27	2.4	.26	0.7	.27	3.1		
7	.19	0.3	.05	-2.3	.22	0.1	.06	-2.0	.04	94
	.26	1.3	.25	5.2	.26	1.2	.26	4.8		
				SEP2000						
1	.45	.0	.04	-2.9	.32	-.2	.04	-.29	.11	95
	.20	.5	.20	4.8	.20	.6	.20	5.4		
2	.21	-2.7	.01	2.3	.17	-2.9	.04	1.5	.05	87
	.20	1.0	.20	19.3	.20	1.2	.20	5.7		
4	.46	-0.2	.03	-2.9	.35	-.4	.04	-2.9	.10	95
	.20	0.4	.20	5.9	.20	.6	.20	4.5		
7	.20	-1.5	.02	3.0	.18	-1.7	.03	2.4	.04	91
	.20	1.0	.20	10.3	.20	1.1	.20	6.6		
				FEB2001						
1	.36	0.2	.07	-2.5	.32	0.1	.06	-2.6	.05	97
	.26	0.7	.26	4.0	.26	0.9	.26	4.8		
2	.17	-2.5	.02	2.3	.16	-2.6	.06	2.1	.05	86
	.26	1.6	.28	10.5	.26	1.7	.28	4.2		
4	.38	0.0	.07	-2.6	.35	-0.1	.07	-2.6	.05	97
	.26	0.7	.26	4.1	.26	0.8	.26	4.1		
7	.16	-1.2	.03	-3.0	.18	-1.4	.05	2.7	.04	91
	.27	1.6	.27	7.8	.27	1.4	.28	5.0		

Reproduced with permission of the copyright owner. Further reproduction prohibited without permission.

Table 7
Spatial Autocorrelation Scales of Model Output

Parameter	Cruise	Across Shelf (km)	Along Shelf (km)
E	MAY2000	6	30–40
	SEP2000	6	30–40
	FEB2001	6	30–40
U	MAY2000	6	25–30
	SEP2000	6	15–30
	FEB2001	6	30–40
V	MAY2000	2–6	15–20
	SEP2000	2–6	15–20
	FEB2001	2–6	15–20

Reproduced with permission of the copyright owner. Further reproduction prohibited without permission.

CHAPTER 5

DISCUSSION

From a methodological point of view, the data assimilation process is a useful and physically coherent way to analyze the tidal and subtidal field in the Virginia inner shelf. As any method, it requires certain choices, namely the value of the bottom drag coefficient, and the number and location of the boundary structure functions. However the choices done for the data assimilation can be more easily justified with a physical basis. A more significant issue is the relative weight that is assigned to the data being assimilated, as well as the importance of the regularization terms used.

The numerical model showed the largest sensitivity to the bottom friction coefficient. A linear bottom drag coefficient was used, and the optimal valued used in these run was 0.15 m s^{-1}. A three dimensional model would be necessary in order to have a better parameterization of the bottom drag in terms of bottom velocity.

For most runs the cost function was reduced close to 30% of the initial value with 60 iterations. This can be seen also in how the model output closely reproduces the ADCP velocities and sea level velocities used to force the model (Figs. 16 and 17, respectively). The assimilation of ADCP data was not successful in recovering the sea level at the stations inside the Chesapeake Bay. In no case the ADCP data were simulated by forcing the model with the sea level. This was expected since the sea level data used was a predicted time series. It would be interesting to see if the measured sea level records, which shown not only the influence of the astronomic tide, can simulate the ADCP variability.

The tidal ellipses obtained with the final runs show a dominant semidiurnal behavior in the three cruises (MAY2000, SEP2000, and FEB2001, Fig. 24). The magnitude of the major axis reaches up to 30 cm s^{-1} and decreases in magnitude at the shelf area just north of the Chesapeake Bay mouth. The tidal ellipses become organized in front the Chesapeake Bay entrance, reflecting the inflows and outflows to and from the Chesapeake Bay . The diurnal ellipses (Fig. 25) show a less consistent distribution in the inner shelf. The average magnitude is less than 10 cm s^{-1}, except for FEB2001, when is up to 15 cm s^{-1}. An independent estimation of the diurnal ellipses was obtained during MAY2000 by measuring a transect for 24 hours. The amplitude of the diurnal tide calculated was 10–15 cm s^{-1}.

The results from the wavelet power spectra analysis of the open boundary conditions (Figs. 20–21) indicate that the main semidiurnal forcing comes from the along shore (or bottom) boundary and one of the across shelf structure functions. These results indicate that the semidiurnal tides on the shelf are better explained by the propagation of a Poincaré wave, and coastal trapped Kelvin wave. The presence of the Poincaré wave is supported

Reproduced with permission of the copyright owner. Further reproduction prohibited without permission.

by the across shore component observed in the semidiurnal ellipses (Fig. 24). The Kelvin wave is indicated by the decrease in magnitude in the across shore distance observed particularly in the MAY2000 and FEB2001 results. At the entrance of the Chesapeake Bay, the semidiurnal cotidal maps are better described as a coastal trapped wave entering the Bay, with the coast as a guide on the right (Northern Hemisphere), amplitudes decreasing away from the coast and phase isolines perpendicular to the coastline.

The mean circulation obtained for the area in the MAY2000 and SEP2000 data assimilation runs was consistent with the wind direction observed while the observations were taken; a the northward direction. The assimilation results from NOV2000 reflect the inadequacy of the data to represent the dynamics in the whole area with such localized measurements. In all cases the mean circulation obtained was parallel to the coastline and rather weak, less than 10 cm s^{-1}, and the residuals not explained by the least squares fit can be large in comparison. The mean circulation obtained from repeated transects in MAY2000 and NOV2000 had magnitudes less than 10 cm s^{-1}, which is consistent with the results obtained for the shelf area.

The diurnal constituent has an amplitude of 8–12 cm, with a phase lag of less than 2 hours. The variance explained by the least squares fit is higher near the Chesapeake Bay and decreases northward for MAY2000 and FEB2001. Considering that the main sources of tidal information are the sea level stations located inside the Chesapeake Bay, the model might have difficulties in propagating the tidal properties against the direction of movement of the coastal trapped wave. It is worth investigating what is the key difference between the assimilation of ADCP records measured in each direction, north and southward. The combination of records measured in both directions decreased significantly the performance of the assimilation.

Larger magnitude semidiurnal ellipses appeared near the Chesapeake Bay mouth. The amplification of tidal amplitudes has been previously described for the Chesapeake Bay (Valle-Levinson et al., 1998), and Delaware Bay (Munchow et al., 1992b). These and other studies (Shay et al., 2001; Whitney, 2003) describe spatial scales for these of the order of tens of kilometers. Whitney (2003) proposed a new parameter to describe the tidal interaction between the estuary and the shelf area. It subdivides the near shelf into an area with high estuarine influence (R_i), and an area with a weaker estuarine influence (R_{ifi}), depending on the shelf bathymetry, ambient shelf tidal velocity and mouth tidal flow. The corresponding values for the Chesapeake and Delaware Bays are $\approx$ 25 and 100 km Whitney (2003).

The analysis of the mean elevation and velocity field were used to obtain an understanding of the dynamic balance in the area. In general, the initial hypothesis was sustained, observing semi-geostrophic dynamics. The along shore dynamics were a balance between

Reproduced with permission of the copyright owner. Further reproduction prohibited without permission.

the Coriolis term, the pressure gradient and the frictional term. The across shore balance was largely geostrophic. Overall, three main dynamic areas were observed; the shelf in front of the Chesapeake bay entrance, the shelf in front of the Delmarva peninsula, and the shelf near the right boundary. Further study is necessary to understand if the results obtained for the area near the right boundary are due to spurious boundary effects or they reflect significant dynamics. These studies should include the Delaware Bay in order to understand the area of the shelf whose dynamics are influenced by these Bays. In the dynamic balance, the relative importance of the frictional term depends also in the value chosen for the linear bottom friction coefficient (r); in this study, the value was chosen as 0.15 m s^1, considering the minimization of the RMS error of withheld sea level data. The spatial scaling analysis showed a characteristic length scale of about 30 km in the along shore direction and 5 km in the across shore direction.

The performance of the model was good in general but was least favorable in the vicinity of the Chesapeake Bay mouth and northern end. This indicates that the dynamic balance represented by the model does not apply to these areas. It is likely that the larger value of the buoyancy frequency N calculated for this area during the cruises (Fig. 6) and nonlinear effects associated with strong lateral shears in the flow influence the dynamics of this areas.

Reproduced with permission of the copyright owner. Further reproduction prohibited without permission.

CHAPTER 6

SUMMARY AND CONCLUSIONS

The tidal and subtidal circulation of the Virginia inner shelf was studied using regional surveys of current velocity and data from sea level stations. These data were assimilated into a numerical model using the variational adjoint technique to obtain the open boundary conditions of the model. The model was validated by comparing the modeled sea level with data predicted by NOAA at sea level stations that were not assimilated into the model. The assimilation of sea level data was not successful to reproduce the circulation in the inner shelf. The ADCP data were insufficient to capture the tidal properties on the shelf, except during the SEP2000 cruise.

The mean circulation in the area is less than 10 cm s^{-1} and is oriented northward along shelf. This was associated with the wind direction. The semidiurnal tidal constituent is dominant and reaches 20-30 cm s^{-1}. The diurnal tidal constituent has a magnitude of less than 10 cm s^{-1}. The spatial distribution of tidal ellipses shows an increase in magnitude near the Chesapeake Bay mouth, and also at the northward end of the model. The propagation of the semidiurnal tide could be explained as a combination of a coastal trapped Kelvin wave and a Poincaré wave that transforms into a coastal trapped Kelvin wave as it moves in to the Chesapeake Bay. The model produced a residual circulation not explained by a least squares fit to a mean circulation and semidiurnal and diurnal tidal constituents. This residual circulation was oriented primarily along shelf and had magnitudes of 30 cm s^{-1}. This could be due to the dynamics of the numerical model, which are linear and do not include the effect of wind stress.

The characteristic spatial scales for the mean flow are anisotropic, with characteristics scales of 20–30 kilometers in the along shelf component and 4–6 km in the across shelf direction. The along shelf dynamic balance was dominated by the frictional, Coriolis and pressure gradient term, while the across shelf balance was predominantly geostrophic. The magnitude of the terms involved in the dynamic balance was different at three areas; near the Chesapeake Bay mouth, the Delmarva shelf between the Chesapeake Bay entrance and the Chincoteague area, and north of the Chincoteague area.

Reproduced with permission of the copyright owner. Further reproduction prohibited without permission.

6.1 FUTURE WORK

The model used in this study had simplified dynamics. The effect of neglected or misrepresented physics will be the object of future research by using a more complex model. A first step will be to add a wind stress term. Since this will be a forcing term and does not involve directly the variables included in the cost function, the adjoint equation does not need to be rewritten. For more complex modification of the dynamics of the numerical model, the adjoint equation must be rewritten, as it is specific for each model formulation or when using nonlinear models to work with more complex data assimilation techniques. The incremental approach (e.g. Lu et al., 2001) allows the combination of a model with simple linear dynamics and the use of a nonlinear model to represent a more complete physical dynamics. Other possibilities are methods developed after the Kalman Filter (Kalman, 1960), such as the Ensemble Kalman Filter (EnKF) (Evensen, 1994). However, approximate Kalman Filters have not been promising for recovering data from moving ADCP measurements (Dowd and Thompson, 1997).

A model run using the measured sea level records, in contrast to predicted values, could be more promising in recovering current variability in the outer shelf. Verified sea level data at several NOAA stations is available every 6 minutes and every hour. The study of this particular area could help to understand the exchange between the inner shelf and the barrier island area of the Delmarva Peninsula, similarly to the studies done by Xie and Eggleston (1999) in North Carolina and Palmico Sound area.

As far as the data assimilation method, a criterion to measure the reduction in cost function value versus the number of parameters, or data points, in the cost function, needs to be developed for deciding the optimal time averaging for the data assimilation runs. Similar criteria exist for autoregressive models, e.g. the Akaike's Information Criterion (Chatfield, 1997). Also, as pointed by Griffin and Thompson (1996), it is necessary to develop a better way to decide what portion of the data record must be withheld in order to validate the model results.

Reproduced with permission of the copyright owner. Further reproduction prohibited without permission.

REFERENCES

Atkinson, L. P., Blanton, J., 1986. Process that affect stratification in shelf waters. In: Mooers, C. (Ed.), Baroclinic processes in continental shelves. Coastal and Estuarine Sciences 3. American Geophysical Union, Washington, D.C., pp. 117–130.

Beardsley, R., Boicourt, W., Hansen, D., 1976. Physical oceanography of the middle atlantic bight. In: Gross, M. (Ed.), American Society of Limnology and Oceanography Special Symposium. pp. 20–34.

Bennett, A., McIntosh, P., 1982. Open ocean modelling as an inverse problem: Tidal theory. Journal of Physical Oceanography 12, 1004–1018.

Bevington, P. R., Robinson, D. K., 1992. Data Reduction and Error Analysis for the Physical Sciences, 2^{nd} Edition. McGraw–Hill, USA.

Bogden, P. S., Malanotte-Rizzoli, P., Signell, R., 1996. Open-ocean boundary conditions from interior data: Local and remote forcing of Masachusstes Bay. Journal of Geophysical Research 101 (C3), 6487–6500.

Bogden, P. S., O'Donnell, J., 1998. Generalized inverse with shipboard current measurements: Tidal and nontidal flows in Long Island Sound. Journal of Marine Research 56, 995–1027.

Chatfield, C., 1997. The Analysis of Time Series. An Introduction, 5th Edition. Texts in Statistical Science. Chapman & Hall, Great Britain.

Csanady, G., Hamilton, P., 1988. Circulation of slopewater. Continental Shelf Research 8(5-7), 565–624.

Das, S., Lardner, R., 1991. On the estimation of parameters of hydraulic models by assimilation of periodic tidal data. Journal of Geophysical Research 96 (C8), 15187–15196.

Dowd, M., Thompson, K., 1996. Extraction of tidal streams from a ship–borne acoustic Doppler current profiler using a statistical–dynamical model. Journal of Geophysical Research 101 ((C4)), 8943–8956.

Dowd, M., Thompson, K., 1997. Forecasting coastal circulation using an approximate Kalman filter based on dynamical modes. Continental Shelf Research 17 (14), 1715–1735.

Egbert, G., 1997. Tidal data inversion: Interpolation and inference. Progress in Oceanography 40, 53–80.

Reproduced with permission of the copyright owner. Further reproduction prohibited without permission.

Epifanio, C., Garvine, R., 2001. Larval transport on the Atlantic continental shelf of North America: A review. Estuarine, Coastal and Shelf Science 52, 51–77.

Evensen, G., 1994. Sequential data assimilation methods with a non-linear quasi-geostrophic model using Monte Carlo methods to forecast error statistics. Journal of Geophysical Research 99 (C5), 10143–10162.

Fang, T., Piegl, L., 1992. Algorithm for Delaunay trangulation and convex hull computation using a sparse matrix. Computer Aided Design 24, 425–436.

Fang, T., Piegl, L., 1993. Delaunay triangulation using a uniform grid. IEEE Computer Graphics and Applications 13, 36–47.

Foreman, M., Freeland, H. J., 1991. A comparison of techniques for tide removal from ship-mounted acoustic Doppler measurements along the southwest coast of Vancouver island. Journal of Geophysical Research 96 (C9), 17007–17021.

Foreman, M. G., Thomson, R. E., 1997. Three-dimensional model simulations of tides and buoyancy currents along the west coast of Vancouver Island. Journal of Physical Oceanography 27, 1300–1324.

Franke, R., 1982. Smooth interpolation of scattered data by local thin plate splines. Computers & Mathematics withs Applications 8 (4), 273–281.

Garvine, R. W., 1995. A dynamical system for classifying buoyant coastal discharges. Continental Shelf Research 15 (13), 1585–1596.

Gill, P. E., Murray, W., Wright, M. H., 1981. Practical Optimization. Academic Press.

Goodrich, D. M., 1988. On meteorological induced flushing in three U.S. east coast estuaries. Estuarine, Coastal and Shelf Science 26, 111–121.

Griffin, D., Thompson, K., 1996. The adjoint method of data assimilation used operationally for shelf circulation. Journal of Geophysical Research 101 (C2), 3457–3477.

Hallock, Z., Pistek, P., Book, J., Miller, J., Shay, L., Perkins, H., 2003. A description of tides near the Chesapeake Bay entrance using in situ data with and adjoint model. Journal of Geophysical Research 108 (C3), 3075, doi:10.1029/2001/JC000820.

Ianniello, J., 1977. Tidally induced residual currents in estuaries of constant breadth and depth. Journal of Marine Research 35, 755–786.

Joyce, T., 1989. On in situ "calibration" of shipboard ADCPs. Journal of Atmospheric and Oceanic Technology 6, 169–172.

Reproduced with permission of the copyright owner. Further reproduction prohibited without permission.

Kalman, R., 1960. A new approach to linear filtering and prediction problems. Journal of Basic Engineering, 35–45.

Kendall, M., Gibbons, J., 1990. Rank Correlation Methods, 5^{th} Edition. Edward Arnold, London.

Lardner, R., Al-Rabeh, A., Gunay, N., 1993. Optimal estimation of parameters for a two-dimensional hydrodynamical model of the Arabian Gulf. Journal of Geophysical Research 98 (C10), 18229–18242.

Lentz, S., Carr, M., Herbers, T., 2001. Barotropics tides in the North Carolina Shelf. Journal of Physical Oceanography 31, 1843–1859.

Li, C., Valle-Levinson, A., Atkinson, L. P., Royer, T. C., 2000. Inference of tidal elevation in shallow water using a vessel-towed acoustic Doppler current profiler. Journal of Geophysical Research 105 (C11), 26225–26236.

Lorenz, E., 1956. Empirical orthogonal functions and statistical weather forecasting. Sci. Rep. 1, M.I.T., Cambridge, MA, 48 pp.

Lu, Y., Thompson, K. R., Wright, D. G., 2001. Tidan currents and mixing in the Gulf of St. Lawrence: and application of the incremental approach to data assimilation. Can. J. Fish. Aquat. Sci. 58, 723–735.

Lynch, D., Naimie, C., Hannah, C., 1998. Hindcasting the Georges Bank circulation. Part I: Detiding. Continental Shelf Research 18, 607–639.

Mesinger, F., Arakawa, A., 1976. Numerical methods used in atmospheric models. GARP Publication Services 14, 64.

Münchow, A., 1992. The formation of a buoyancy driven coastal current. Ph.D. thesis, University of Delaware, 205 pp.

Munchow, A., Garvine, R., Pfeiffer, T., 1992a. Subtidal currents from a shipboard acoutic Doppler current profiler in tidally dominated waters. Continental Shelf Research 12 (4), 499–515.

Munchow, A., Masse, A., Garvine, R., 1992b. Astronomical and nonlinear tidal currents in a coupled estuary shelf system. Continental Shelf Research 12 (4), 471–498.

Noble, M., Butman, B., Williams, E., 1983. On the longshelf structure and dynamics of subtidal currents on the eastern United States continental shelf. Journal of Physical Oceanography 13, 2125–2147.

Reproduced with permission of the copyright owner. Further reproduction prohibited without permission.

Ou, H. W., Beardsley, R. C., Mayer, D., Boicourt, W. C., Butman, B., 1981. An analysis of subtidal current fluctuations in the Middle Atlantic Bight. Journal of Physical Oceanography 11, 1383–1392.

Palma, E., Matano, R., 1998. On the implementation of passive open boundary conditions for a general circulation model: The barotropic mode. Journal of Geophysical Research 103 (C1), 1319–1341.

Panteleev, G., Maksimenko, N., de Young, B., Reiss, C., Yamagata, T., 2000. Anisotropic optimization of the current field with the variational method. Oceanology 40 (4), 451–457, translated from Okeanologiya.

Paraso, M., Valle-Levinson, A., 1996. Meteorological incluences on sea level and water temperature in the lower Chesapeake Bay. Estuaries 19 (3), 548–561.

Pedlosky, J., 1987. Geophysical Fluid Dynamics, 2^{nd} Edition. Springer-Verlag, New York, USA.

Press, W. H., Teukolsky, S. A., Vetterling, W. T., Flannery, B. P., 1992. Numerical Recipes in Fortran 77 - The Art of Scientific Computing, 2^{nd} Edition. Cambridge University Press, Cambridge, UK.

Qiu, L.-J., Er, M.-H., 1995. Wavelet spectrogram of noisy signals. Int. J. Elec. 79, 665–677.

Redfield, A. C., 1958. The influence of the continental shelf on the tide of the Atlantic coast of the United States. Journal of Marine Research 17, 432–448.

Reyes-Hernandez, C., 2001. Tidal and subtidal lateral structures of density and velocity in the Chesapeake Bay entrance. Ph.D. thesis, Old Dominion University, 170 pp.

Salas-Monreal, D., 2002. Sea level slopes and volume fluxes produced by atmospheric forcing in Chesapeake Bay. Master's thesis, Old Dominion University, Norfolk, VA, USA.

Sanders, T. M., Garvine, R. W., 1996. Frontal observations of the Delaware Coastal Current source region. Continental Shelf Research 16 (8), 1009–1021.

Sasaki, Y., 1970. Some basic formalisms in numerical variational analysis. Monthyl Weather Review 98, 875–883.

Shay, L. K., Cook, T. M., Hallock, Z. R., Haus, B. K., Graber, H. C., Martinez, J., 2001. The strength of the m_2 tide at the Chesapeake Bay mouth. Journal of Physical Oceanography 31, 427–449.

Reproduced with permission of the copyright owner. Further reproduction prohibited without permission.

Sherman, K., Grosslein, M., Mountain, D., Busch, D., O'Reilly, J., Theroux, R., 1988. The continental shelf ecosystem off the northeast coast of the United States. In: Postma, H., Zijlstra, J. (Eds.), Continental Shelves. Ecosystems of the World Series No. 27. Elsevier, Amsterdam, pp. 279–339.

Simpson, J., Mitchelson-Jacob, E., Hill, A., 1990. Flow structure in a channel from an acoustic Doppler current profiler. Continental Shelf Research 10(6), 589–603.

Spitz, Y., Klinck, J., 1998. Estimate of bottom and surface stress during a spring–neap tide cycle by dynamical assimilation of tide gauge observations in the Chesapeake Bay. Journal of Geophysical Research 103 (C6), 12761–12782.

Thacker, W. C., 1988. Fittin models to inadequate data by enforcing spatial and temporal smoothness. Journal of Geophysical Research 93 (C9), 10655–10665.

Thompson, K. R., Griffin, D. A., 1998. A model of the circulation on the outer Scotian Shelf with open boundary conditions inferred by data assimilation. Journal of Geophysical Research 103 (C13), 30641–30660.

Torrence, C., Compo, G. P., 1998. A practical guide to wavelet analysis. Bulletin of the American Meteorological Society 79, 61–78.

Trump, C. L., Marmorino, G. O., 1997. Calibrating a gyrocompass using ADCP and DGPS data. Journal of Atmospheric and Oceanic Technology 14 (1), 211–214.

Ullman, D. S., Wilson, R. E., 1998. Model parameter estimation from data assimilation modeling: Temporal and spatial variability of the bottom drag coefficient. Journal of Geophysical Research 103 (C3), 5531–5549.

UNESCO, 1981. Tenth report of the joint panel on oceanographic tables and standards. Tech. Rep. 36, UNESCO, Paris, France.

Valle-Levinson, A., Klinck, J., Wheless, G., 1996. Inflows/outflows at the transition between a coastal plain estuary and the coastal ocean. Continental Shelf Research 16 (14), 1819–1847.

Valle-Levinson, A., Li, C., Royer, T. C., Atkinson, L. P., 1998. Flow patterns at the Chesapeake Bay entrance. Continental Shelf Research 18, 1157–1177.

Valle-Levinson, A., Wong, K.-C., Bosley, K. T., 2001. Observations of the wind–induced exchange at the entrance to Chesapeake Bay. Journal of Marine Research 59, 391–416.

Whitney, M. M., 2003. Simulating the Delaware Coastal Current. Ph.D. thesis, University of Delaware, 284 pp.

Reproduced with permission of the copyright owner. Further reproduction prohibited without permission.

Wilks, D., 1995. Statistical Methods in the Atmospheric Sciences. Academic Press.

Wong, K.-C., 1998a. On the variability in the vertical structure of the Delaware coastal current. Continental Shelf Research 18, 929–940.

Wong, K.-C., 1998b. The seasonal and subtidal variability on the source region of the Delaware coastal current. Estuarine, Coastal and Shelf Science 47, 1–19.

Wong, K.-C., 1999. The wind driven currents on the Middle Atlantic Bight inner shelf. Continental Shelf Research 19, 757–773.

Wong, K.-C., Münchow, A., 1995. Buoyancy forced interaction between estuary and inner shelf: Observation. Continental Shelf Research 15 (1), 59–88.

Wong, K.-C., Valle-Levinson, A., 2002. On the relative importance of the remote and local wind effects on the subtidal exchange at the entrance to the Chesapeake Bay. Journal of Marine Research 60, 477–498.

Xie, L., Eggleston, D., 1999. Computer simulations of wind-induced estuarine circulation patterns and estuary-shelf exchange processes: The potential role of wind forcing on larval transport. Estuarine, Coastal and Shelf Science 49, 221–234.

Yankovsky, A., Garvine, R., Münchow, A., 2000. Mesoscale currents on the inner New Jersey shelf driven by the interaction of buoyancy and wind forcing. Journal of Physical Oceanography 30, 2214–2230.

Zhang, A., Wei, E., Parker, B. B., 2003. Optimal estimation of tidal open boundary conditions using predicted tides and adjoint data assimilation technique. Continental Shelf Research 23, 1055–1070, DOI:10.1016/S0278-4343(03)00105-5.

Reproduced with permission of the copyright owner. Further reproduction prohibited without permission.

APPENDIX A

SCALING ANALYSIS

Consider the equations of motion for a thin shell in a rotating Earth:

Across shelf flow:

$$\frac{\partial u}{\partial t} + u\frac{\partial u}{\partial x} + v\frac{\partial u}{\partial y} + w\frac{\partial u}{\partial z} = -\alpha\frac{\partial P}{\partial x} + fv - 2\Omega\cos\phi w + F_x + F_y + F_z \tag{A-1}$$

Along shelf flow:

$$\frac{\partial v}{\partial t} + u\frac{\partial v}{\partial x} + v\frac{\partial v}{\partial y} + w\frac{\partial v}{\partial z} = -\alpha\frac{\partial P}{\partial y} - fu + F_x + F_y + F_z \tag{A-2}$$

Considerations:

- Steady state conditions,

$$\frac{\partial}{\partial t} \approx 0$$

- The Ekman Layer depth ($\delta = \sqrt{2A_z/f}$) is $\approx$ 50 m. However, A_z depends on the wind stress and stratification.
- The Coriolis parameter ($|f| = 2\Omega\sin\phi$) has an approximate value of 0.86×10^{-4} for the Delmarva shelf (37°N).
- The frictional terms (F_z) can be scaled in three ways:

$$F_z = \frac{\tau_b}{\rho H} \tag{A-3}$$

$$F_z = \frac{\tau_w}{\rho H} \tag{A-4}$$

$$F_Z = \frac{A_z U}{H^2} \tag{A-5}$$

For the upper layer, values of τ_w can be found in the literature, while for the bottom layer τ can be calculated from a quadratic drag formula

$$\tau_b = \rho C_D U^2 \tag{A-6}$$

with $C_D = 2.5 \times 10^{-3}$, $\rho_w = 1000$ kg m^{-3} and u bottom velocity (u or v).

Reproduced with permission of the copyright owner. Further reproduction prohibited without permission.

- We use the average values of $A_{x,y} = 10^2$ m^2 s^{-1} and $A_z = 10^{-2}$ m^2 s^{-1}. Upper limit values found in the literature are $A_{x,y} = 10^5$ m^2 s^{-1} and $A_z = 10^{-1}$ m^2 s^{-1}.
- In Eq. (A-1) the term $-2\Omega \cos\phi w$ is omitted ($\approx 10^{-7}$).

A.1 ACROSS SHELF CIRCULATION

$$u\frac{\partial u}{\partial x} + v\frac{\partial u}{\partial y} + w\frac{\partial u}{\partial z} = -\alpha\frac{\partial P}{\partial x} + fv + A_x\frac{\partial^2 u}{\partial x^2} + A_y\frac{\partial^2 u}{\partial y^2} + A_z\frac{\partial^2 u}{\partial z^2}$$

$$\frac{UU}{L_x} + \frac{VU}{L_y} + \frac{WU}{H} = ? + fV + A_x\frac{U}{L_x} + A_y\frac{U}{L_y} + F_z \tag{A-7}$$

The question mark represent the barotropic contribution, which can not be scaled due to its variance. For this analysis, this term is be ignored. Here the bottom stress represent the frictional force F_z, eq (A-3).

$$\frac{10^{-4}}{10^4} + \frac{10^{-3}}{10^5} + \frac{10^{-6}}{10^1} = ? + 10^{-5} + 10^2\frac{10^{-2}}{10^8} + 10^2\frac{10^{-2}}{10^{10}} + \frac{10^3 2.5\times 10^{-3}10^{-4}}{10^3\cdot 10^1} \tag{A-8}$$

$$10^{-8} + 10^{-8} + 10^{-7} = ? + 10^{-5} + 10^{-8} + 10^{-10} + 10^{-8} \tag{A-9}$$

Dividing by the Coriolis term (10^{-5})

$$10^{-3} + 10^{-3} + 10^{-2} = ? + 1 + 10^{-3} + 10^{-5} + 10^{-3} \tag{A-10}$$

For this direction the momentum balance is geostrophic with corrections at 1% order due to nonlinear terms.

A.2 ALONG SHELF CIRCULATION

$$u\frac{\partial v}{\partial x} + v\frac{\partial v}{\partial y} + w\frac{\partial v}{\partial z} = -\alpha\frac{\partial P}{\partial y} - fu + A_x\frac{\partial^2 v}{\partial x^2} + A_y\frac{\partial^2 v}{\partial y^2} + A_z\frac{\partial^2 v}{\partial z^2}$$

$$\frac{UV}{L_x} + \frac{VV}{L_y} + \frac{WV}{H} = ? - fU + A_x\frac{V}{L_x} + A_y\frac{V}{L_y} + F_z \tag{A-11}$$

The question mark represent the barotropic contribution, which can not be scaled due to its variance. For this analysis, this term is be ignored. Here, the bottom stress represent the frictional force F_z, eq (A-3).

$$\frac{10^{-3}}{10^4} + \frac{10^{-2}}{10^5} + \frac{10^{-5}}{10^1} = ? - 10^{-6} + 10^2\frac{10^{-1}}{10^8} + 10^2\frac{10^{-1}}{10^{10}} + \frac{10^3 2.5\times 10^{-3}10^{-2}}{10^3\cdot 10^1} \tag{A-12}$$

Reproduced with permission of the copyright owner. Further reproduction prohibited without permission.

Dividing by the Coriolis term (10^{-6})

$$10^{-1} + 10^{-1} + 1 = ? - 1 + 10^{-1} + 10^{-3} + 1 \tag{A-13}$$

The momentum balance is between the pressure gradient, Coriolis terms, bottom drag and nonlinear terms.

Reproduced with permission of the copyright owner. Further reproduction prohibited without permission.

APPENDIX B

ASSIMILATION MODEL DETAILS

The linear shallow water equations were nondimensionalized dividing the dynamic terms by fU, where f is the Coriolis and U is a velocity scale, taken here as 1 m s^{-1}. The depth h was nondimensionalized by $H_{\max}$, the maximum depth. In this case, $H_{\max} = 40$ m. The model uses finite difference and an Arakawa C grid (Mesinger and Arakawa, 1976). The time integration interval was set to $\delta t = 6.25$ min, based on the CFL condition. The u, v, and η fields from the numerical model were saved every hour. The minimization of the cost function was based on the linear conjugate–gradient algorithm of Gill et al. (1981)

The grid size is 128×134 η points. Of those, approximately 6500 correspond to "wet" points. Considering the u, v, and η fields, there are $\approx$ 19500 initial conditions. Instead of defining the initial conditions or a parameterization of them as something to be found by the data assimilation, each runs starts three days before assimilating data to spin up de the model.

The four structure functions, two for the bottom open boundary condition and two for the right boundary condition, were calculated every 1.5 h. Each day of data assimilation had then 4×16 = 64 control variables, per day, to be defined. Three days of spin up represent 192 "initial" control variables. so, for one day of data assimilation we had 254 control variables, for two days 318, an so forth.

Unless regularization terms are added, more data points than open boundary parameters are needed for the fit. A useful analogy is when a time series is fitted by least squares to a semidiurnal tidal function. Just three parameters need to be determined; mean current, amplitude, and phase, but more than three data points are used for the fit.

Each sea level station assimilated had hourly elevation, providing then 24 data points, per day, per station. An average of four sea level stations were used in each experiment. ADCP data were averaged in 10 minute intervals, giving 144 data points per day. For one day of data assimilation we needed the 144 data points form the ADCP record, plus 110 data from the sea level record, i.e. 5 sea level stations ($5 \times 24 = 120$ data points). For two days of assimilation, we have 288 data points from the ADCP, and as calculated before, we have 318 variables. Therefore we need at least 40 data points from the sea level record, i.e. a minimum of two stations ($2 \times 24 = 48$). The ADCP data set, collected every minute, could be averaged into 5 minute intervals in order to increase the number of data points available for assimilation, however it is unknown if a five minute interval will provide statistically independent data. The same question arises for the 20 minute interval, but further averaging would reduce the amount of data available and thus increasing the ill-condition of the problem. Further study is needed also in the effect of changes in the

Reproduced with permission of the copyright owner. Further reproduction prohibited without permission.

grid size and number and location of the boundary structures.

Reproduced with permission of the copyright owner. Further reproduction prohibited without permission.

APPENDIX C

NUMERICAL MODEL RUNS

The following tables summarize the main input and output results from the data assimilation runs.

The following description applies to Tables 8– 12. The **Run** column is a unique identifier for each model setup. The **Sea Level Stations** are referred by a number, and their location is shown in Fig. 1. The sea level stations indicated in the table were not assimilated in the model. The **Weight Ratio** column indicates the relative weight of each term in the cost function; σ_a for the ADCP term, σ_s for the sea level term, σ_v for the vorticity term, and σ_t for the tidal term. The **Final J %** value shows what percentage of the initial value is left after **n** iterations. Subscripts denote the number of iterations. **aRMS** and **sRMS** are the root-mean-square-error of the withheld ADCP and sea level data, respectively. The **Note** in the last column shows the portion of the ADCP record being analyzed in each run.

Tables 13–17 provide the following information. The **Run** column is a unique identifier for each model setup. The **Sea Level Stations** are referred by a number, and their location is shown in Fig. 1. The sea level stations indicated in the table were not assimilated in the model. No ADCP data were withheld for these runs. The **Weight Ratio** column indicates the weight ratio between the ADCP term and the sea level (σ_a/σ_s). The vorticity term and the tidal term were set to ∞ in all these runs. r is the value of the linear bottom drag coefficient used in the model run. The **Final J_{10}** column shows what percentage of the initial value is left after 10 iterations. If a larger number of iterations was done, the subscript is changed to the final number of iterations (e.g. J_{60} for 60 iterations).

- Note explanations for Table 8: **north** indicates the model was run for the time when the northward portion of the track was surveyed, **south** indicates the model was run for the time when the southward portion of the track was surveyed, **all** indicates the model was run for the time when the whole track was surveyed, **reps** indicates the model was run for the time when the a track was repeated for 24 hours. **top** indicates the model was run for a 24 hour interval covering the northernmost portion of the cruise track.

- Note explanations for Table 9: Since this track consisted only of a 24 h survey, the whole period was modeled, and just portions of the track were withheld for verification purposes.

- Note explanations for Table 11: **1** stands for the first track repeated for 13 hours, **m**

Reproduced with permission of the copyright owner. Further reproduction prohibited without permission.

for the survey track done in the middle, and **2** stands for the second track repeated for 13 hours.

- Note explanations for Table 12: **north** indicates the model was run for the time when the northward portion of the track was surveyed, **south** indicates the model was run for the time when the southward portion of the track was surveyed, **all** indicates the model was run for the time when the whole track was surveyed, **all(north)** indicates the model was run for the time when the whole track was surveyed, but just the north portion was assimilated.

- Note explanations for Table 17: Runs 66a, 66b, and 66c assimilate different intervals, 24 hours long, of the ADCP record. All the other runs assimilate the whole ADCP record, except run 51.

Table 8
Regularization Terms. MAY2000

Run	Sea Level Stations	Weight Ratio $\sigma_a/\sigma_s/\sigma_v/\sigma_t$	Final J %	aRMS (cm s^{-1})	sRMS (cm)	Note
m1	1,2,4,7	1.0/0.1/1500/∞	17_{60}	17	6	north/south
m2	1,2,4,7	1.0/0.1/500 /∞	24_{60}	34	6	reps
m3	1,2,4,7	1.0/0.1/500 /∞	37_{60}	10	6	top
m4	1,2,4,7	1.0/0.1/500 /∞	29_{60}	8	7	all
m5	1,2,4,7	1.0/0.1/1000/∞	21_{60}	17	6	north/south
m6	1,2,4,7	1.0/0.1/250 /∞	41_{60}	8	9	all
m7	1,2,4,7	1.0/0.1/500 /∞	27_{60}	6	7	north
m8	1,2,4,7	1.0/0.1/500 /∞	37_{60}	17	6	south
m9	1,2,4,7	1.0/0.1/1000/∞	17_{60}	4	6	north
m11	1,2,4,7	1.0/0.1/1000/∞	30_{60}	26	5	south
m12	1,2,4,7	1.0/0.1/1250/∞	22_{60}	22	5	south

Reproduced with permission of the copyright owner. Further reproduction prohibited without permission.

Table 9
Regularization Terms. SEP2000

Run	Sea Level Stations	Weight Ratio $\sigma_a/\sigma_s/\sigma_v/\sigma_t$	Final J %	aRMS (cm s^{-1})	sRMS (cm)
s1	1,2,4,7	1.0/0.1/1000/∞	11_{40}	11	19
s2	1,2,4,7	1.0/0.1/1500/∞	16_{40}	8	6
s3	1,2,4,7	1.0/0.1/750 /∞	23_{40}	12	6
s4	1,2,4,7	1.0/0.1/2000/∞	13_{40}	6	6
s5	1,2,4,7	1.0/0.1/500 /∞	29_{60}	7	7
s6	1,2,4,7	1.0/0.1/250 /∞	42_{40}	6	10
s6a	1,2,4,7	1.0/0.1/250 /∞	40_{40}	6	10
s6b	1,2,4,7	1.0/0.1/250 /∞	44_{40}	11	10
s6c	1,2,4,7	1.0/0.1/250 /∞	41_{40}	6	10
s6d	1,2,4,7	1.0/0.1/250 /∞	44_{40}	11	10
s6e	1,2,4,7	1.0/0.1/250 /∞	43_{40}	9	10
s7	1,2,4,7	1.0/0.1/5000/∞	09_{40}	18	6
s8	1,2,4,7	1.0/0.1/1000/∞	20_{60}	10	6
s9	1,2,4,7	1.0/0.1/100 /∞	60_{40}	9	15
s10	1,2,4,7	1.0/0.1/10 /∞	90_{40}	14	22
s11	1,2,4,7	1.0/0.1/1 /∞	99_{40}	16	26
s12	1,2,4,7	1.0/0.1/∞/∞	5_{40}	29	9
t1	1,2,4,7	1.0/0.1/∞/500	3_{60}	26	13
t2	1,2,4,7	1.0/0.1/∞/250	3_{60}	26	13
t3	1,2,4,7	1.0/0.1/∞/100	3_{60}	27	13
t5	1,2,4,7	1.0/0.1/∞/10	4_{60}	21	13
t6	1,2,4,7	1.0/0.1/∞/1	4_{60}	15	13
t7	1,2,4,7	1.0/0.1/∞/.1	4_{60}	10	13
t8	1,2,4,7	1.0/0.1/∞/5000	3_{60}	26	14
t8a	1,2,4,7	1.0/0.1/∞/.01	5_{60}	9	12
s6a	1,2,4,7	1.0/0.1/250 /∞	40_{40}	6	10
s6b	1,2,4,7	1.0/0.1/250 /∞	44_{40}	11	10
s6c	1,2,4,7	1.0/0.1/250 /∞	41_{40}	6	10
s6d	1,2,4,7	1.0/0.1/250 /∞	44_{40}	11	10
s6e	1,2,4,7	1.0/0.1/250 /∞	43_{40}	9	10
s7	1,2,4,7	1.0/0.1/5000/∞	09_{40}	18	6
s8	1,2,4,7	1.0/0.1/1000/∞	20_{60}	10	6
s9	1,2,4,7	1.0/0.1/100 /∞	60_{40}	9	15
s10	1,2,4,7	1.0/0.1/10 /∞	90_{40}	14	22
s11	1,2,4,7	1.0/0.1/1 /∞	99_{40}	16	26
s12	1,2,4,7	1.0/0.1/∞/∞	5_{40}	29	9

Reproduced with permission of the copyright owner. Further reproduction prohibited without permission.

Table 10
Regularization Terms. SEP2000 (Cont.)

Run	Sea Level Stations	Weight Ratio $\sigma_a/\sigma_s/\sigma_v/\sigma_t$	Final J %	aRMS (cm s^{-1})	sRMS (cm)
t1	1,2,4,7	$1.0/0.1/\infty/500$	3_{60}	26	13
t2	1,2,4,7	$1.0/0.1/\infty/250$	3_{60}	26	13
t3	1,2,4,7	$1.0/0.1/\infty/100$	3_{60}	27	13
t5	1,2,4,7	$1.0/0.1/\infty/10$	4_{60}	21	13
t6	1,2,4,7	$1.0/0.1/\infty/1$	4_{60}	15	13
t7	1,2,4,7	$1.0/0.1/\infty/.1$	4_{60}	10	13
t8	1,2,4,7	$1.0/0.1/\infty/5000$	3_{60}	26	14
t8a	1,2,4,7	$1.0/0.1/\infty/.01$	5_{60}	9	12
t9	1,2,4,7	$1.0/0.1/\infty/.001$	5_{60}	9	12
t10	1,2,4,7	$1.0/0.1/\infty/.0001$	5_{60}	9	12
s001	1,2,4,7	$1.0/0.1/\infty/.0001$	10_{60}	10	9
s002	1,2,4,7	$1.0/0.1/\infty/.00001$	8_{60}	9	20
s003	1,2,4,7	$1.0/0.1/\infty/.000001$	9_{60}	19	20
s004	1,2,4,7	$1.0/0.1/500$ /.000001	32_{60}	6	9
s005	3,5,6	$1.0/0.1/500$ /∞	21_{60}	13	6

Table 11
Regularization Terms. NOV2000

Run	Sea Level Stations	Weight Ratio $\sigma_a/\sigma_s/\sigma_v/\sigma_t$	Final J %	aRMS (cm s^{-1})	sRMS (cm)	Note
n1	1,2,4,7	$1.0/0.1/500$ /∞	32_{60}	13	8	1/m/2
n2	1,2,4,7	$1.0/0.1/500$ /∞	31_{60}	16	9	1/m
n3	1,2,4,7	$1.0/0.1/500$ /∞	29_{60}	14	9	1
n4	1,2,4,7	$1.0/0.1/500$ /∞	27_{60}	19	8	m
n5	1,2,4,7	$1.0/0.1/250$ /∞	46_{60}	11	12	1/m/2
n6	1,2,4,7	$1.0/0.1/750$ /∞	25_{60}	15	7	1/m/2
n7	1,2,4,7	$1.0/0.1/1000/\infty$	21_{60}	16	8	1/m/2
n001	1,2,4,7	$1.0/0.1/\infty/.001$	3_{60}	15	17	1
n002	1,2,4,7	$1.0/0.1/\infty/.0001$	3_{60}	17	16	1
n003	1,2,4,7	$1.0/0.1/\infty/.001$	1_{60}	22	13	m
n004	1,2,4,7	$1.0/0.1/\infty/.0001$	1_{60}	22	13	m
n005	1,2,4,7	$1.0/0.1/\infty/.001$	2_{60}	10	13	2
n006	1,2,4,7	$1.0/0.1/\infty/.0001$	2_{60}	10	12	2

Reproduced with permission of the copyright owner. Further reproduction prohibited without permission.

Table 12
Regularization Terms. FEB2001

Run	Sea Level Stations	Weight Ratio $\sigma_a/\sigma_s/\sigma_v/\sigma_t$	Final J %	aRMS (cm s^{-1})	sRMS (cm)	Note
f4	1,2,4,7	$1.0/0.1/500/\infty$	31_{60}	6	5	all(north)
f5	1,2,4,7	$1.0/0.1/500/\infty$	32_{60}	15	5	all(south)
f6	1,2,4,7	$1.0/0.1/500/\infty$	31_{60}	11	5	all(middle)
fh1	1,2,4,7	$1.0/0.1/500/\infty$	30_{60}	9	5	north/south
fh3	1,2,4,7	$1.0/0.1/250/\infty$	45_{60}	9	8	north/south
fh4	1,2,4,7	$1.0/0.1/500/\infty$	32_{60}	4	5	north
fh5	1,2,4,7	$1.0/0.1/\infty/.0001$	45_{60}	4	6	north
f001	1,2,4,7	$1.0/0.1/500/\infty$	23_{60}	22	6	south
f002	1,2,4,7	$1.0/0.1/\infty/.0001$	21_{60}	21	6	south
f003	1,2,4,7	$1.0/0.1/1000/\infty$	20_{60}	3	5	north
f004	1,2,4,7	$1.0/0.1/1000/\infty$	21_{60}	21	6	south
f005	1,2,4,7	$1.0/0.1/\infty/.0001$	21_{60}	21	6	north/south

Table 13
Cost Function - MAY2000 ($r = 0.15$ m s^{-1})

Run	Sea Level Stations	Weight Ratio σ_a/σ_s	sRMS (cm)	Final J_{10} %
00	2,5,6	1.80	7	14
01	2,5,6	6.50	7	15
02	2,5,6	2.00	9	14
03	2,5,6	1.16	8	15
04	2,5,6	0.40	11	15
05	1,2,3,4,5,6,7	1.00/inf	29	11
06	2,5,6	inf/1.00	6	1
07	2,5,6	100.	17	3
08	2,5,6	20.0	7	5
09a	2,5,6	10.0	7	7
09b	2,4,7	0.10	15	8 (J_{60})
09c	1,2,4,7	10.0	7	7 (J_{60})
11	2,5,6	0.75	20	15
12	2,5,6	0.25	8	14
13	2,5,6	0.15	16	14
14	2,5,6	0.85	9	15
15a	2,5,6	10.0	7	7
15b	2,5,6	10.0	7	5 (J_{60})
16	2,5,6	2.00	8	13
17	2,5,6	1.33	8	14
18	2,5,6	6.66	7	11
19	2,5,6	4.00	7	9
20	2,5,6	1.18	8	15

Reproduced with permission of the copyright owner. Further reproduction prohibited without permission.

Table 14
Cost Function - MAY2000 ($r = 0.15$ m s^{-1}) (Cont.)

Run	Sea Level Stations	Weight Ratio σ_a/σ_s	sRMS (cm)	Final J_{10} %
21	2,5,6	1.00	8	16
22	2,5,6	2.00	8	14
23	2,5,6	3.00	7	12
24	2,5,6	4.00	7	11
25	2,5,6	5.00	7	10
26	2,5,6	6.00	7	9
27	2,5,6	1.00	8	15
28	2,5,6	0.33	11	14
29	2,5,6	3.00	7	12

Table 15
Cost Function - SEP2000

Run	Sea Level Stations	Weight Ratio σ_a/σ_s	r (m s^{-1})	sRMS (cm)	Final J_{10} %	Δt ADCP (min)
30	–	1.0	0.15	7	10	
31	–	inf/1.0	0.15	4	3	
32	1,2,3,4,5,6,7	1.0/inf	0.15	4	11	
33	1,3,6	1.0	0.15	9	11	
34	3,6	1.0	0.15	8	10	
35	3	1.0	0.15	8	10	
36	2,5	1.0	0.15	7	10	10
37	2,5	1.0	0.15	6	7	20
38	2,5	1.0	0.15	5	7	30
39	2,5	1.0	0.15	5	6	40
40	2,5	1.0	0.15	5	6	50
41	2,5	1.0	0.15	5	4	60
42a	2,5	1.0	0.15	6	10	10
42b	2,4,7	0.1	0.15	10	9(J_{60})	10
42c	1,2,4,7	10.0	0.15	8	5(J_{60})	10
42d	1,2,4,7	10.0	0.15	6	7	10
43	2,5	1.0	0.20	6	10	10
44	2,5	1.0	0.10	7	10	10
45	2,5	1.0	0.30	7	11	10
46	2,5	1.0	0.06	7	10	10
47	2,5	1.0	0.40	8	12	10
48	2,5	1.0	0.80	12	18	10
49	2,5	1.0	0.01	8	10	10

Table 16
Cost Function - NOV2000

Run	Sea Level Stations	Weight Ratio σ_a/σ_s	r (m s^{-1})	sRMS (cm)	Final J_{10} %
e1	3,5,6	10.0	0.15	5	3
e3	3,5,6	inf/1.0	0.15	24	1
e4	2,3,4,5,6	10.0	0.15	5	4

Reproduced with permission of the copyright owner. Further reproduction prohibited without permission.

Table 17
Cost Function - FEB2001

Run	Sea Level Stations	Weight Ratio σ_a/σ_s	r (m s^{-1})	sRMS (cm)	Final J_{10} %
50a	–	1.0	0.15	5	17
50b	–	1.0	0.15	3	12 (J_{60})
51	–	inf/1.0	0.15	3	3
52	1,2,3,4,5,6,7	1.0/inf	0.15	22	22
53	2,4,7	1.0	0.15	6	19
54	4,7	1.0	0.15	6	19
55	7	1.0	0.15	5	17
59a	1,2,4,7	10.0	0.15	4	6 (J_{60})
59b	1,2,4,7	10.0	0.15	5	9
60a	3,7	1.0	0.15	6	18
60b	3,7	1.0	0.15	7	14 (J_{30})
60c	3,7	1.0	0.15	6	13 (J_{60})
60d	2,4,7	0.1	0.15	11	16 (J_{60})
61	–	inf/1.0	1.25	11	28
62	1,2,3,4,5,6,7	1.0/inf	0.55	7	22
63	3,7	1.0	0.30	6	19
64	3,7	1.0	0.20	6	18
65	3,7	1.0	0.10	6	19
66a	3,7	1.0	0.015	9	21
66b	3,7	1.0	0.015	9	15
66c	3,7	1.0	0.015	14	20
67	3,7	1.0	1.50	12	30
68	3,7	1.0	0.50	7	22
69	3,7	1.0	0.75	9	24
70	3,7	1.0	0.25	6	19
71	3,7	1.0	0.35	6	20
72	3,7	1.0	0.15	6	18
73	3,7	1.0	0.45	7	21
74	3,7	1.0	0.65	8	24
75	3,7	1.0	0.85	9	25
76	3,7	1.0	0.95	10	26
77	3,7	1.0	3.00	16	37
78	3,7	1.0	4.50	17	45
79	3,7	1.0	0.05	17	20
80	3,7	1.0	0.00	7	20
81	3,7	1.0	0.175	6	18
82	3,7	1.0	0.125	6	19

Reproduced with permission of the copyright owner. Further reproduction prohibited without permission.

VITA

Héctor Hito Sepúlveda
Department of Ocean, Earth, and Atmospheric Sciences
406 Ocean/Physics Building
Old Dominion University
Norfolk, VA, 23529

PERSONAL DATA
Born in August 19th 1972 in Santiago, Chile
to Héctor Sepúlveda Sepúlveda and Carmen Paz Allende Bussi.

EDUCATION
B.Sc. in Physics from the Faculty of Sciences, University of Chile,
Las Palmeras 3425, Santiago, Chile (1996).

Reproduced with permission of the copyright owner. Further reproduction prohibited without permission.